HYPERSONIC FLOW OVER A YAWED CIRCULAR CONE

Thesis by

Richard R. Tracy

In Partial Fulfillment of the Requirements

For the Degree of

Doctor of Philosophy

California Institute of Technology

Pasadena, California

1964

ACKNOWLEDGMENTS

Beyond the appreciation due to those of the GALCIT faculty and staff whose continuing effort underlies every research project, and the U. S. taxpayers, through whose generosity and wisdom a portion of this research was underwritten by the Hypersonic Research Project sponsored by the U. S. Army Research Office and the Advanced Research Projects Agency, the author is particularly grateful to:

Lockheed Aircraft Corporation who, through the Lockheed Leadership Foundation, contributed financially to the author's graduate studies;

Mr. William H. Bowen for his advice and support in the design of the test equipment;

the staff of the Aeronautics Machine Shop under Mr. C. A. Bartsch, and especially Messrs. G. [illegible]son and [illegible] McDonald for their unusual skill in constructing the exp[illegible]

Messrs. S. Roman, J. Van Dijk, and G. Van Hal[illegible]yn for their assistance in conducting the wind tunnel tests, and Mr. P. Baloga, under whose guidance the wind tunnel operations were performed;

Mrs. Truus van Harreveld for her unrele[illegible] care in the numerical computations;

Mr. J. Gibbs, at that time the Regional Sa[illegible]es Representative for the Transducer Division, Consolidated Electrodynamics Corporation, who furnished the excellent pressure transducer that was instrumental in the acquisition of the surface pressure data;

Mr. H. Kolkowitz, president of Computermat Incorporated, who

constructed the program, and contributed the IBM 1650 computer time required for the determination of the shock shape coefficients;

Mrs. Gerry Van Gieson for her able and tireless typing of the manuscript;

Mr. E. F. Ward, President of Task Corporation, for his patience and encouragement; and to

Professors Lester Lees and Toshi Kubota, who suggested the problem, and whose continued guidance has been essential to the completion of this research and invaluable to the author.

With the recognition that her inspiration and perseverence were fundamentally associated with its inception and completion, this work is dedicated to my wife, Jo.

ABSTRACT

A 10° semi-apex, circular cone is tested in air at Mach 8 and at yaw angles to 24°; surface pressure, heat transfer, and pitot-pressure throughout the flow field are presented. The nominal surface temperature is 40 % of the free stream stagnation temperature, and the Reynolds number, based on cone generator length, is varied from 0.5×10^5 to 4.2×10^5. Heat transfer is measured at higher surface temperature ratios (up to 56 %) and Reynolds numbers (up to 7.3×10^5) by reducing the free stream stagnation temperature. All raw data consist of continuous circumferential distributions of each quantity and are included in a supplement.

The surface pressure data are compared with the theories of Stone-Kopal and Cheng; Reshotko's theory of heat transfer to the windward generator is compared with experiment. The probe data delineate the boundary between viscous and inviscid flow and determine the shape of the outer shock wave as well as the secondary shocks which appear in the flow field at large yaw. The probe data are sufficient to determine the flow field in the plane of symmetry and permit an approximate representation of the Mach number profiles of the separated viscous flow in the leeward meridian plane beyond a moderate yaw angle.

TABLE OF CONTENTS

LIST OF FIGURES

Supplemental Figures

LIST OF SYMBOLS

A	constant (Equations A-4, A-14)
a_n	Fourier coefficients
B	constant (Equation A-14)
C_p	pressure coefficient
c_p, c_v	specific heats
E	voltage (volts, unless specified)
f	function (Equation A-1)
H_w'	quantity related to gradient of total enthalpy at wall
h	heat transfer coefficient
k	cross flow parameter (defined by Equation III-4), conductivity (B. T. U./ft. s. ^oR)
L	characteristic length (Equation A-3)
M	Mach number
m	exponent (Equation A-14)
n	index of Fourier series
p	pressure (p. s. i.)
q	heat flux (B. T. U./ft.^{2}s.)
Re	Reynolds number per unit length (ft.$^{-1}$)
r	radial coordinate of spherical-polar system
T	temperature (^oR)
t	thickness (in.)
U_∞	velocity of the undisturbed flow
u	radial component of velocity
v	component of velocity normal to radius in meridional plane

w	circumferential component of velocity
x	distance along cone generator from apex (in.)
y	coordinate normal to x and tangent to cone
z	coordinate normal to x and normal to cone (in.)
α	yaw angle
γ	ratio of specific heats
δ	boundary layer thickness (in.)
Δ	small change or difference, as specified
ϵ	error (defined by Equations A-7a, A-11a)
θ	lattitude angle of spherical-polar coordinate system
ϕ	longitude (circumferential) angle of spherical-polar coordinate system
∇^2	Laplacian operator (= div • grad)

Subscripts

aw	quantity at insulated surface
b	quantity at base of low conductivity layer (on heat transfer model)
c	quantity at cone surface (flow quantities external to boundary layer)
r	referred to radial direction
s	quantity at (or just behind) shock
t	quantity at reservoir conditions
w	quantity at surface (at base of boundary layer)
x	referred to cone generator length
θ	referred to θ- direction
ϕ	referred to ϕ- direction

Subscripts (Continued)

∞ quantity in the undisturbed flow

o quantity related to the unyawed cone

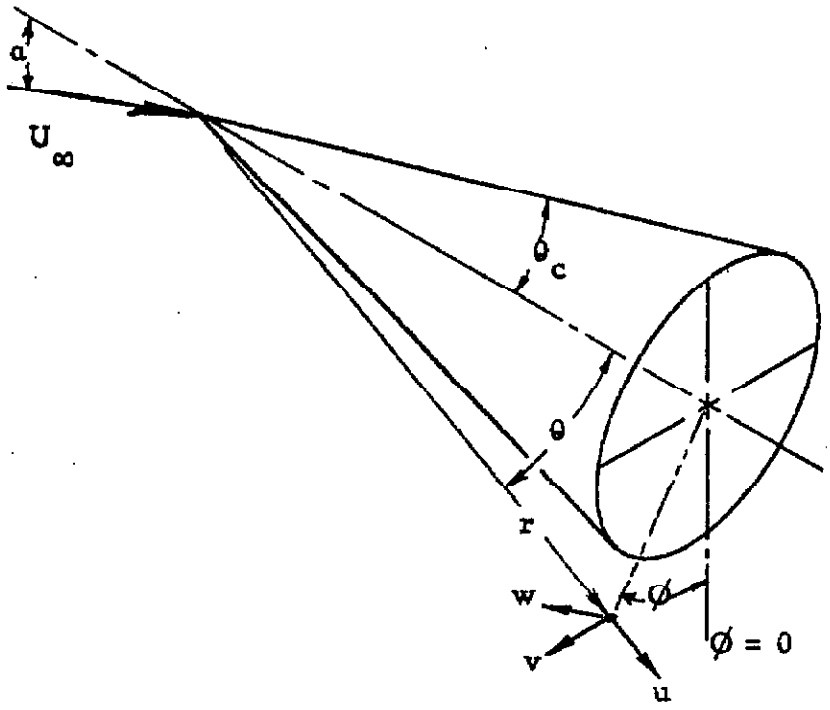

SPHERICAL-POLAR COORDINATE SYSTEM
AND ASSOCIATED VELOCITY COMPONENTS

I. INTRODUCTION

The supersonic flow of a gas over a yawed circular cone has been the object of numerous studies, none of which has been able to provide a clear comprehension of the complete problem. The reasons for the widespread interest are apparent:

(1) The circular cone is a fundamental shape to which other more general pointed bodies approximate.

(2) With the idealization of an inviscid fluid, the flow field is conical, that is, the variables of the flow no longer depend upon the radius from the apex.

The causes underlying the failure of the investigations to yield a generally valid conception of the phenomena are not as apparent. Because of the essential non-linearity of the inviscid equations of motion approximate methods of solution must be employed. Aside from the general methods of linearized supersonic theory and the hypersonic small disturbance theory, the approximate treatments are based primarily on the exact solution for the unyawed cone[1]. The linearizations about this solution[4], and the expansion of the variables in powers of yaw[2, 3] each gave solutions which were shown to omit an essential aspect of the flow field[5]. A modified power series theory[6] corrected this difficulty but was still unable to represent the flow near the lee side of the cone.

With the exception of Newtonian flow theory, all of the theories are restricted to relatively small yaw angles. Even within the yaw range of their formulation, there is no theory (including an isolated numerical integration[7]) which can quantitatively describe the entire flow field.

A still more fundamental problem exists. Each of the inviscid theories relies upon the validity of the Prandtl boundary layer concept; however, none attempt its demonstration. There are no direct measurements of the extent of the viscous region evident in the literature. The additional approximations contained in these theories prevent a conclusive indirect verification of the Prandtl concept by comparison of the theory with the numerous measurements of surface pressure[15-19] and heat transfer[20-24].

It is the purpose of this study to provide an experimental basis for the determination of the limits of the existing theoretical framework, and to augment the understanding of the phenomena which have eluded theoretical description.

The program adopted for the attainment of these objectives consists of a thorough experimental study of a cooled, 10° semi-apex cone at a Mach number of 8. The basic measurements consist of surface pressure, heat transfer, and a complete survey of the pitot-pressure in the flow field. Major emphasis is placed on the acquisition of detailed data for one set of flow parameters over a wide range of yaw.

The three basic tests are described and the data are presented. The remaining sections are devoted to the comparison of appropriate theories with the data, and discussions of the significance of the phenomena which are observed.

II. EXPERIMENTAL STUDIES

II. 1. Scope

Many experimental studies of circular cones at yaw are reported in the literature. Those tests covered a wide range of Mach number, Reynolds number, and cone angle. The measurements were of surface pressure or of local heat transfer and recovery factor. There do not appear to be any boundary layer measurements, nor surveys of any portions of the flow field. In each instance, the pressure and heat transfer measurements were made at discrete locations on the cone, so that no detailed examination of the circumferential distributions is possible.

The attainment of the objective of this investigation demands a detailed case study, and for this reason no exhaustive variation of parameters is attempted; specifically, only the yaw angle and, to a limited extent, the Reynolds number are varied.

The model is a 10^{o} semi-apex circular cone. The tests were conducted at a nominal Mach number of 8. The majority of the data was taken at a Reynolds number of 4×10^{5} (based on distance from the apex), and at a wall temperature ratio ($T_w/T_{t\infty}$) of 0.4. A limited variation of the latter parameters was introduced. The yaw angle was varied from zero to 24^{o}.

Surface pressure, pitot-pressure, and heat transfer rate were recorded continuously around the full cone circumference in each case. The pitot-pressure surveys were made in circular paths at various radii from the cone axis.

Neither static pressure nor total temperature was recorded in

the flow field. The variations in flow direction were too great to permit the recovery of useful static pressure data. A total temperature probe demarks regions of non-isoenergetic flow, i. e., viscous zones; however, in general, these boundaries were defined satisfactorily by the pitot-pressure data. (A "cold-wire" probe would be of value in distinguishing the edge of the boundary layer when it is adjacent to an isoenergetic flow of high vorticity.)

II. 2. Facility

II. 2. 1. Wind Tunnel

All of the tests described herein were conducted in "leg 2" of the GALCIT hypersonic facility. The facility consists of a compressor plant and dryer which supply either of two test sections (legs). Leg 2 is comprised of a nichrome-wire heater, a symmetrical, flexible-plate nozzle, a variable second throat, and an after-cooler. Further details of the facility can be found in Reference 26 . A photograph of the test section with the North sidewall removed appears in Figure 1.

The nozzle plates were adjusted for a nominal Mach number of 8. With this geometry the test section is approximately 7-1/4 inches square. The maximum supply conditions normally available are 250 p. s. i. g. and 900^{o}F. The tunnel can be operated at substantially lower pressure and enthalpy; however, at a supply pressure much below 100 p. s. i. g. the flow uniformity begins to deteriorate, and difficulty is experienced in maintaining the flow with a high drag model configuration (e. g., the present cone model at large yaw). The equilibrium properties of air indicate the possibility of condensation at temperatures

below about 850°F. The wind tunnel calibration, performed at the conclusion of the tests, is presented in Appendix B.

Tests were conducted at two pressures: $p_{t\infty}$ = 245 and 115 p. s. i. g. and at one temperature: $T_{t\infty}$ = 900°F. (The latter was varied for one series of heat transfer measurements, described in Section II. 3. 3.) The supply pressure and temperature were controlled within $\pm$0. 5 psi and $\pm$ 3°F, respectively. These tolerances were occasionally exceeded momentarily, as the result of transients in the controlling systems. The free-stream Reynolds numbers associated with the two supply conditions (129. 3 and 259. 3 p. s. i. a.; 900°F) were 0. 62 x 10^6 and 1. 25 x 10^6 per foot.

II. 2. 2. Model Support System

The original model support system, which was employed for preliminary tests, consists of a pair of vertical struts passing through the upper tunnel wall in tandem, aft of the test section. The struts are moved vertically by means of lead screws. Differential motion is controlled by a gear box so that a sting suspended from the struts can be pitched about any one of three centers or translated vertically. The strut positions are determined from the readings of two Veeder-Root counters.

Following the preliminary tests, this model support system was abandoned in favor of a yaw-sector type of model support system, which is mounted from a side wall as shown in Figure 1. Details of the support system are given below and in the drawing.

The spindle contains inlet and outlet coolant passages as well

as an instrumentation passage and is threaded to receive the model. The bearings which support the spindle are ball-radial-thrust ABEC class 7 and are seated in the tapered housing. Alignment between model and spindle is maintained by seating the back face of the model directly against the inner race of the forward bearing. The aft bearing outer race is pre-loaded in the direction of the prevailing drag force.

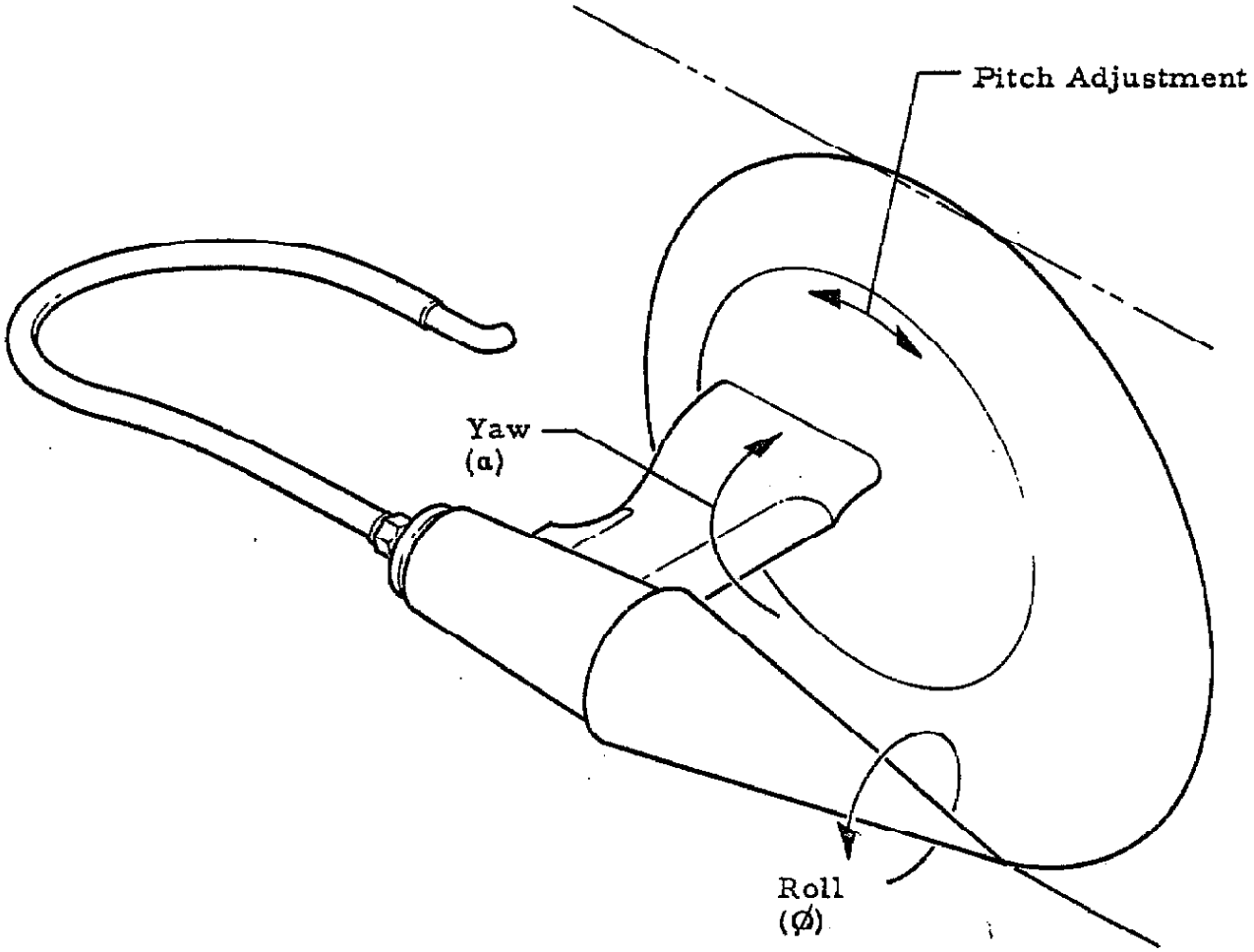

The spindle is rotated by a 2:1 right angle bevel reduction gear; the bevel drive-gear shaft passes through a horizontal strut which supports the housing. Inlet and return coolant passages in the strut

communicate with those in the spindle through a sealed manifold. The horizontal strut is machined to a circular planform at its inboard end. This circular sector slides through a slot in the mounting block as the model is yawed. The strut is attached to an arm which swings on a vertical axle-pin defining the center of yaw. The arm supporting the strut also carries the roll-drive motor, the roll position potentiometer, the yaw position lead-screw trunion, and the yaw position indicator pointer. Yaw positioning is accomplished manually by means of a lead screw and the yaw angle is read directly on a machine divided protractor. Either of two, constant speed, reversible, Bodine motors was used to provide model rolling rates of 0.7 or 3.7 degrees per second.

The complete support system is self contained and is installed as a unit in the South sidewall of the wind tunnel where it replaces the viewing port (thus precluding the use of the schlieren system). Small adjustments in pitch were made by rotating the entire assembly in the port. The center of yaw rotation lies in the tunnel wall 3.6 in. aft of the cone apex. This location keeps the model approximately centered in the test core for yaw angles up to about 30°.

An instrumentation shield encased the pressure tubing and the thermocouple leads between the aft end of the spindle and the point where the leads emerged from the tunnel through the South sidewall. The shield was a flexible metal hose through which a portion of the return coolant was passed. The length of the shield was the minimum that permitted compliance with the rolling and yawing motions imposed.

This mechanism permitted rapid and very accurate yaw settings

with negligible oscillation of the model axis during rotation. The total eccentricity of the model tip through a complete revolution measured 0.002 in. This figure includes the eccentricity of the model, the spindle, and the bearings, and constitutes an angular error of about 0.01°. The absolute accuracy of the yaw settings is considered to be within $\pm 0.05^{\circ}$; the repeatability was within $\pm 0.02^{\circ}$.

At the beginning of the wind tunnel tests the model axis was aligned with the flow direction by equalizing the pressures first at $\phi = 0^{\circ}$ and 180°, and then at 90° and 270°. The yaw position indicator was set and the port secured. The alignment was checked at the beginning of each test, but further adjustments were unnecessary.

II. 3. Test Equipment and Procedure

II. 3. 1. Preliminary Surveys

II. 3. 1. 1. Base Pressure Effects

In two-dimensional flows, the extent of a separated region is largely governed by the geometry in the reattachment zone. When the separated region communicates with the base flow behind a body, the extent of the separated region over the body is affected by any disturbances in the base pressure. Such a disturbance is caused by a strut and sting supporting the model. In the present problem, it is apparent that any gross separation of the flow from the cone surface extends to, and includes the base flow. Consequently, it was necessary to ascertain the influence, if any, of disturbances in the base region on the cone surface pressure for the yaw range of these tests.

An uncooled, 10° semi-apex cone model was constructed of brass and suspended in the tunnel using the original support system. A special dog-leg sting was constructed as shown in the sketch.

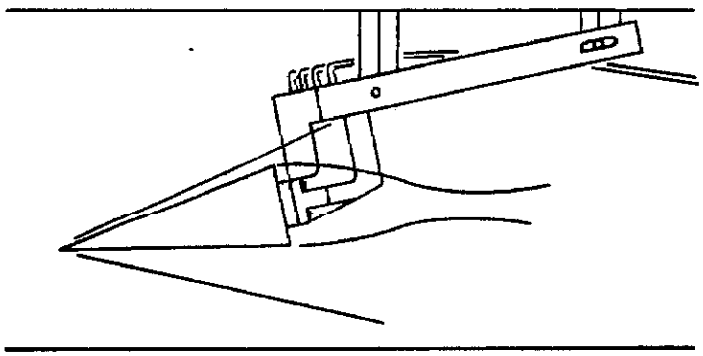

Negative Angle of Attack

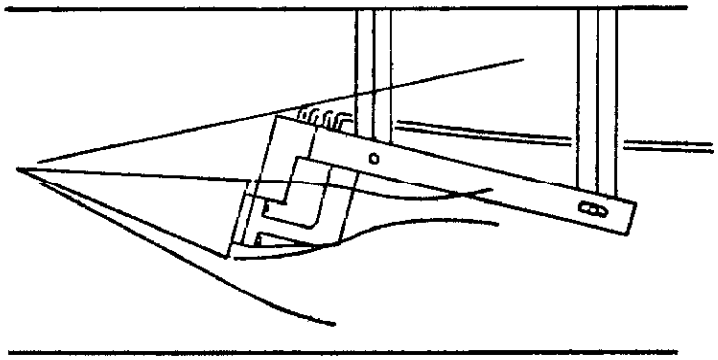

Positive Angle of Attack

The sting itself is well above the model axis, where its influence is isolated from the base or near-wake region. Only a very thin, doubly cusped strut enters the wake region. The model was provided with three surface pressure orifices located 0.50 in. from the base of the cone at the top, side, and bottom cone generators. A fourth, base-pressure orifice was positioned on the aft face of the cone at the horizontal centerline. The pressure passages in the cone communicated

with passages in the strut which led to four copper tubes attached to the upper surface of the sting. The joint between the model and the strut necessitated the use of 'O'-ring seals and these limited the maximum supply temperature to 750°F.

With the model at a negative angle of attack* (nose down), the sting remained clear of the wake and only the thin strut entered the viscous region. Positive pitch, however, caused the sting to be driven into the wake and base flow region.

Pressure measurements were made on a silicone oil micromanometer with a vacuum reference. The vacuum reference pressure was maintained below 10 micron Hg and was monitored with a McCleod gage. The overall inaccuracy of each pressure measurement did not exceed $\pm$ 0.25 mm. of silicone oil. The maximum error in the angle of attack was $\pm$ 0.25°. Pressure readings were made at angle of attack increments of 2° or less for both positive and negative angles up to 20°. This sequence was repeated at two tunnel pressures -- 100 p. s. i. g. and 250 p. s. i. g. -- with a supply temperature of 750°F. The model temperature, registered by an imbedded thermocouple, indicated that the cone was in thermal equilibrium and at adiabatic conditions during the tests.

No effect of free-stream Reynolds number of the base pressure could be discerned. However, the primary test objective was achieved. With negative angle of attack the leeward surface pressure decreased from its initial value at a continuously diminished rate until, at 20° it was still twice the base pressure and decreasing only very slowly.

---

* The term "yaw" is avoided in describing the preliminary tests in order to maintain the explicit distinction between the model arrangement and support system of these preliminary surveys and that of the later tests.

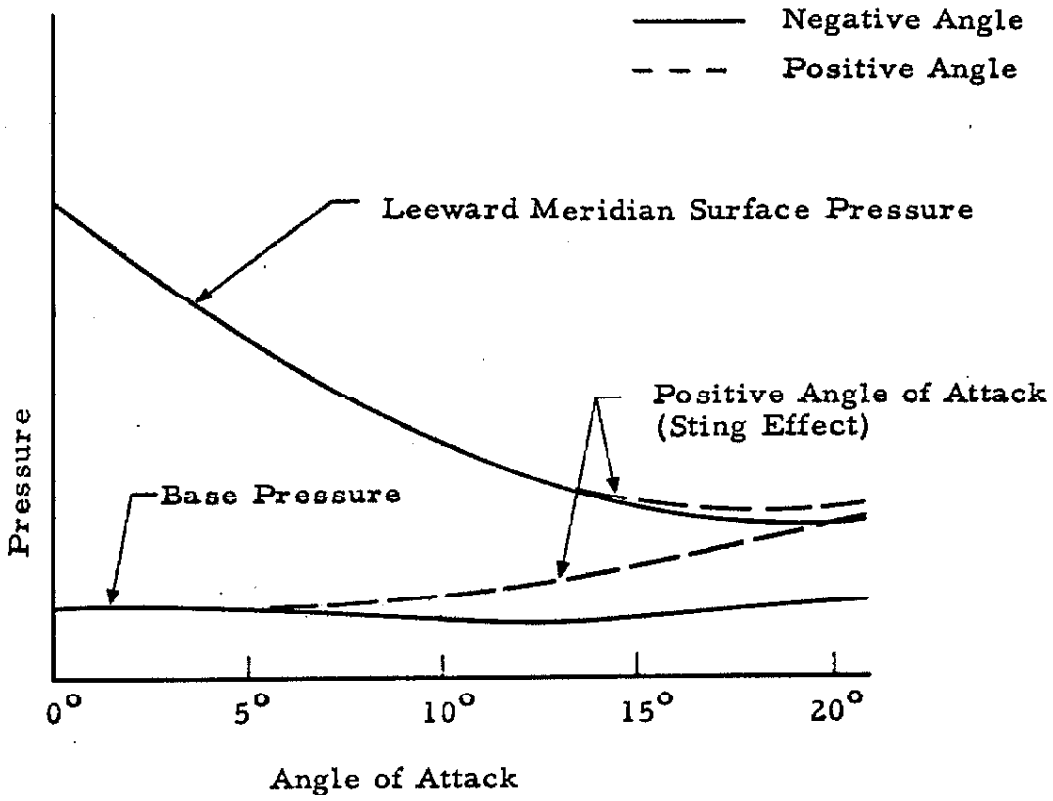

Even at very large negative angles the lee side of the cone was able to support pressures more than double the existing base pressure, thus eliminating the possibility of a subsonic communication between the two regions.

A marked difference was noted for positive angles of attack, when the sting was driven into the base and wake regions. In this case the base pressure began to rise strongly beyond about 5°, and at 12° had attained a value 50 % greater than at the same angle in the negative direction. At a 16° angle of attack the base pressure had risen to about 70 % of the existing leeward surface pressure. Beyond that angle, as the base pressure continued to approach the leeward surface pressure, the surface pressure became nearly constant, and showed an unmistakable

influence of the base pressure. That is, beyond about 16° the leeward surface pressure at a positive angle departed from that exhibited for negative angles, and a subsonic communication between the cone lee side and the base region must have existed.

This result indicates that tests of a finite length cone, even at large angles of attack, can be considered to represent the behavior of the idealized semi-infinite cone as long as reasonable precaution is taken in the design of the supporting structure to prevent the generation of abnormally large base pressures.

II. 3. 1. 2. Flow Visualization

Using the model and sting of the foregoing tests, limited visual observations were made. These consisted of schlieren photographs and observations of the flow directions at the model surface.

Schlieren Visualization

With the tunnel at its maximum pressure ($p_{t\infty}$ = 250 psig) and nominal temperature ($T_{t\infty}$ = 900°F) the flow was observed normal to the plane of symmetry through the schlieren system over the entire angle of attack range. Schlieren photographs were made at several representative angles.

Because of the relatively low density and the three-dimensional character of the flow field, the schlieren effect was very weak. At zero angle of attack the shock wave and boundary layer were visible; however, at even very small angles the shock wave and boundary layer could not be seen on the leeward side.

The photographs were thus indicative of very little except that the shock strength and density rapidly decrease on the lee side of the cone. The boundary layer thickness in the windward meridian plane was a small fraction of the shock layer thickness, and the shock wave there was measurably straight. The conditions accompanying a conical flow field appear to exist in the windward meridian plane.

Surface Flow Patterns

The following procedure was adopted to make surface flow observations: The brass model was polished and cleaned; then ordinary roofing tar was melted and applied in circular bands to the cone surface.

At approximately 350°F the tar behaved like a heavy oil; at temperature much in excess of 400°F the viscosity became so low that the tar spread into a discoloring film on the cone surface. The starting sequence of leg 2 requires approximately 20 minutes, during which time the supply temperature is increased to at least 750°F. Because of the starting requirement it was necessary to provide a means of temporarily insulating the tar-coated model.

A layer of ice, approximately 1/4 inch thick was cast around the model in the form of a truncated cone, and the model was quickly installed on the strut and the starting sequence initiated. By the time the flow was established, the last of the ice had disappeared. Since flow could be established only with the model axial and near the floor of the test section, the angle of attack which could be attained was limited to that which could be achieved after the model was raised into the test section core, and before the tar began to flow excessively. At this point

the angle was held and the wind tunnel heater was turned off. When the tar had hardened sufficiently, the compressors were shut down. The model was removed, photographed, and wrapped in a circular sector of polar graph paper. Upon heating in an oven, some of the tar was absorbed by the paper leaving a distinguishable pattern superimposed over the coordinate grid.

The flow conditions could not be well defined for these tests. The tunnel supply pressure ranged from 150 to 220 p. s. i. g. and the temperature from 750° - 850°F. The model wall temperature ratio was about 0. 6 before the heater was shut off; however, the surface patterns belong to a higher wall temperature ratio, probably very close to unity.

The surface flow patterns from a test at approximately 11° angle of attack are presented in Figure 3. Two stagnation lines are visible approximately 20° on either side of the leeward cone generator. Although the direction of the surface shear stress between these lines cannot be determined, the pattern is certainly indicative of a reversal of the circumferential component of the velocity near the leeward meridian.

These "stagnation lines" appear to lie on cone generators and persist toward the apex; the resolution of the tar patterns is insufficient to study the origin of these lines. The flow associated with these patterns is apparently conical over at least 90 % of the cone length (4. 25 in.). These stagnation lines were present at somewhat lower angles of attack, and persisted nearly unchanged to the maximum angle of the tests.

The circumferential distribution of the angle of the limiting streamlines is

essentially similar at every radius where the patterns are discernible, again indicating the existence of conical flow. The presence of a conical flow field is a necessary but not sufficient condition to confirm the existence of a thin boundary layer.

The large angle between the limiting streamlines and the cone generators, especially near the sides of the cone, exhibits the expected effect of the circumferential pressure gradient on the low velocity fluid near the surface.

II. 3. 2. Surface Pressure Measurements

Models

The two brass models used for surface pressure measurements are illustrated in the sketch. Model No. 1 had a static pressure orifice

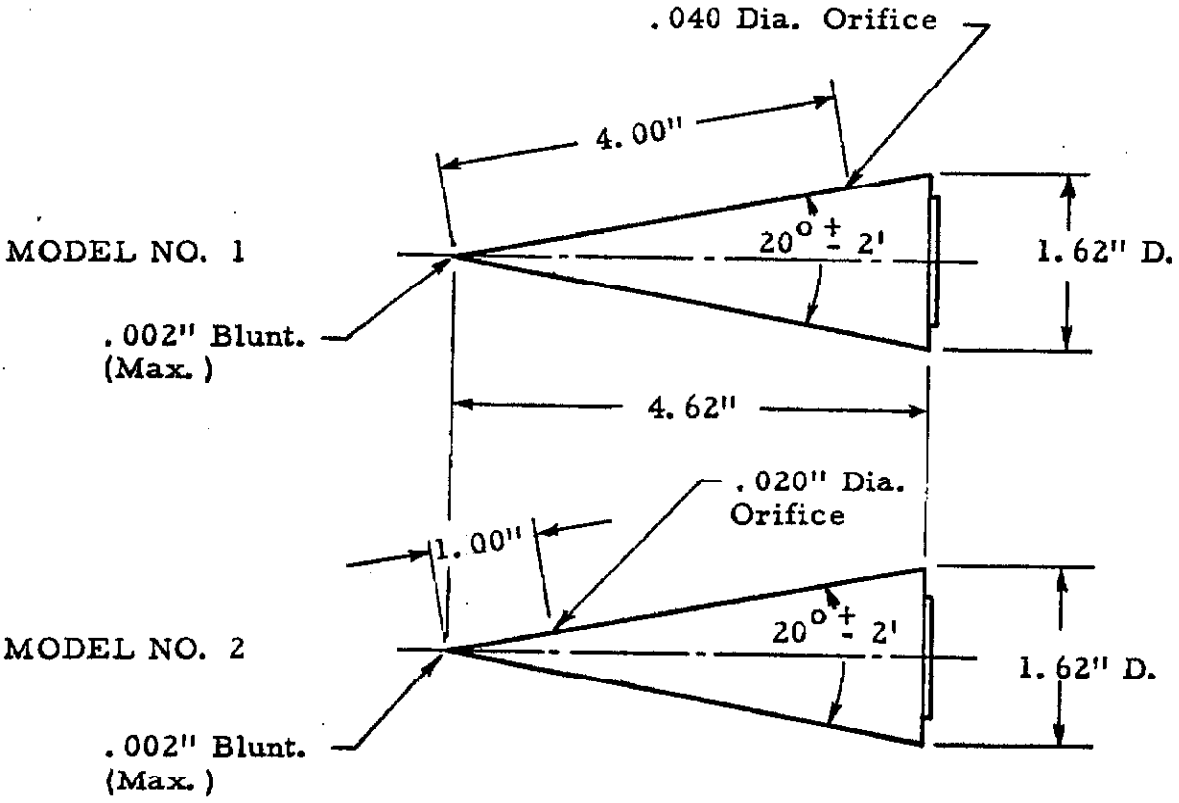

of 0.040 in. diameter located 4.00 in. from the cone apex. A copper-constantan thermocouple was located 180° from the orifice at the cone surface. The model had a conical cavity in which the coolant was circulated. The wall thickness decreased from 3/16 in. near the base to 1/16 in. at the forward end of the cavity, about 0.6 in. aft of the cone apex. Model No. 2 had a static pressure orifice of 0.020 in. diameter located 1.00 in. from the apex and a copper-constantan thermocouple located opposite it at the surface. The coolant cavity in Model No. 2 was similar to that of Model No. 1. Copper pressure tube (0.06 in. O.D. x 0.04 in. I.D.) was connected to the orifice of each model and extended aft through the instrumentation passage in the spindle. Nose bluntness and apex angle were very carefully controlled during fabrication to within the tolerances shown. The equipment and procedures for testing these models were identical.

Equipment

A schematic diagram of the test setup appears in the sketch on the next page. A 1/16 in. inside diameter saran tube was used between the copper pressure tube from the model and the pressure transducer. The transducer was situated as closely as possible to the point where the pressure tubing emerged from the tunnel in order to minimize the pneumatic response time.

The pressure transducer employed a fully active bridge comprised of unbounded strain gages. The device was produced by the Transducer Division, Consolidated Electrodynamics Corporation, as the prototype model for their $\frac{1}{2}$ p.s.i.a. transducer series. It generated

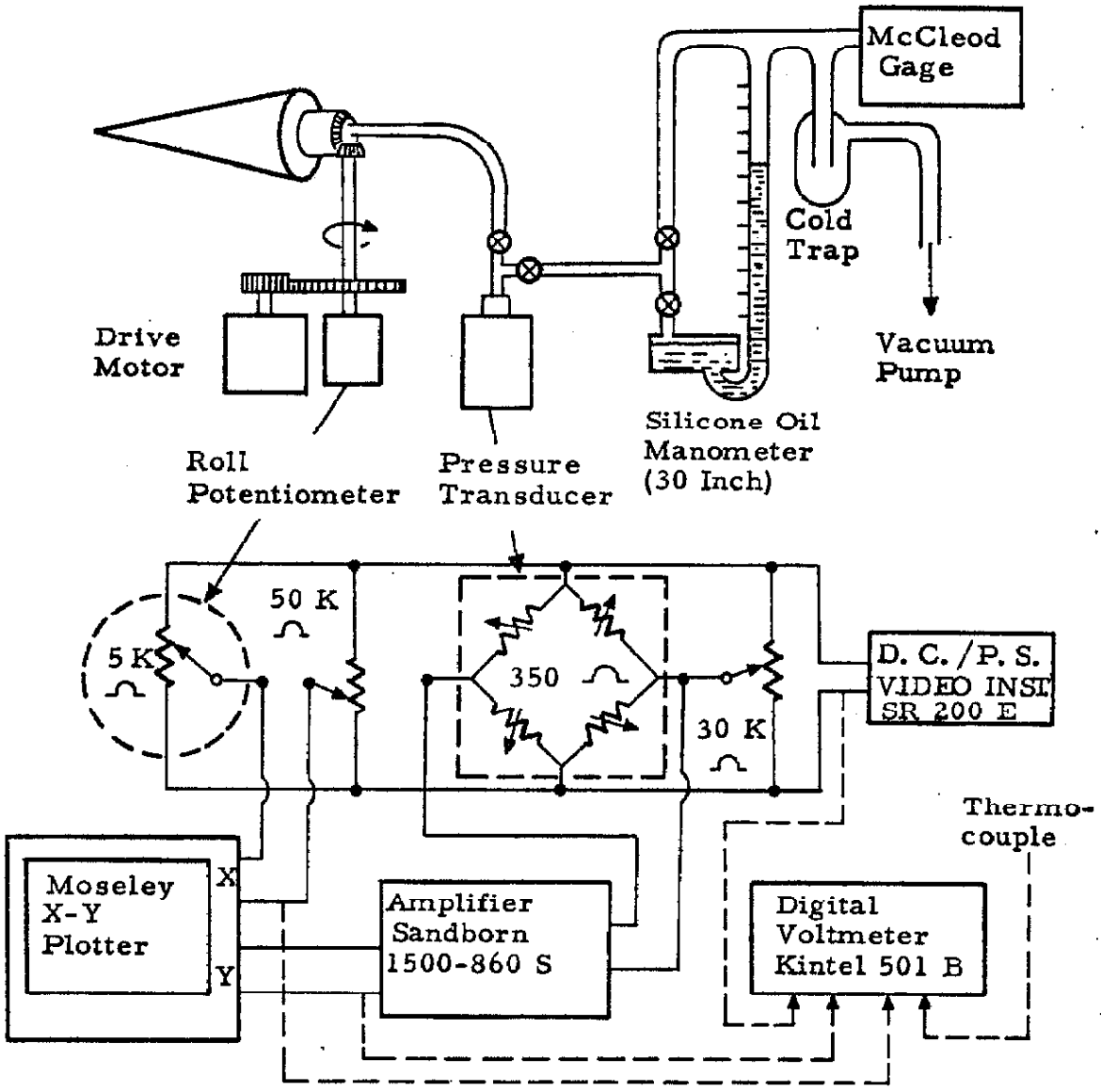

a nominal output of 27 milli-volts at $\frac{1}{2}$ p. s. i. a. with 5 volts D. C. excitation. An overpressure stop limited the pressure range to 0. 7 p. s. i. a. The transducer was encased in a vessel and maintained in a low-pressure environment during all tests as a precautionary measure. The transducer was calibrated several times and found to be very stable.

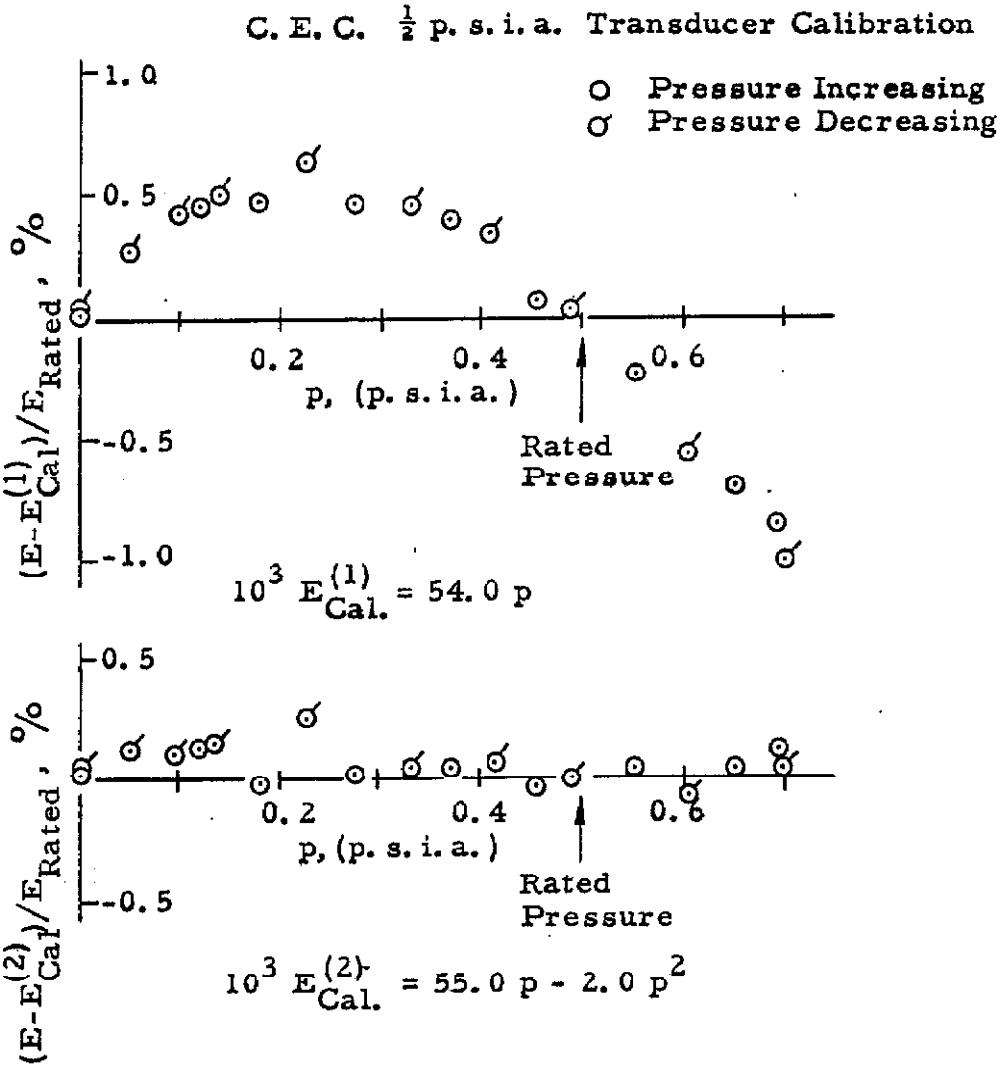

The deviations of the output voltage (E) from a linear function of pressure ($E^{(1)}_{CAL} \times 10^3 = 54.0\ p$) and from a quadratic function ($E^{(2)}_{CAL} \times 10^3 = 55.0\ p - 2.0\ p^2$) are shown. All of the data were reduced using the quadratic calibration voltage ($E^{(2)}_{CAL}$), and the remaining error attributed to the transducer is within ± 0.2 %. The resolution and repeatability of very low pressures was consistently better than 0.01 % of full scale. In all cases, the significance of the data was limited by the accuracy of the data plotter.

The transducer signals were amplified by a Sanborn 1500 - 860 S low-level amplifier. The amplification could be pre-selected at any of several values between 10 and 1000. Long-time stability and linearity were consistently within $\pm$ 0.1 %. The D. C. excitation voltage for the transducer and roll position potentiometer was provided by a Video Instruments, Model SR 200 E,D. C. power supply. Its output remained sensibly constant over an 8 hour period.

The roll position transducer was a three-turn, 5000 ohm, 1/10 % linearity Helipot, attached directly to the drive shaft of the bevel gear set. Two turns of the potentiometer constituted a single revolution of the model. The potentiometer was connected in a bridge circuit with a second potentiometer which permitted a null adjustment.

A Moseley X-Y Plotter recorded the amplified pressure signal as a function of circumferential position. For each axis there were a number of choices of both fixed and variable sensitivity available. The linearity of each axis was found to be generally better than the 0.5 % claimed.

Thermocouple output as well as the excitation voltage, the potentiometer output, and the amplified signal from the pressure transducer were monitored on a Kintel 501 B digital voltmeter sensitive to $\pm$ 0.1 millivolt.

A thirty-inch silicone oil manometer was used to calibrate the transducer. A manometer reference pressure of 5 micron Hg was maintained by a vacuum pump and cold trap and measured by a McCleod gage. This vacuum was also used to evacuate the transducer for the determination of the absolute output level.

The model coolant was tap water supplied at 10 ± 2 p. s. i. g. and $65 \pm 5^{\circ}$ F.

Procedure

Following model installation and electronic equipment warm-up, the X- axis (roll position) scale sensitivity and zero were set using a height gage to ascertain that the pressure orifice was horizontal ($\phi = 0$) before and after one revolution. The model cooling water was turned on and the tunnel started. In all cases, the pressure transducer cavity was kept evacuated between tests. The amplifier null and the amplification ratio were checked and reset, and the transducer output signal level was set to zero (allowing for the finite pressure indicated by the McCleod gage).

When the flow was established, the transducer was isolated from the vacuum system and exposed to the model pressure. The model alignment with the flow was checked by the method described in Section II. 2. 2. Misalignments of as little as 0.01° could be detected easily. Before each trace was made the amplifier input was short-circuited and the Y-axis of the plotter was reset. Following a series of traces the pressure transducer was evacuated in order to check its null signal. At least one spot check of the absolute pressure level was made during each series of traces by recording the manometer reading, the voltmeter display of the amplified transducer output, and the plotter ordinate.

Full 360° traces were made at yaw angles between zero and 24° with the amplifier gain set at 100:1 and 200:1 for supply pressures of 245 and 115 p. s. i. g., respectively, and with a Y- axis sensitivity of 5 volts, full scale. Details of the pressure distribution on the leeward

side of the cone were recorded with the Y- axis sensitivity increased to 1 volt, full scale.

The model was rolled at 0. 7 degree per second during these tests; however, the finite response time of the pressure measuring system introduced no perceptible error, except on the leeward side of the cone at large yaw angles with the 115 p. s. i. a. supply pressure. There, the time lag introduced errors not exceeding 0. 0005 p. s. i. a.

Presentation of Results

The surface pressure distributions which are shown in the supplement (Figures S1 - S4), were traced directly from the original Moseley plots. The pressure scale, which gives the ratio of surface pressure to supply pressure ($p_c/p_{t\infty}$), has been made non-linear in accordance with the transducer calibration. The primary effect of the time response mentioned above is an apparent local shift in the circumferential coordinate. The "shift" is at most about 2°, which is within the absolute accuracy of the ϕ- values of the curves. In the neighborhood of the leeward meridian, the circumferential locations of particular phenomena, such as the pressure minima, can be determined to within about $\frac{1}{2}^\circ$ by utilizing the symmetry about the plane of yaw.

The traces taken at zero yaw are an indication of the uniformity of the flow. The low pressures at $\phi = 0^\circ$, 180° and 360° of Figure S1b could be produced by a flow divergence of 0.14° from the cone axis in the horizontal plane. At the reduced supply pressure (Figure S2b) the apparent divergence in the horizontal plane is reduced to about 0.06° (Axisymmetric non-uniformities cannot be detected in these tests.)

At the forward orifice location (Model No. 2) the non-uniformity, from Figure S3 and Figure S4 appears to be an upward flow inclination of about 0.08° at 245 p. s. i. g. and 0.07° at 115 p. s. i. g.

The flow conditions pertaining to each of the foregoing tests are listed in Table I.

II. 3. 3. Heat Transfer Measurements

It is not the intention of this test to confirm the theoretical value of the heat transfer to an unyawed cone, but rather to ascertain the variation of heat transfer caused by yaw. The quantity to be determined experimentally is the ratio of the local heat transfer coefficient, h, at yaw, to that at the same location of the unyawed cone, h_o. This normalized heat transfer coefficient, (h/h_o), can be found directly without an absolute calibration of the thermometric elements, if the signal that is recorded depends linearly upon only the local heat transfer coefficient. Then the signal at zero yaw defines $(h/h_o) = 1$ and all of the plotted signals are normalized accordingly.

The thermoelectric transducer employed in this test is a thermopile: a pair of thermo-junctions disposed on either side of an electrically insulating layer of low thermal conductivity. For a heat meter of this type a number of effects can cause the electrical signal to depart from a purely local and linear dependence upon the heat transfer coefficient. These effects can be classified as follows: (1) lateral heat conduction; (2) variations in the physical properties of the thermometric elements; (3) thermodynamic potential effects. A detailed discussion of each effect appears in Appendix A.

The pertinent result is that the error caused by lateral conduction is proportional to the square of the thickness of the low conductivity layer. The remaining errors each increase with the temperature difference across the insulating layer which, in turn, is proportional to the thickness of the layer. Consequently, a layer of minimum thickness is desirable.

On the other hand, there is a minimum signal level demanded by the data acquisition system; thus for a given heat flux and thermoelectric constant, the thickness of the layer which can be employed is inversely proportional to its thermal conductivity.

The metallic oxides are commonly employed as low conductivity coatings; however, the achievement of low porosity and good surface finish is difficult. This problem is overcome by applying a dispersion coating of fluorocarbon plastic, and furthermore, the thermal conductivity of these plastics is typically an order of magnitude less than that of the oxides.

Model

The material selected for the low conductivity layer on the heat transfer model was a thermoplastic fluorocarbon noted for good surface finish and low porosity and classified as "F. E. P." teflon. The model itself was fabricated of commercially pure copper. Its external dimensions and coolant cavity were the same as those of the surface pressure models.

The model dimensions and heat meter construction are illustrated in the sketch. Constantan wires were soldered into holes in the copper

model at points 1.0 and 4.0 in. from the apex along a generator. A single 0.002 in. diameter copper wire, to which two 0.001 in. diameter constantan wires had been spotwelded was bonded to the surface of the teflon along the same cone generator. These copper-constantan junctions were placed directly over the two constantan wires in the model. Four constantan leads and a single copper wire that was common to each of the four thermocouples were brought out from the model.

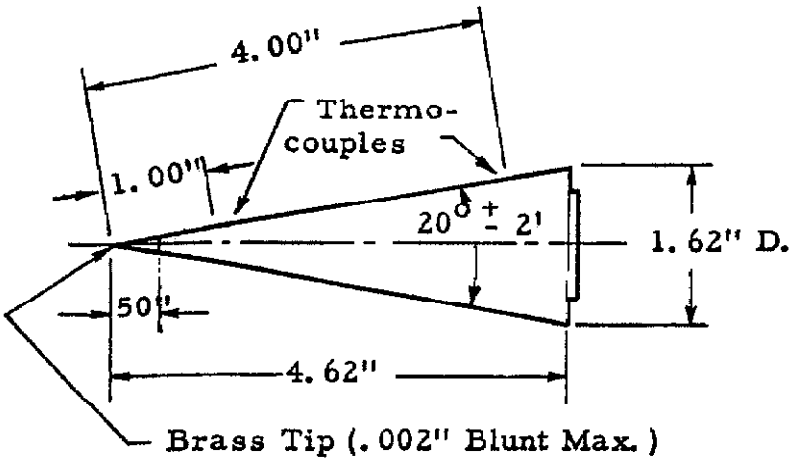

HEAT TRANSFER MODEL

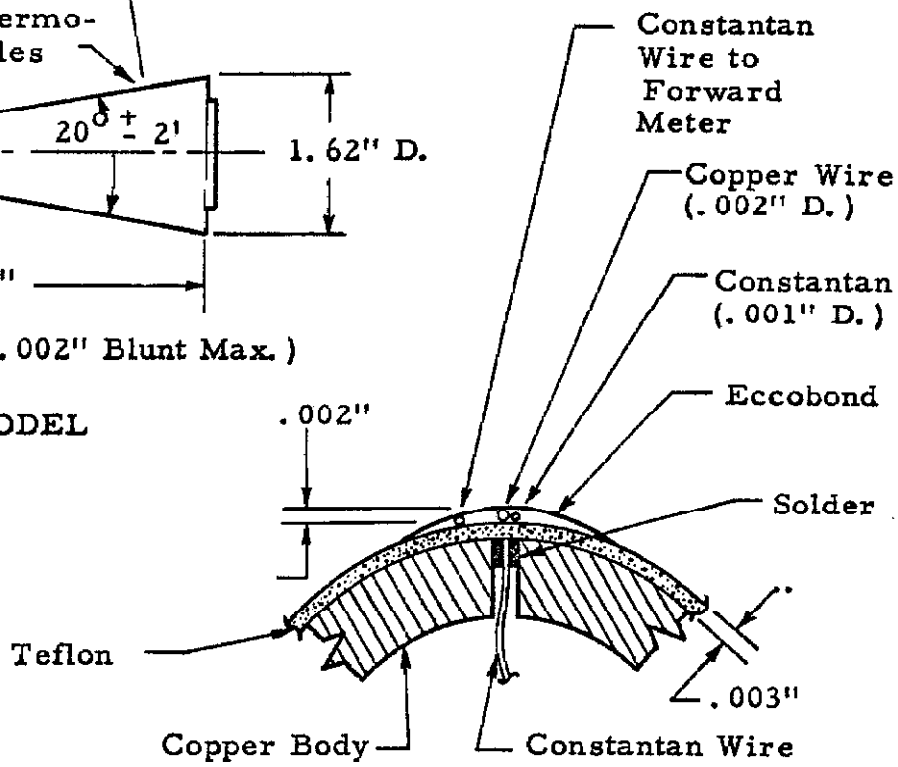

DETAIL OF AFT HEAT METER

The Eccobond "52" epoxy used to secure the wires to the teflon was filed and polished until the copper wire was just exposed and the epoxy faired smoothly. The resulting "mound" on the cone surface was approximately 0.002 in. high.

The teflon coat was specified to be 0.003 in. thick; a calculation of the thickness from the observed temperature difference, the theoretical heat transfer at zero yaw, and the manufacturer's heat conductivity value (4.0×10^{-5} B. T. U./sec. ft. $^{\circ}$R) agreed to within 10 % at both forward and aft measuring stations.

A brass tip 0.5 in. long was used at the cone apex. It was threaded into the copper model after the teflon was applied and enabled a very sharp point to be made and maintained. There was no more than 0.0005 in. of discontinuity between the tip and the remainder of the cone. The coolant cavity did not include the brass tip, so that conduction to the copper cone through the joint provided the only cooling of this portion of the model.

Equipment

The electronic equipment used in this test was the same as that employed for the surface pressure measurements. The thermocouple leads were brought out through the instrumentation shield and connected to a selector switch as shown in the diagram. The switch permitted a selection of either of two modes for each of the two measuring stations: (1) the voltage difference between the external and internal thermocouples; (2) the voltage difference between either of the internal thermocouples and a reference junction. The reference junctions were copper-constantan, and were immersed in an isothermal bath of melting ice. The particular mode being recorded was amplified by the Sanborn amplifier. Its output and that of the roll position potentiometer were recorded on the Moseley X-Y plotter and monitored on the Kintel digital voltmeter.

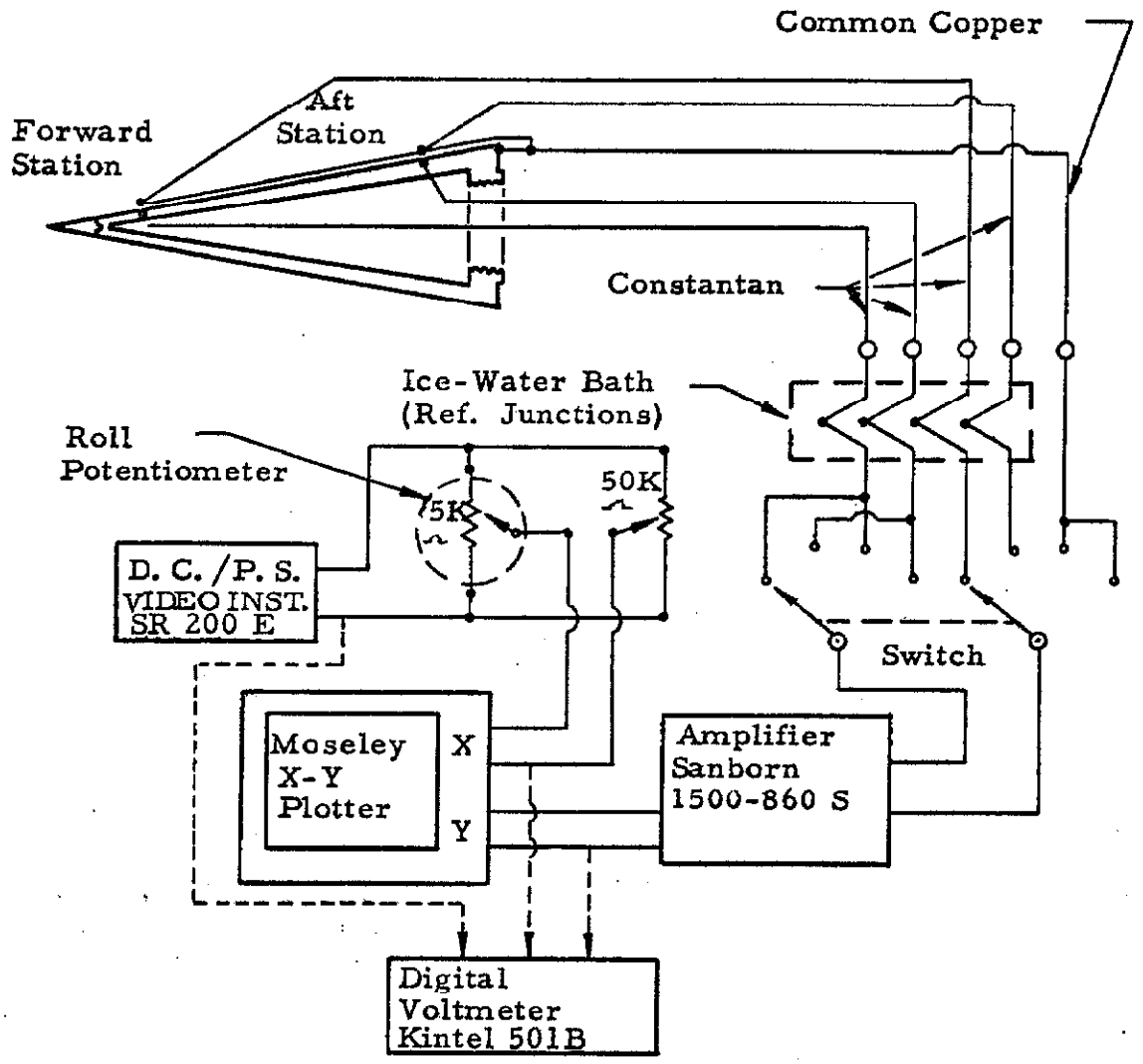

The accuracy of the electronic instrumentation was discussed in Section II. 3. 2. The inaccuracies attributable to the model construction are calculated in Appendix A. Under the worst circumstances, the algebraic total of the errors adds to 0. 8 %. However, this result is unconservative because the 5. 8 % error caused by thermocouple non-linearity and by increased thermodynamic potential is nearly cancelled by the 4. 6 % error based on the assumed variation of the teflon

conductivity with temperature. The latter was included to represent the upper limit of the conductivity variation. Thus, it is more conservative to suppose constant conductivity. Then, the maximum error in the measured heat transfer coefficient is about 6.0 % of that at zero yaw; i.e., the error in the normalized heat transfer coefficient is $\Delta(h/h_o) = \pm 0.06$.

Procedure

The model roll angle was related to the X- axis position on the Moseley just as for the surface pressure tests. The pre-amplifier was set and calibrated at 500:1 amplification for all tests. After the tunnel had reached steady conditions, the Y- axis sensitivity of the Moseley was adjusted so that the signal produced by the temperature difference across the insulating layer at the aft station of the unyawed cone gave 25 % of full Y- scale deflection. Traces were then made by plotting the voltage difference between outer and inner thermocouples at yaw angles from 0° to 24°. The plotter ordinate and its input signal as observed on the digital voltmeter were recorded at one point near full scale to calibrate the Y- axis. The model was rolled at 3.7 degrees per second during these tests. Because of the very short response time of the thermometric system, no measurable difference was observed between the continuous data and steady-state points.

The yaw settings were repeated, and the temperature at the base of the teflon coat was observed. Since this temperature varied little from its value with the cone unyawed, it was recorded only at the windward and leeward meridians at each yaw angle in order to verify the

order of magnitude of the variation, and to provide a record of the nominal wall temperature. A calibrated Y- scale sensitivity was employed when recording these base temperature values.

The procedure was repeated at the forward measuring station. The measurements were made at both forward and aft stations for tunnel supply pressures of 245 and 115 p. s. i. g. at a supply temperature of 900°F.

Two runs were made at successively reduced supply temperatures to obtain a higher wall temperature ratio, $T_w/T_{t\infty}$. These measurements were made at the aft thermocouple station with a supply pressure of 245 p. s. i. g. and at supply temperatures of 700° and 500°F. The maximum yaw angles which could be attained were 20° and 16°, respectively because of the difficulty in maintaining the wind tunnel flow at the low supply temperatures.

Presentation of Results

Photographic reproductions of the original Moseley plots of the thermocouple output difference across the teflon coat at the aft measuring station* are presented in the supplement (Figures S5 - S8). The ordinate of each plot is in units of (h/h_o), the ratio of the heat transfer coefficient to that at zero yaw.

The data indicate the presence of an unsteady phenomena of unknown origin, but small amplitude. The plots of the output difference at the aft station exhibit irregular oscillations characterized by a

---

* The data from the forward measuring station exhibit an approximate 50 % reduction of the effect of yaw on heat transfer, and are considered to include an unidentified, gross error.

period of about 0.5 second and an amplitude of about 0.5 % of the observed steady signal.

The traces at zero yaw at the aft station indicate the existence of the flow divergence in the horizontal plane noted earlier from the surface pressure data. (Slight reductions of heat transfer appear at $\phi = 90^{\circ}$ and 270°, indicating the possibility of some flow divergence in the vertical plane as well.) The flow divergence that would be required to account for these data is about 2.5 times as great as that indicated by the pressure data. This discrepancy is attributed to a difference between the sensitivity of the two variables to non-uniformities of the flow, rather than to a significant change in the wind tunnel flow between tests. Both surface pressure and heat transfer tests were repeated with precisely the same results.

The flow conditions for these tests are indicated in Table II, along with the nominal temperature difference across the teflon coat at zero yaw.

II. 3. 4. Pitot Pressure Measurements

In order to obtain data for the determination of the shock wave shape and for a study of the entire flow field, a series of tests was conducted in which a pitot-probe was suspended from the model. The probe traversed circumferentially around the model axis as the model was rotated. These tests were sufficient to define the flow field quantitatively only in the plane of symmetry; elsewhere, the domains of the field were mapped.

Model

The model was of brass and was identical to the surface pressure models, with the addition of a sleeve normal to the cone surface into which a probe was inserted. A seal and retainer at the outboard end

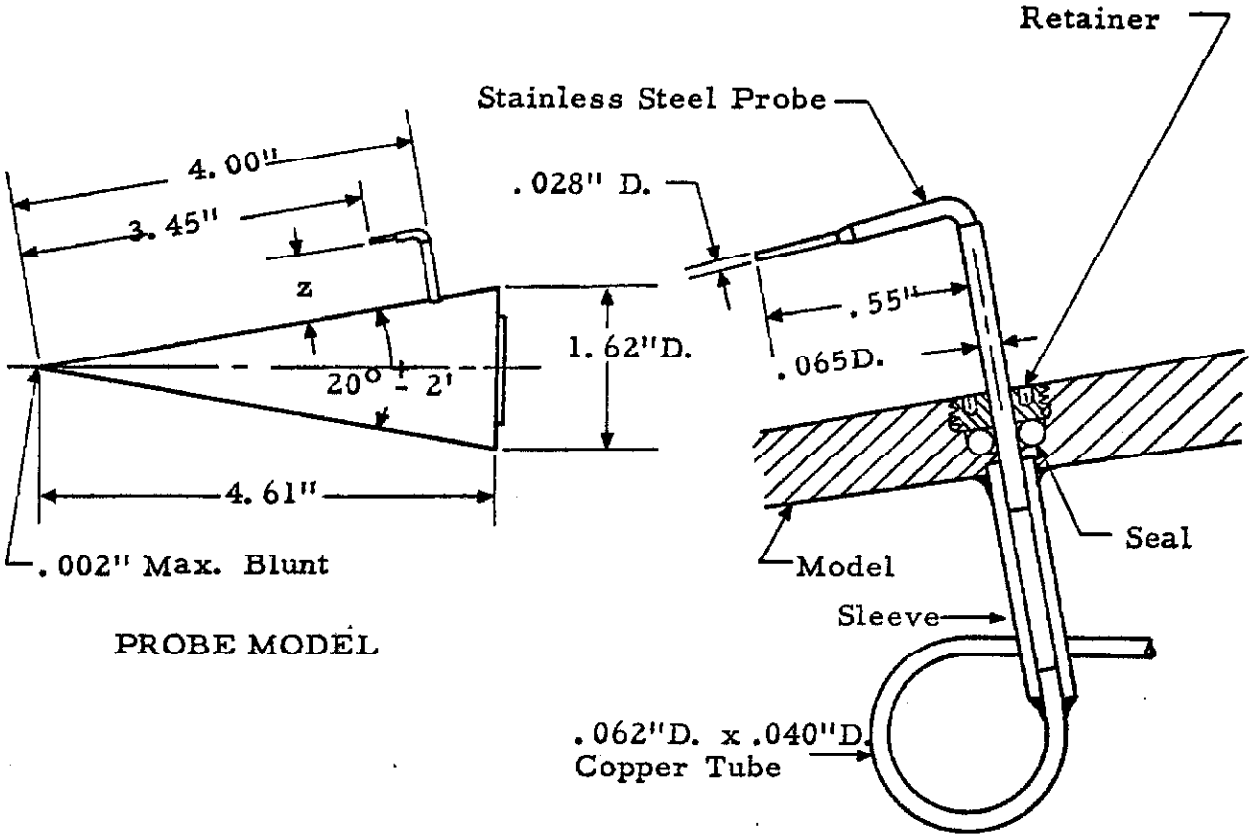

of the sleeve held the probe at a pre-set height and prevented leakage. The lower end of the sleeve communicated with copper pressure tubing which led aft through the spindle. The model and probe detail are sketched.

Four probes were made with stems of different lengths so

that probe settings from the surface to 1.5 in. above the surface were possible. The probe stem was 0.065 in. diameter, and the tip was stepped down to a diameter of 0.028 in. with an orifice of 0.014 in. diameter, as illustrated. The probe forward face was flat and normal to the cone surface.

A copper-constantan thermocouple was provided in the surface of the cone at a distance of 4.0 in. from the apex on the side opposite the probe.

The probe diameter was of the same order as the boundary layer thickness on the unyawed cone and consequently unsuitable for the determination of boundary layer profiles where the boundary layer thickness remained of that order. In addition, there existed the possibility that the shock wave produced by the probe could substantially thicken or even separate the boundary layer ahead of the stem when the probe was just outside the boundary layer. A quantitative estimate of the error from this source cannot be made.

There is a systematic error in the measured pitot-pressure caused by the probe misalignment relative to the local flow. The fraction of true pitot-pressure that is registered by the probe is plotted as a function of the probe misalignment. The data was obtained with the probe in the free-stream at $M = 7.95$ and $Re = 2900$, based on the probe diameter. For a misalignment of 10° or less, the error from this source is negligible.

In general, the misalignment cannot be determined; however, in the meridian plane of symmetry, the shock shape (determined from the probe-shock intersections) provides a means of calculating the probe

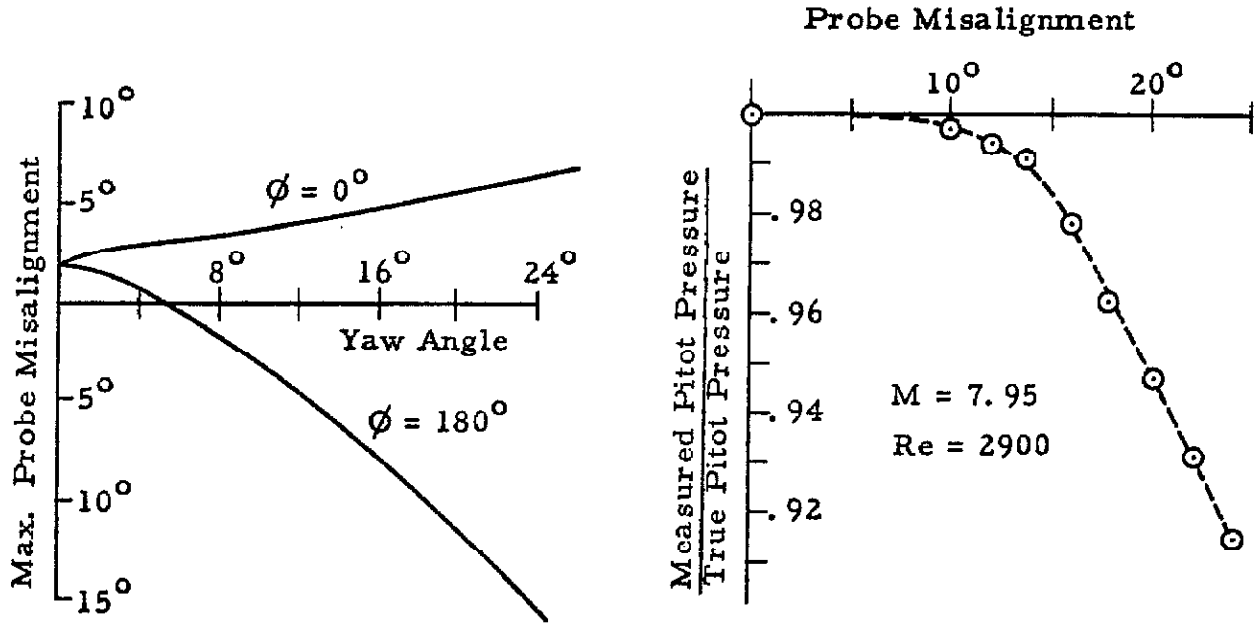

misalignment just behind the shock. The probe misalignment decreases to zero at the cone surface. The maximum probe misalignment is less than 6° in the windward plane of symmetry; consequently the accompanying error is negligible. In the leeward plane of symmetry an appreciable error is incurred because of the probe misalignment beyond about 18° of yaw. The probe error caused by the misalignment near the shock in the leeward plane of symmetry reaches 2.0 % at 24° of yaw.

Elsewhere, the error from this source cannot be determined. However, near the shock in the vicinity of $\phi = 90^{\circ}$ and 270° the probe misalignment may be of the same magnitude as the yaw angle and the error from this source could reach 8 %.

Equipment

The installation of the model in the tunnel and the electronic apparatus used for amplifying and recording the pressure and the roll position signals were identical to those of the surface pressure test. The pressure transducer and the manometer were replaced by units of greater pressure range. The transducer utilized a 350 ohm bridge of unbonded strain gages. Atmospheric pressure was used as a reference so that 10 volts of D. C. excitation could be applied without damaging the strain gages. The results of the transducer calibration are shown in the figure, which shows the deviation of the output voltage from a linear function of the pressure. The deviation of the output does not exceed $\pm$ 0.15 % of the maximum pitot-pressures measured in these tests (approximately 9 p. s. i. a.). An 800 mm. Hg micro-manometer was employed. The least reading was 0.01 mm. Hg; observations of a given pressure were repeatable to $\pm$ 0.1 mm. Hg.

Statham 15 p.s.i.g. Transducer Calibration

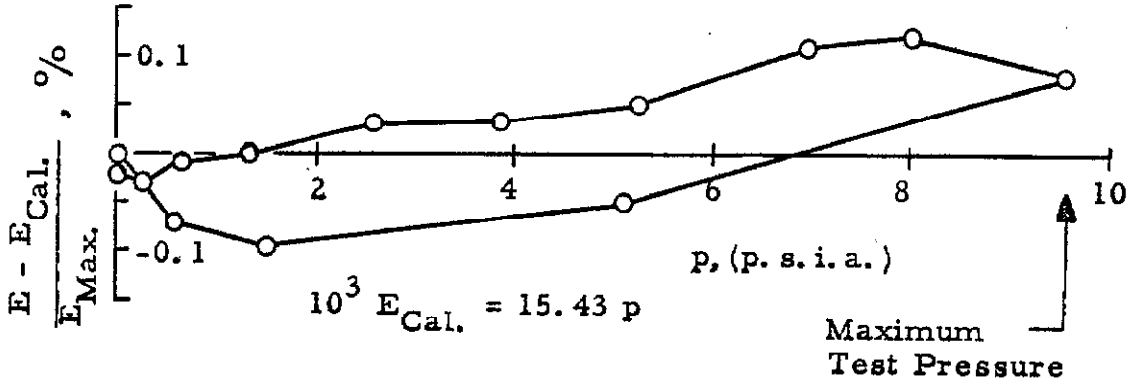

The output level of the transducer varied in proportion to changes of the atmospheric reference pressure. The variation was as much as 0.8 mm. Hg from start to finish of a sequence of runs, during which it was not practical to reset the transducer signal level. The errors total approximately 1.5 mm. Hg, or about 0.3 % of the maximum pitot-pressure at the 245 p.s.i.g. supply pressure. To this must be added the error caused by probe misalignment.

Procedure

The procedure for setting the X- axis of the Moseley in correspondence with the circumferential position of the probe was identical to that employed in the surface pressure and heat transfer tests. The probe height from the surface was set by means of a "telescope gage" to within $\pm$ 0.002 in. Allowance was made for the probe tip diameter so that the heights (z- values) refer to the centerline of the probe orifice. (For heights under 0.15 in. ground drill-blanks were used as "go, no-go" gages between the probe tip and the model surface.) The probe was visually aligned with its meridian plane to within $\pm$ 1°.

After each probe setting, the entire pressure system was checked for leaks. (The probe seal gave difficulty on only one occasion.) Each sequence was preceded by a direct calibration of the pressure scale (Y- axis) of the plotter. Pressures of approximately half and full range were observed on the manometer and recorded along with the plotter ordinate.

The manometer was isolated from the pressure measuring system and a trace was made by rotating the model and probe around its

axis at zero yaw. When the probe tip was outside the unyawed shock, this trace was a plot of the pitot-pressure in the free stream at a particular radius. The model was yawed until the probe just entered the shock wave on the leeward side. Successive traces were made of that portion of the probe path in the disturbed flow field at yaw angles up to 24°. At the completion of this sequence the transducer was evacuated and the residual signal recorded.

It was necessary to shut down the wind tunnel in order to reset the height of the probe. Thus the compatibility of a family of traces belonging to several probe heights at a given yaw angle depends upon the repeatability of the pressure measuring system and of the wind tunnel flow conditions. A number of settings were repeated and, generally the data agreed to well within the stated measuring accuracy.

Presentation of Data

The data is presented in the supplement (Figures S9 - S14). The original Moseley records have been traced directly, but have been regrouped so that each plot contains a complete family of traces for all the probe settings at one yaw angle. Data is presented for yaw angles of 4°, 8°, 12°, 16°, and 24°. All of the data belong to the following flow conditions.

$M_\infty = 7.95$

$p_{t\infty} = 259.3$ p. s. i. a.

$T_{t\infty} = 900^\circ F$

$T_w/T_{t\infty} = 0.41$

$Re_{\infty, x} = 3.6 \times 10^5$

The probe-boundary layer interaction appears as a slight rise in pitot pressure at the edge of the viscous layer, e. g. Figure S9, $z = 0.050$ in., $\phi = 120^\circ$.

III. EVALUATION OF THE DATA

In the following sections, the test data are reduced to forms suitable for evaluation and comparison with the predictions of the most appropriate theories for surface pressure, heat transfer, and other quantities of the flow. In order to facilitate a comprehension of the physical significance of the quantitative results, the discussion is preceeded by a presentation of the geometry of the flow field found from the probe studies.

III. 1. The Flow Field of the Yawed Cone

III. 1. 1. Geometry of the Flow Field

The families of probe traces in Figures S9 - S14 display distinct domains of characteristic behavior. The boundaries of these domains

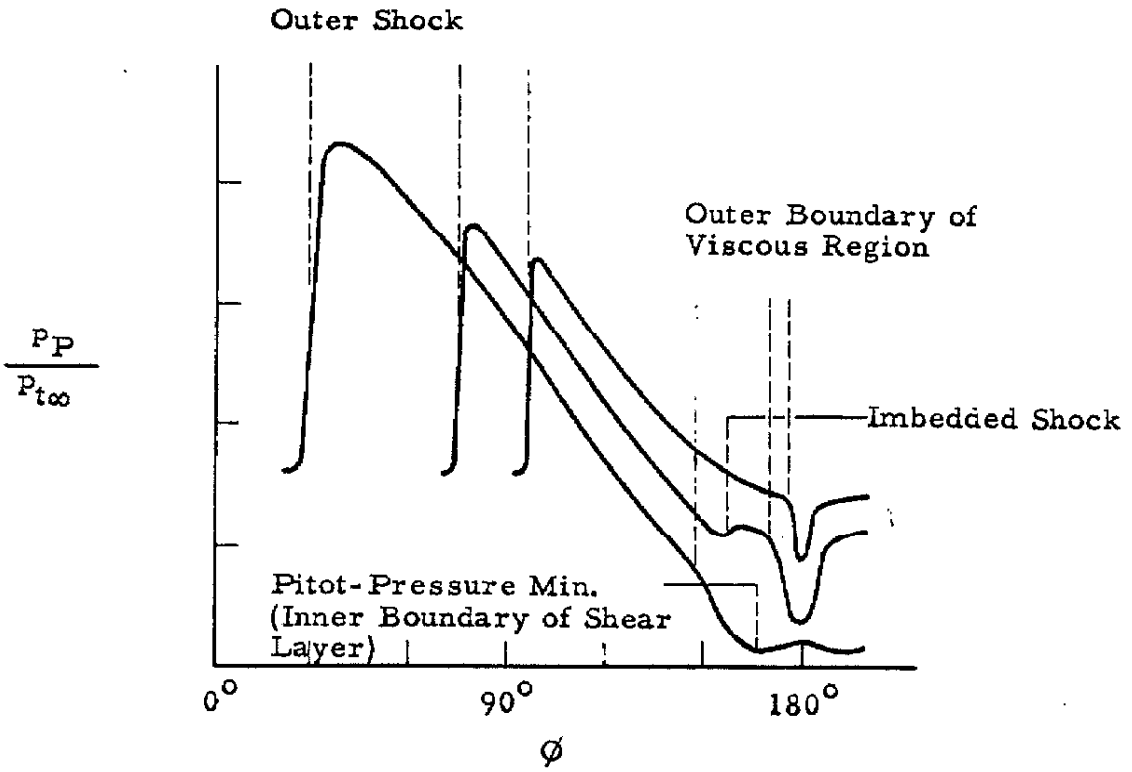

CRITERIA FOR DEFINING DOMAINS OF FIELD FROM PITOT-PRESSURE TRACES

have been determined according to the criteria indicated by the sketch and are plotted in Figures 4a-4f. Each figure represents the intersection of the flow field with the spherical, θ - ϕ surface. On each of Figures 4, the yaw angle is indicated by a filled, circular symbol. The location of this point is the projection of the free stream direction through the apex onto the spherical surface.

III. 1. 1. 1. The Outer Shock

The outer boundary appearing on each of Figures 4 is the shock wave that encloses the flow field of the cone. The shock position in the windward plane of symmetry has been found from a cross-plot (see Figure 6); the character of the probe-shock intersections in the windward quadrants indicates that the variation of the shock layer thickness there is slight. In the leeward quadrants the probe-shock intersections are definitive.

The shock wave was represented analytically by the following expression:

$$(\theta_s - \theta_c)^{-1} = \sum_{n=0}^{N} a_n \cos(n\phi) \qquad \text{(III-1)}$$

The first three coefficients are plotted against yaw angle in Figure 5. The coefficients were determined for N = 2 and N = 5, and in each case the analytic shape matched the data within the experimental accuracy.

III. 1. 1. 2. The Viscous Region

The most significant aspect of the flow field that is evident in Figures 4a-4f is the rapidity of the growth of the viscous layer over the

leeward portion of the cone. The region of extreme growth is confined to a localized "hump" extending about 30° to either side of the leeward meridian. Elsewhere on the leeward half of the cone the growth of the boundary layer with yaw is less rapid. Except near the pronounced "hump", the shape defined by the outer edge of the boundary layer remains nearly circular at all yaw angles. This nearly circular displacement shape is not concentric with the conical body, but is increasingly shifted to leeward with yaw.

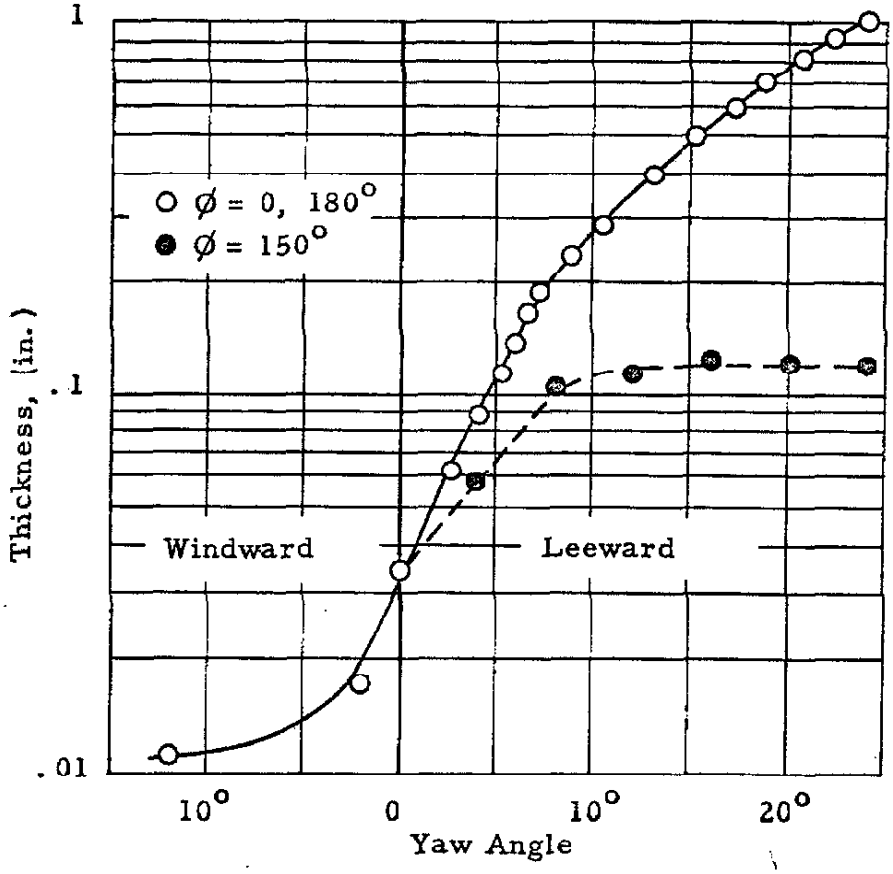

THICKNESS OF VISCOUS LAYER

The initial growth of the viscous layer over the leeward portion of the cone is approximately an exponential function of yaw. This

behavior, both at $\phi = 180^{\circ}$ and at $\phi = 150^{\circ}$, as well as the commensurate reduction of thickness in the windward meridian, is illustrated in the figure on page 38. The normalized boundary layer thickness in the plane of symmetry can be represented as

$$(\delta/\delta_o) = \exp.\left[- (5/2)(\alpha/\theta_c) \right] \quad ; \quad (2^{\circ} > \alpha > - 8^{\circ}) \quad , \quad \text{(III-2)}$$

where positive and negative α refer to the windward and leeward meridians, respectively. The derivative of this ratio with yaw at zero yaw is comparable to the value found by Moore[11] for the displacement thickness of an insulated cone.

It is clear that the presence of the viscous "hump", even at very small yaw angles, alters the inviscid flow over the leeward portion of the cone, and that this interaction is a fundamental aspect of the flow, at least locally. However, the boundary layer over the remainder of the cone remains of moderate thickness and apparently produces no qualitative change in the effective displacement shape of the body.

The behavior of the viscous flow can be seen to undergo a qualitative change beyond 8° of yaw. In fact, there is a concurrence of phenomena at approximately 8° of yaw which are listed below:

(1) The second derivative of the surface pressure, $(d^2 p_c/d\phi^2)$, vanishes at the leeward meridian. (See Section III. 2. 1. 2.)

(2) The growth of the viscous "hump" ceases to be an exponential function of yaw.

(3) The boundary layer thickness on either side of the "hump" ceases to grow significantly with further yaw

(4) The velocity component lying in the θ - ϕ plane (normal to

the radius) becomes sonic in some portions of the flow field. The circumferential velocity component alone is nearly sonic near the shock.

The second derivative of the pressure vanishes at the yaw angle for which the leeward cone generator becomes a rear stagnation line of the inviscid flow, as indicated by the sketches of the external inviscid streamline projections on the cone surface. At larger yaw a pressure

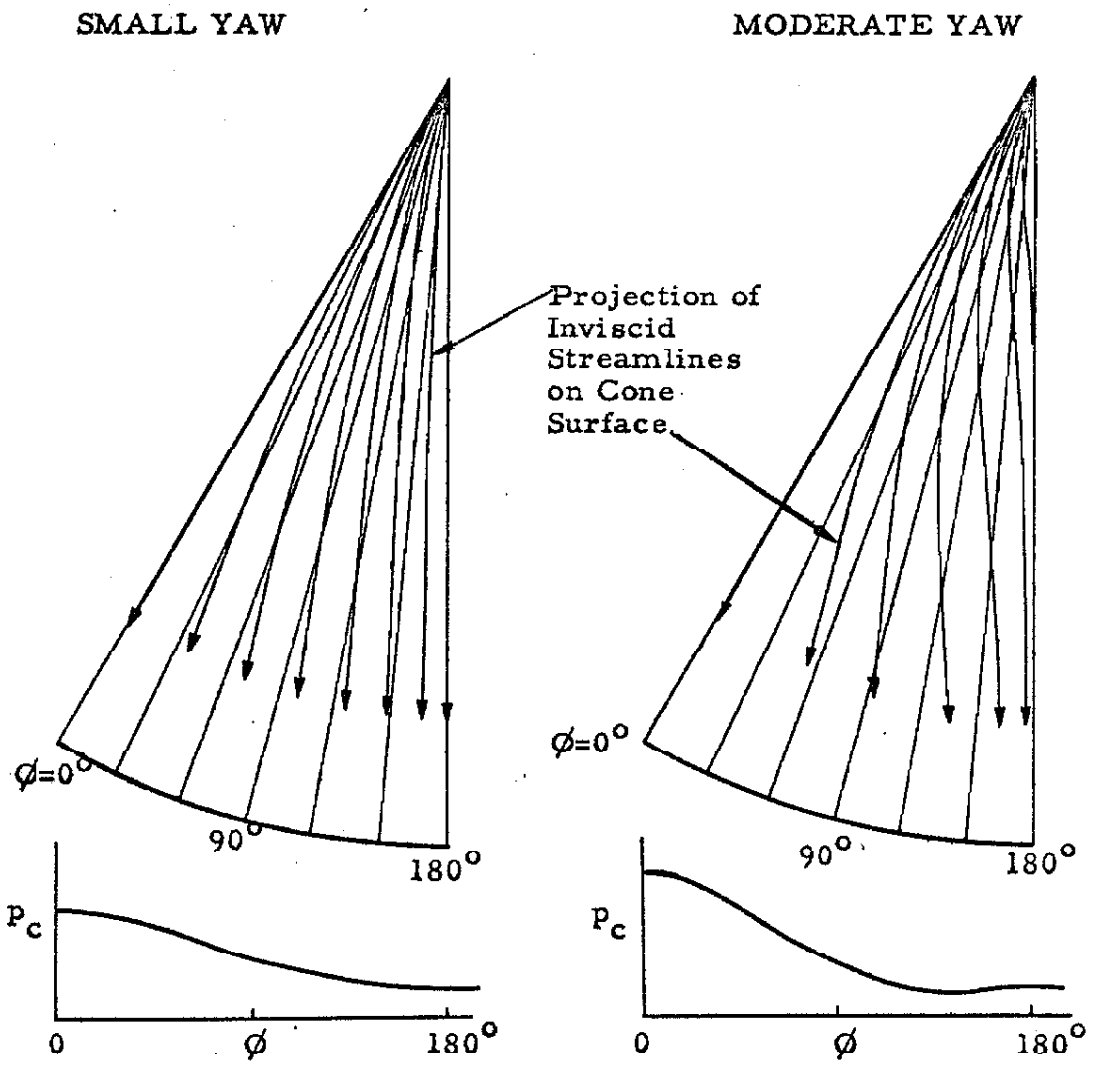

recovery near the leeward meridian is associated with the compressive turning of the inviscid streamlines (see sketch). The adverse pressure gradient has a more pronounced effect on the low velocity fluid in the boundary layer and the circumferential component of velocity near the base of the boundary layer is reversed. This mechanism tends to oppose the convection of fluid into the viscous layer at the leeward meridian and thus affects the further growth of the viscous layer with yaw.

A second effect which accompanies the appearance of a leeward stagnation line (of the inviscid flow) is the divergence of the streamlines from the cone surface in the leeward meridian plane. Thus the requirement that the viscous flow entrain fluid from the external flow imposes a new mode of growth upon the boundary layer.

Beyond 12° of yaw (Figures 4c-4f), the inner edge of the shear layer which bounds the viscous "hump" is demarked. The location of the circumferential minima of each pitot-pressure trace was used to define this boundary, as illustrated by the sketch in Section III. 1. 1. These curves are extended to the minima of the surface pressure at the cone.

The portion of the total flow field that is occupied by the viscous flow in the plane of symmetry is presented in Figure 6. The outer edge of the viscous flow is seen to remain above the cone apex at all yaw angles. The thickness of the viscous region in the leeward meridian becomes a large fraction of the total shock layer even at moderate yaw.

III. 1. 1. 3. Imbedded Shocks

Beyond 16° of yaw shock waves appear imbedded in the inviscid flow field. Their existence is not surprising in view of the supersonic velocity component in the θ - ϕ plane and the compressive flow turning demanded by symmetry at the leeward meridian. In particular, the shocks deflect the flow from the large viscous "hump" in much the same way as the separation shocks in the two dimensional flow over a circular cylinder, e. g., Reference 25. Although there are several important differences between the flow over a cone at large yaw and that around a circular cylinder, one essential similarity lies in the effect of viscosity at the rear stagnation point. The viscous and inviscid flows interact and grossly alter the effective body shape in such a way that recompression occurs far upstream of the leeward generator. The structure of the "inviscid", supersonic flow in the lee of the cylinder is indeterminate; viscosity provides the mechanism whereby the ambiguity of the recompression process is removed.

Despite the fundamental role of viscosity in producing a grossly different effective body shape at the lee side of a cylinder, the geometry of the flow, e. g., the location of flow separation, is nearly independent of Reynolds number. The same conclusion can be reached regarding the role of viscosity in locating the imbedded shocks (and in controlling the effective shape of the viscous "hump") at the lee side of the cone. That is, the imbedded shocks and the viscous hump are essentially conical. The primary support for this statement comes from a series of traces made at a Reynolds number reduced by 50 %. These traces display the same pattern of imbedded shocks, and each is displaced to

windward by only about 1^{o}. Similarly, the shape of the viscous hump was found to be nearly independent of Reynolds number at large yaw.

III. 1. 2. Theoretical Description of the Inviscid Flow Field

The theories that have been developed specifically to describe the flow about a yawed circular cone are based upon the flow about the unyawed cone. These theories also regard the surface of the cone as the appropriate inner boundary condition, i. e., the boundary layer is assumed to remain thin over the entire cone surface.

The Stone theory, which formed the basis for the computations by Kopal[2, 3], is a perturbation analysis of the variables of the flow about their values at zero yaw[1]. The variables are represented by Fourier series in the circumferential angle, ϕ, at each order of the analysis; e. g., to first order in yaw, the variables, including the entropy, vary sinusoidally around the cone. The meridional planes are surfaces of constant entropy, and consequently these planes are stream surfaces.

III. 1. 2. 1. The Vortical Layer

Although this representation is correct for zero yaw, it was shown by Ferri[5] to be fundamentally incorrect for a yawed cone. The cone surface is also a stream surface and must posess constant entropy. The streamlines crossing the shock in the windward meridian reach the cone and envelop it. The streamlines entering the flow field in the other meridians approach the cone surface nearly meridionally, then turn and flow to leeward near the cone surface. Near the surface, the closely spaced stream surfaces each possess different entropy because of the

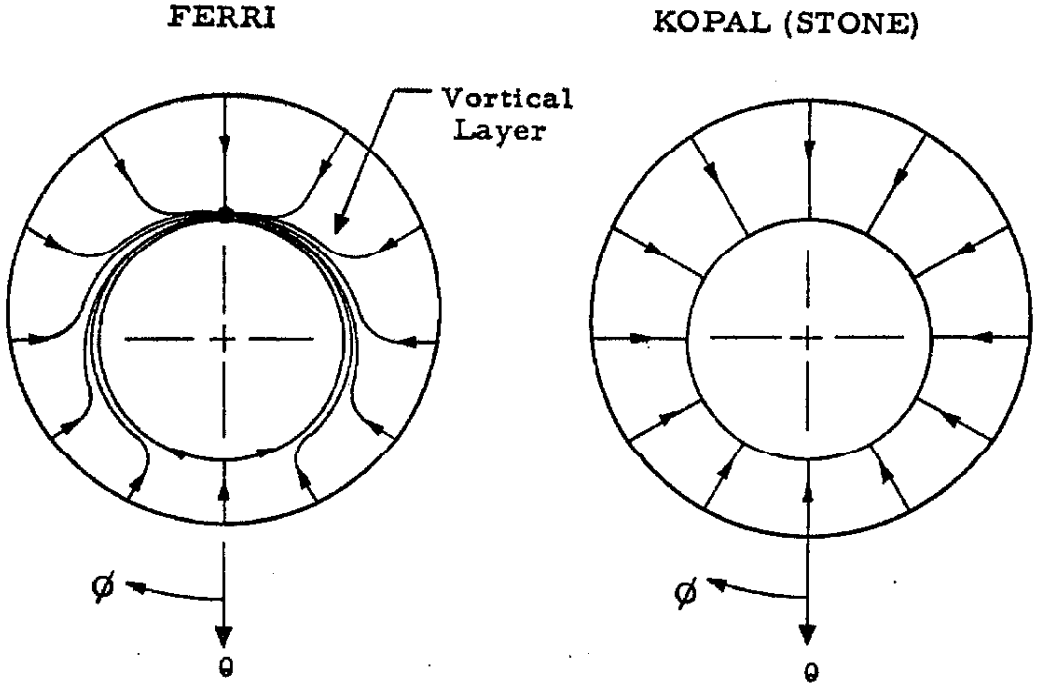

circumferential variation of the strength of the shock wave; consequently there is a thin layer in which the entropy varies rapidly with distance from the cone. This entropy layer is commonly referred to as the vortical layer because of the variation of the radial velocity component through the layer.

The density and radial component of velocity given by Kopal are basically in error near the surface, even to first order in yaw. Ferri proposed to correct the radial component of velocity and the density at the cone surface by applying the Bernoulli equation along the surface streamline. The surface pressure and circumferential component of velocity given by Kopal are used along with the radial component of velocity at the windward generator where the vortical layer vanishes.

The surface correction procedure breaks down when applied to

the second order theory. In that approximation, even the normal and circumferential velocity components, (v and w), as well as the surface pressure may be affected by the presence of the vortical layer.

Cheng[6] employed the shock layer concept and represented the variables of the flow in a double power series in yaw and compressibility, $(\gamma - 1)/(\gamma + 1)$. The resulting explicit expressions for the variables define a flow field which exhibits the same error as the Stone theory near the cone surface. However, Cheng then used his first order results for the circumferential and normal components of velocity near the surface to obtain an explicit expression for the entropy distribution, correct to first order, throughout the flow field (except in the neighborhood of the point $\theta = \theta_c$, $\phi = \pi$, where the inviscid equations become singular and the entropy is multi-valued). Thus the stream surfaces were defined, and the correct expressions for the radial velocity component and density were obtained. These were used with the differential equations to verify that the vortical layer did not alter the original results for v, w, or p (in fact the correction to the pressure appeared only in the third order effect of yaw). The sketch on page 46 shows the streamlines and shock shape given by the first order Cheng theory. The shock shape and the streamline directions at the shock are in satisfactory agreement with the probe data at 4° of yaw. It is noteworthy that at only 4° of yaw, the stream surfaces already deviate considerably from the meridian planes, even near the shock wave. The disparity in shock angle near the leeward meridian is comparable to the thickness of the viscous layer there. The comparison is graphic evidence of the error incurred by the inviscid theories in neglecting

the displacement effect of the viscous layer near the leeward meridian.

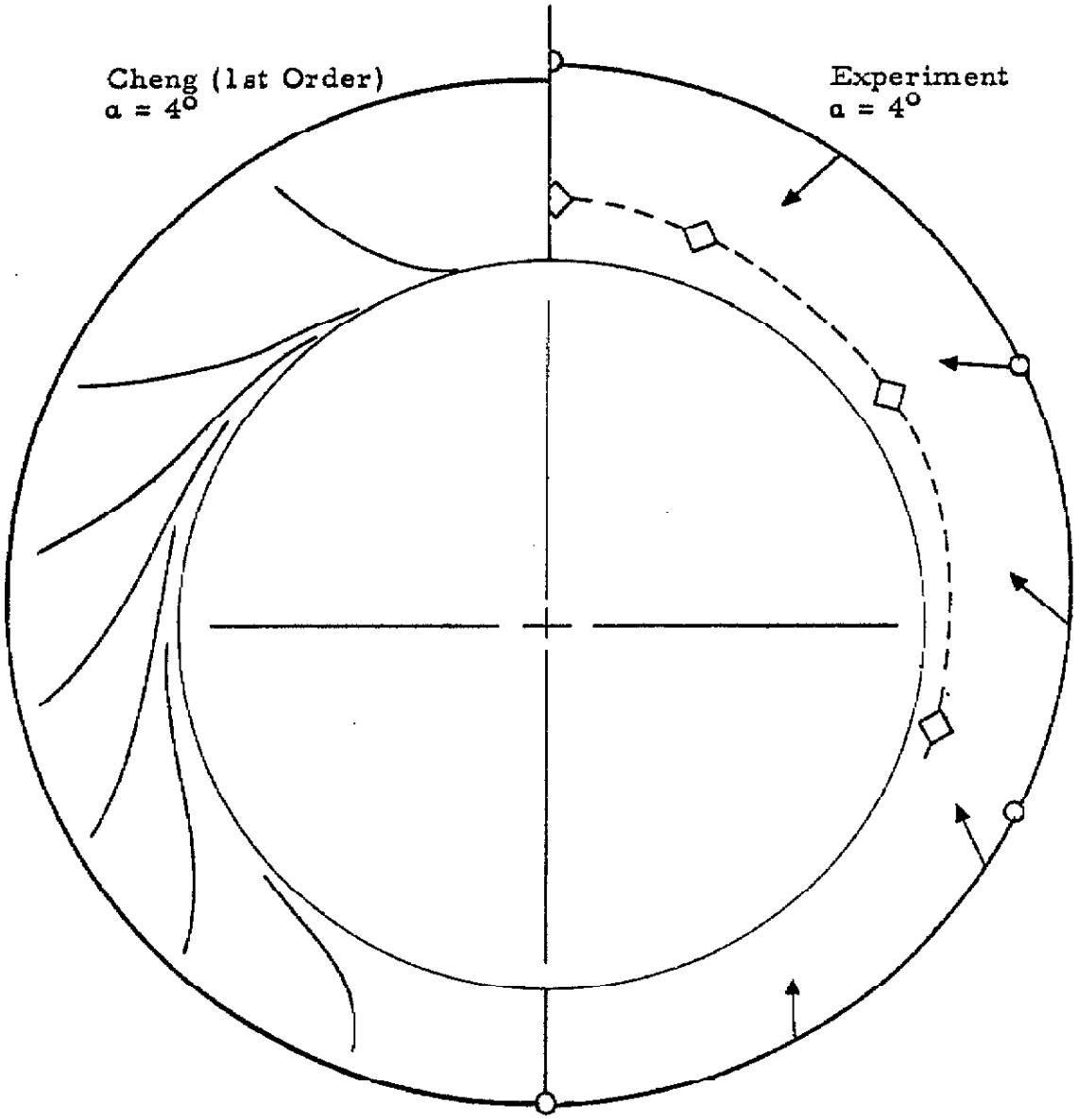

The requirements of the Cheng theory that $\gamma \longrightarrow 1$ and $M_\infty \sin \theta_c >> 1$ were not realized in these tests and, consequently, some of the agreement is fortuitous. Specifically, the shock layer given by Cheng for the unyawed 10° cone at $M_\infty = 7.95$ and $\gamma = 1.4$ is 20 % thicker than the Taylor-Maccoll (exact) value. A similar increase was found in the test because of the displacement effect of the boundary layer.

III. 1. 2. 2. The Vortical Singularity

The flow field given by Cheng for small yaw exhibits all of the qualitative features found by Stocker and Mauger from numerical integrations of the equations of inviscid, conical flow for the case of a circular cone with $\theta_c = 20^\circ$ at $M_\infty = 3.53$. However, when the yaw angle was increased to 15° (comparable to approximately 7.5° of yaw in the present case) they were unable to define a circular body without a "bump" on the leeward side of the cone.

Their integration proceeded inward from the shock along the streamlines; each step of the integration corresponded to an increment in radial distance along the streamline. Points in the flow field which are reached by a streamline only in the limit $r \longrightarrow \infty$, e.g., the singularities at $\theta = \theta_c$, $\phi = 0, \pi$, cannot be reached by a finite number of steps of integration. Consequently, the integration of streamlines near the windward meridian could not progress beyond the windward stagnation line (singularity). The body shape was actually approximated by the streamlines near it in the vortical layer. At sufficiently large yaw, the vortical singularity (which represents the $\theta - \phi$ value of the angular direction into which all the streamlines flow as $r \longrightarrow \infty$) moves off the cone surface into the leeward meridian plane. The low density flow near

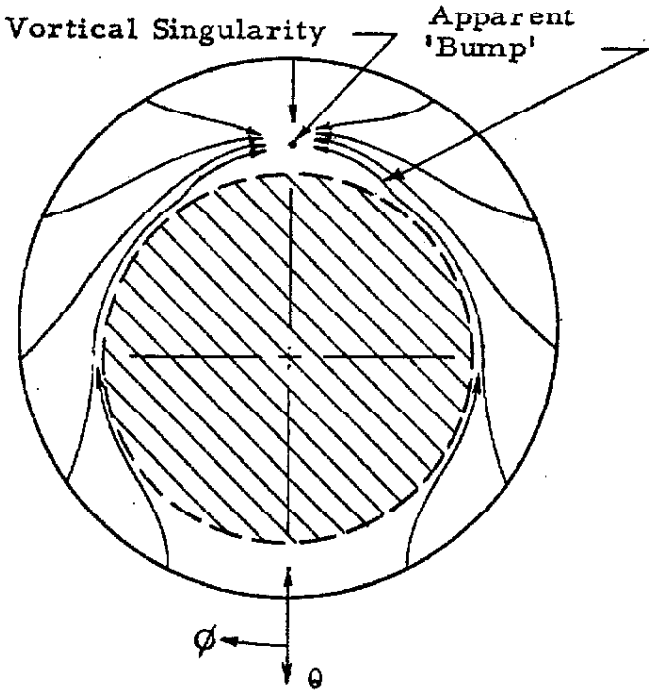

the leeward meridian causes a divergence of the streamlines from one another and from the body so that a streamline near (but not at) the surface traces the shape that was observed as it approached the vortical singularity.

This calculation supports Ferri's hypothesis that the vortical singularity may move off of the body in certain instances. In a real fluid, the region between the "bump" and the body must be occupied by a viscous flow. *

---

* It is interesting to note the two inviscid flows that are possible in this vicinity. The sketch at the left depicts a conventional leeward stagnation line from which the flow streams outboard toward the vortical singularity. The flow depicted in the sketch on the right requires that the adverse pressure gradient which develops near the leeward meridian at moderate yaw should be sufficient to reverse the circumferential velocity component of the low density fluid at the base of the vortical layer. Such a behavior is a case of inviscid separation. The numerical integration scheme of Stocker and Mauger cannot reveal either of these flows explicitly; however, the behavior of the circumferential component of velocity along the last streamline computed should give some indication of the flow beneath.

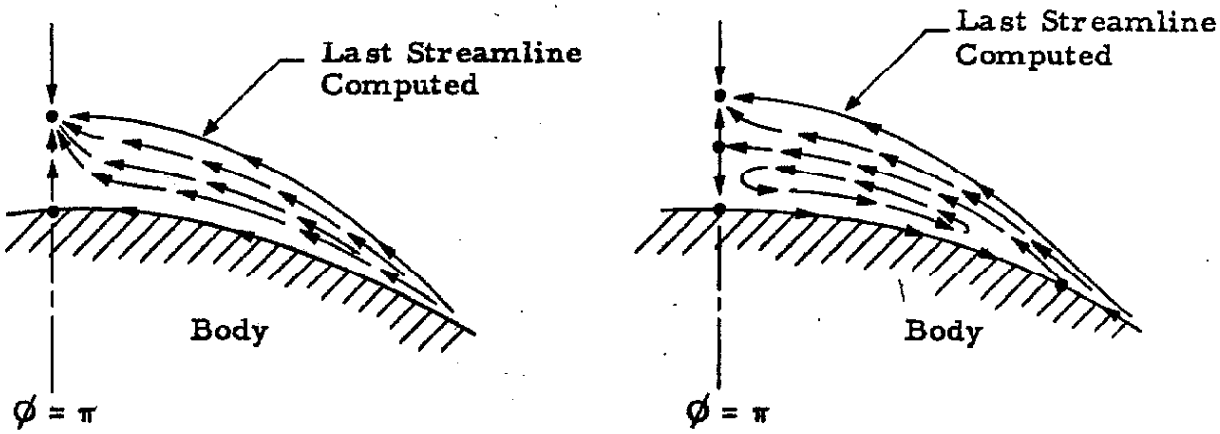

III. 1. 2. 3. Limitations of the Inviscid Theories

All of the inviscid theories have been developed to describe the flow about the yawed circular cone; however, the experimental data have indicated that the displacement shape of the body is non-circular near the leeward meridian, even at very small yaw. Only numerical integration can provide the flow about such a cone.

Even disregarding the departure of the effective shape from circular, the perturbation analyses only give the flow variables as derivatives with respect to yaw, evaluated at zero yaw. The error at finite yaw caused by neglecting higher derivatives has not been ascertained nor is the limit of series convergence known. The error in the Kopal values at the cone surface appears in the derivatives themselves and is distinct from the problem of series convergence.

Cheng's solutions exhibit a defect common to shock layer theory; namely, the exaggeration of centrifugal forces to the extent that sub-vacuum pressures result. No provision has been made to permit the shock layer to separate from the body as demanded by the physics of the flow, if indeed, a near vacuum shock layer can be considered representative of any real flow.

Other methods, such as Newtonian theory and the incompressible cross-flow theory of Allen[8] are valuable aids in estimating surface pressure, but they are not considered to be rational theories for the flow field.

III. 2. Comparison of Theory with Experimental Results

In the following sections the experimental surface pressure and heat transfer data are presented along with the predictions of the forgoing theories. Emphasis will be placed on distinguishing between the effects of viscosity and those attributable to the approximations within the framework of inviscid theory.

III. 2. 1. Surface Pressure

Representative data from the Supplemental Figures S1 - S4 have been reduced to pressure coefficients and are presented in Figures 7, 8, and 9. The data are compared with the Stone-Kopal and Cheng inviscid theories, as well as the prediction of the uncorrected Newtonian approximation. The Allen theory for an incompressible cross flow component of velocity is compared at small yaw.

A practical obstacle to the use of the Stone-Kopal theory in the hypersonic regime is the termination of the second order tabulations at relatively low free-stream Mach numbers, e. g., $M_\infty = 4.07$ for the 10° semi-apex cone being studied. The second order pressure coefficients were determined from the Newtonian approximation and were found to be qualitatively similar to the Kopal values in the range below $M_\infty = 4.07$, where a comparison could be made. Consequently, the Newtonian results were used to guide the extrapolation of the Kopal coefficients to higher Mach numbers. The following values were used for the second order pressure computation at $M_\infty = 7.95$ for $\theta_c = 10^\circ$ (using the notation of References 1, 2, and 3):

$$(p_o/p)_s = -37.1$$

$$(p_2/p)_s = 6.9 \quad .$$

The indeterminacy of the extrapolation is such that the second order pressure effects may misrepresent those of Stone's theory by as much as 15 %.

III. 2. 1. 1. Variation with Yaw in Meridian Planes

Because the inviscid theories of Stone-Kopal and Cheng employ an expansion in powers of the yaw angle, they must fail to describe the flow properly at sufficiently large yaw. The breakdown is examined in Figure 7 where the experimental surface pressures* in coefficient form are compared with the theoretical predictions in three meridian planes: windward ($\phi = 0^{\circ}$), side ($\phi = 90^{\circ}$), and leeward ($\phi = 180^{\circ}$).

At zero yaw, the experimental pressure equals the Taylor-Maccoll value for a 10.5° cone. If parabolic boundary layer growth is assumed, the local angle of the displacement thickness accounts for only about half of the 0.5° discrepancy. The remainder may be caused by an axisymmetric flow convergence in the wind tunnel. (At the forward measuring station (Model No. 2) the surface pressure at zero yaw is consistent with the local boundary layer displacement angle.)

Windward Meridian

The measured pressure on the windward meridian exhibits a rate of increase with yaw angle which is less than that of the theories, and which can be attributed to viscous effects over only a very small yaw range. That is, on the windward meridian the boundary layer rapidly

---

* The data from Model No. 1, tested at $p_{t\infty} = 245$ p. s. i. g., are plotted in order to minimize the departure of the test conditions from "inviscid behavior".

becomes thinner and its meridianal profile becomes fuller, both of which effects promotes a reduction of its displacement effect there; however, that mechanism appeared to be complete by about 3° of yaw.

Beyond about 8° of yaw the theoretical pressures exceed those measured and become increasingly in error with larger yaw. The boundary layer is very thin in the windward meridian; hence the theoretical error must be entirely the result of the limited number of terms in the expansion in powers of yaw. The expansion parameter is actually (α/θ_c), and it is by no means small at 8°. The degree of approximation which the theories are able to provide at much larger yaw is the fortunate consequence of the actual behavior, which is evidently very nearly proportional to $\sin^2(\theta_c + \alpha)$.

The Newtonian approximation on the windward meridian provides a very good estimate of the pressure at all yaw angles.

Side Meridian

The Cheng and Kopal curves for the surface pressure show a qualitative departure from the data in the meridian plane at the side of the cone ($\phi = 90^{\circ}$). Only second and higher, even order terms account for any variation with yaw in this plane, and the theories, carried only to second order, are limited to a simple quadratic reduction of pressure with yaw. This behavior is confirmed by the data at small yaw. However, beyond about 8° - 10° of yaw, the measured pressures rise, in essential opposition to the theoretical trend. Since no noticeable difference in pressure was observed at lower Reynolds numbers and in view of the thin boundary layer that persists, the failure of the theories

beyond 8° of yaw is again indicative of the necessity of higher order terms. It is noteworthy that terms of at least fourth order become appreciable beyond about 8° of yaw.

The Newtonian pressure falls below the data and the inclusion of a centrifugal force correction would worsen the approximation. This fact is evident in the Cheng theory which predicts a vacuum at the side of the cone near 24° yaw.

Leeward Meridian

The Kopal theoretical values in the leeward meridian represent the data well up to a yaw angle of 8°, beyond which the theory indicates rising pressure whereas the observed trend is a continual gradual decrease. In fact, considering the very rapid growth of the viscous "hump" at the leeward side of the cone, which undoubtedly acts to elevate the pressure, the theoretical agreement at 8° of yaw is in part fortuitous. The true "inviscid" behavior may be more nearly represented by the Cheng theory; however the question is entirely academic.

The behavior of the theories at large yaw is certainly incorrect because of an inadequate number of terms, so that they cannot be used to evaluate the error caused by viscous effects. The tests at the forward station gave only slightly higher pressure coefficients at the leeward meridian. However, this near-independence of Reynolds number is consistent with the probe data, which demonstrated that the viscous thickness at large yaw was nearly unchanged at reduced Reynolds number (Figure 6).

III. 2. 1. 2. Circumferential Distribution

Comparison with Higher Order Theories

The circumferential distributions of surface pressure are presented in Figure 8, and are again compared with the Cheng, Kopal and Newtonian theoretical values. At small and moderate yaw (Figure 8a) the distributions are fairly well represented by the Kopal theory. At 8^{o} yaw the second derivative of the experimental pressure, $(d^2p_c/d\phi^2)$, vanishes at the leeward meridian, and although the theories of Cheng and Stone no longer correctly represent the leeward distribution, each predicts very closely the yaw angle at which this derivative vanishes.

At the leeward meridian a pressure recovery is evident and the pressure minimum moves rapidly away from the leeward meridian as the yaw is increased past 8^{o}. The raw data (e. g., Supplemental Figure S1b) indicate that the pressure minimum reaches its most windward position of $\phi = 142^{o}$ at 12^{o} yaw.

The similarity between the pressure minimum predicted by Kopal and that found experimentally at 12^{o} yaw (and beyond) is entirely superficial. The cross-flow velocity component is supersonic in much of the flow field, and a pressure recovery over the leeward portion of the cone can not be anticipated by an inviscid theory. The Kopal and Cheng theories give such a result because they are formally applicable to the cone only at zero yaw. That is, to any order of analysis, the cross-flow velocity component is always regarded as subsonic and the pressure distribution exhibits the characteristic subsonic recovery. This behavior can be qualitatively correct only in cases involving slender cones at relatively low Mach numbers where the cross-flow component

of the velocity is still subsonic at large values of (α/θ_c).

In the present case, the location and magnitude of the pressure recovery are governed by a strong viscous interaction at the leeward side of the cone, which exhibits a mechanism similar to that found at the lee side of a circular cylinder in two-dimensional supersonic flow. The similarity between the detailed pressure distributions over the leeward portion of the cone (Supplemental Figures S1 - S4) and those found for a cylinder (Reference 25) is a dramatic confirmation of this fact.

The pressure recovery predictions of the yaw expansion theories are probably not particularly significant even when applied to a case involving a subsonic cross-flow component. The predicted pressure distribution over the leeward portion of the cone is qualitatively dependent upon the number of terms retained. In the leeward meridian, the theoretical power series expression for the pressure is an alternating series whose terms are of similar magnitude at the yaw angle for which a pressure recovery may be anticipated.

On the basis of the observed boundary layer thickness and, to some extent, by analogy with the two-dimensional flow over a circular cylinder, the experimental pressure distribution is considered to be closely approximated by the "inviscid" pressure distribution over the windward portion of the cone and at least aft to $\phi = 120^\circ$. Farther to leeward, and certainly beyond $\phi = 150^\circ$, the pressure distribution and flow field are dominated by the viscous interaction.

In summary, it is seen that both of the second order theories represent the data satisfactorily on the windward portion of the cone at

a yaw angle somewhat greater than that for which additional terms are required elsewhere. The Kopal theory yields satisfactory pressure distributions over most of the remainder of the cone to about 8° of yaw. At greater yaw angles terms to at least fourth order in yaw are significant. However, an extension to higher order seems somewhat futile in the face of the question of convergence, the inability to represent the supersonic cross-flow component, and the fundamental role of viscosity in the flow over the leeward third of the cone.

Comparison with Theories for Small Yaw

The circumferential pressure distributions at 4° and 8° of yaw are compared with Allen's linearized theory and with the first order results of Kopal in Figure 9. If a displacement allowance is made for a boundary layer, both theories represent the data at 4° yaw reasonably well, but are inadequate at 8°.

At 4° of yaw Allen's theory is qualitatively better, even though it is quantitatively less accurate over most of the cone. The essential difference between the Allen pressure expression and the first order result of Kopal is the addition of a term equal to the pressure distribution on a circular cylinder in an incompressible stream whose velocity is $U_{\infty} \sin \alpha$. This additional term is qualitatively correct at small yaw and suggests that the observed pressures can be synthesized by adding, instead, the experimental pressure distribution on a cylinder at the Mach and Reynolds numbers of the normal component of the free stream. This concept implies viscous separation even at very small angles, and severely mislocates the separation that is observed at large yaw angles.

It is clear that the phenomenon of boundary layer separation on the cone, while in some respects apparently similar to that on a cylinder does not depend simply upon the Mach and Reynolds numbers of the cross flow component, nor are the conditions accompanying its onset to be correctly inferred from the simple resolution of the external flow into parallel and normal components.

III. 2. 2. Heat Transfer

In the subsequent sections some of the results of the heat transfer experiments are presented along with the available theory. The only rigorous discussion of heat transfer to a yawed cone is that of Reshotko[13]. Reshotko and Beckwith[14] analyze the yawed, infinite circular cylinder, a problem that is formally the limiting case of a slender cone at very large yaw. In both of these theories the analysis is restricted to the windward plane of symmetry.

The heat transfer to the windward (or leeward) generator of a yawed cone, normalized by the heat transfer to the unyawed cone is

$$\frac{h}{h_o} = \frac{H_w'}{H_{w_o}'} \sqrt{\frac{P_c u_c}{(P_c u_c)_o}} \quad , \tag{III-3}$$

where H_w' is the wall temperature gradient computed by Reshotko[13]. This variable depends upon three parameters of the inviscid flow evaluated in the plane of symmetry:

(1) The cross flow parameter, k, defined by

$$k = (2/3) \frac{(dw_c/d\phi)}{u_c \sin \theta_c} \quad . \tag{III-4}$$

(2) The surface Mach number, M_c, in the form $(\gamma-1)M_c^2/2$.

(3) The wall temperature ratio, $(T_w/T_{t\infty})$.

In addition the surface pressure and radial component of velocity which appear in equation (III-3) must be found in order to complete the calculation.

The variation of these inviscid flow parameters with yaw angle is plotted in Figure 10. In each case, these results were obtained by taking the value of the parameter and its derivative with yaw, both at zero yaw, from the tabulations of Kopal. The extension to larger yaw was based on the value from Newtonian theory. In the case of the cross-flow parameter, an alternative form for k was used, since the Newtonian circumferential velocity is considerably in error:

$$k = \frac{1}{3}\left\{\pm\sqrt{1-\frac{4(d^2p_c/d\phi^2)}{\gamma p_c M_\xi^2 \sin^2\theta_c}} - 1\right\}_{\phi=0,\pi} . \quad \text{(III-5)}$$

The positive sign is to be taken for $k > -(1/3)$, i. e., on the windward meridian at all yaw angles and on the leeward meridian below a small yaw angle. This expression follows directly from the circumferential momentum equation after it is differentiated with respect to ϕ and evaluated at the cone surface, and in the plane of symmetry.

The inadequacy of the inviscid theories near the leeward side of the cone, even at relatively small yaw, poses a fundamental problem in determining quantities of the external flow there. Thus, even if the solutions to the boundary layer equations were available (and applicable) in the leeward meridian plane, a method for obtaining the inviscid behavior is lacking. However, the most important variable is the

cross-flow parameter, k, and there is one yaw angle at which k can be accurately defined from experimental pressure data. On the leeward meridian when $(d^2p_c/d\phi^2) = 0$, equation (III-5) gives the result, $k = -(2/3)$. This value occurs at a yaw angle of 8° in the present tests.

III. 2. 2. 1. The Windward Meridian

The data taken at the aft heat transfer measuring station ($x = 4.0$ in) are cross plotted against yaw angle in Figure 11. Data at four supply conditions are presented. (The supply temperature was reduced for two of the tests in order to achieve a higher wall temperature ratio.)

The theoretical calculations of (h/h_o) are found to agree with the experimental data up to a yaw angle of 20°. There is no perceptible Reynolds number effect observed between the data at the two tunnel pressures.

The more rapid increase of heat transfer with yaw in the first 2° or 3° is noticeable in the data and is predicted by the theory. Presumably this phenomena is related to the initially very rapid rate of decrease of the boundary layer thickness with yaw.

At yaw angles in excess of 20° an apparently systematic rise in the rate of increase of heat transfer ratio with yaw is observed. In this range, the heat transfer to a yawed circular cylinder has been calculated using the method of Reference 14 with the following exception: The analogy between the yawed cylinder and the slender cone at large yaw is interpreted by Moore and by Reshotko to require that the cone be replaced by a circular cylinder whose axis is parallel to that of the cone. To do so would place the yawed cylinder curves below those of the

cone. The curves of Figure 11 are obtained by replacing the cone by a cylinder whose axis is parallel to the windward cone generator. The limited data in this range supports this procedure.

In fact, there is no explicit conflict with theory in so doing, since the analogy simply shows that neglecting terms of the order of the cone half-angle with respect to those of the order of yaw in the boundary layer equations results in the equations valid for the yawed cylinder. No analysis is made of the effect of the neglected terms, nor are the criteria for the external flow specified any more precisely. The experimental data of Reference 22 also support the yawed cylinder analogy more closely when the cylinder axis is parallel to the windward cone generator.

The data from the tests at constant supply pressure (259.3 p. s. i. a.) and lowered supply temperatures (1160°R and 960°R) are presented in order to indicate the effect of higher wall temperature ratios. The support for the validity of this data, in view of the condensation which may have existed in the flow, is the lack of any qualitative departure of the distributions of heat transfer around the cone from those found at the normal supply temperature. The data from these tests appear to support the theoretically predicted wall temperature effect upon the heat transfer to the windward meridian.

The agreement of the theoretical calculations with experiment is considered to justify the procedures employed for the approximate calculation of the external, inviscid flow, as well as the boundary layer theory developed in Reference 13.

III. 2. 2. 2. The Leeward Meridian

The Boundary Layer Equations

There are no tabulated solutions to the boundary layer equations in the leeward meridian. Moore[12] cites the indeterminacy of these solutions, even at small yaw, as indicative of a breakdown of the validity of restricting the boundary layer equations to the leeward plane of symmetry. He argued that the boundary layer in that plane was influenced by the influx of fluid from the boundary layer at either side of the leeward meridian.

The viscous flow in the neighborhood of the leeward meridian represents the end point of the boundary layer flow over the entire cone. The mass flow (and consequently the thickness) of the boundary layer is essentially dependent upon the history of the boundary layer flow to that point, and this information is not contained in the equations or boundary conditions localized to the leeward meridian plane. On the other hand, the simplification of the boundary layer equations in the leeward meridian plane results from the deletion of terms which, by symmetry, do in fact vanish there. The multiplicity of solutions is not uncommon in boundary layer theory and in this case implies that there is more than one state in which a viscous flow may exist under the prescribed local conditions. Only one of these states represents the end point of the complete boundary layer flow about the cone. Thus, except for an indeterminate thickness, the equations, restricted to the leeward plane of symmetry, give a correct solution to the viscous flow, within the approximations inherent in boundary layer theory.

A question remains concerning the adequacy of boundary layer equations, in general, to represent the viscous flow near the leeward meridian, in view of the large viscous thickness there. Although the probe data show that the boundary layer thickens very rapidly, this growth is not "catastrophic". Even the large "hump" at 8^{o} of yaw corresponds to the thickness of the boundary layer on a similar cone, unyawed, at a Reynolds number of 10^{4}.

It is argued here that for a moderate range of yaw, the boundary layer equations, restricted to the leeward meridian are essentially valid, but that the unique, quantitative determination of the leeward meridional boundary layer requires a knowledge of the viscous flow (and consequently the coupled inviscid flow) that exists over the remainder of the cone.

There is one yaw angle at which the external flow permits a considerable simplification of the meridional boundary layer equations. At $k = -(2/3)$ the equations are satisfied when the radial and circumferential velocity profiles each obey a Blasius-like equation. Linear transformations of the dependent and independent variables are required to achieve the Blasius form; then the velocity and enthalpy gradients are $1/\sqrt{3}$ of their values for the unyawed cone, and the thickness is greater by a factor of $\sqrt{3}$.

It was noted previously that $k = -(2/3)$ when $(d^{2}p_{c}/d\phi^{2}) = 0$ in the leeward meridian. It is interesting to observe that in this case the external flow near the leeward cone generator is locally one-dimensional and thus, the Blasius profile seems to be appropriate.

Experimental Results

Using the result, $H_w'/H_{wo}' = 1/\sqrt{3}$ in equation (III-3), the heat transfer in the leeward meridian at 8° of yaw ($k = -2/3$) has been indicated in Figure 11. The predicted value of $(h/h_o) = 0.34$ is approximately 100 % higher than the value measured.

This disagreement is not surprising in the light of the indeterminacy of the boundary layer thickness and in the associated enthalpy gradient at the wall. There is also the possibility that the Blasius profile is not the appropriate solution at all (numerical integration is required to find any other solutions). In any case it is not possible to attribute the discrepancy to experimental errors: The experimental error in the heat transfer ratio is less than 10 % of the measured local value, and the pressure-velocity product used in the heat transfer calculation can be related to the experimental data within 10 % . There is no theoretical dependence on wall temperature ratio or Mach number, so that the major discrepancy lies in the theoretically predicted gradient of the enthalpy at the wall, $H_w'/H_{wo}' = 1/\sqrt{3}$.

The onset of a rise in the heat transfer coefficient is evident at 10° yaw. This phenomenon is identified with boundary layer separation and appears to be fully developed at 16° of yaw. For yaw angles greater than about 16° and at a Reynolds number of 4.2×10^5, the heat transfer coefficient at the leeward meridian has risen to nearly 50 % of the unyawed cone value. In this range of yaw, the normalized heat transfer coefficient (h/h_o) is approximately proportional to the square root of Reynolds number. Thus, the absolute value of the heat transfer coefficient is independent of the Reynolds number. This Reynolds number

independence is also evident in the data taken at reduced supply temperature. The sketch presents the normalized heat transfer coefficient,

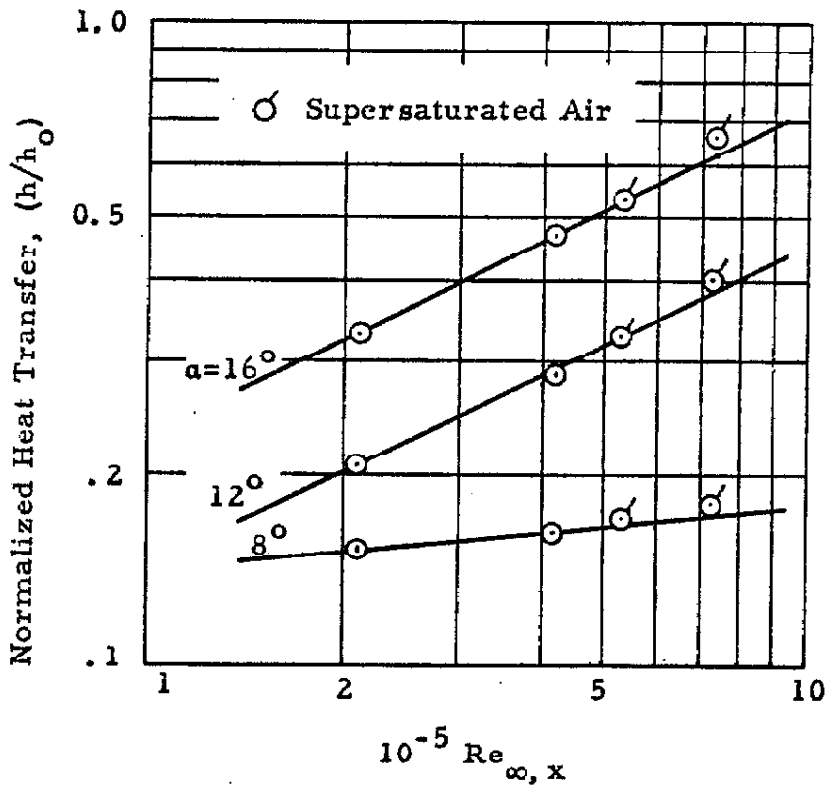

(h/h_o), plotted against Reynolds number for $\alpha = 8^\circ$, 12°, and 16°. This figure clearly displays the qualitative change in the behavior of the viscous flow between 8° yaw and 12°. At 8° yaw the Reynolds number dependency of the heat transfer is nearly the same as that found on the unyawed cone, i.e., $h \sim (Re)^{-\frac{1}{2}}$, whereas at a yaw angle of 12° or more the heat transfer is practically independent of Reynolds number.

The Reynolds number dependency at yaw angles below 8° is consistent with the growth of a conventional boundary layer in the absence of a pressure gradient. That is, the profiles in the leeward meridian are apparently similar with respect to a Blasius normal

coordinate.

The lack of dependence of heat transfer upon Reynolds number beyond 12° yaw could be caused by shear layer profiles that are invariant with radial distance.* A similar independence of Reynolds number was observed in the extent of the separated region at large yaw, i.e., the separated region is essentially conical.

III. 2. 2. 3. Circumferential Distribution

No quantitative theoretical comparison of the circumferential distribution of heat transfer can be made because of the lack of solutions to the full boundary layer equations. Three qualitative features of the distributions shown in Figures S5 through S8 are noteworthy, however.

(1) At a yaw angle of between 3° and 4° a pronounced depression appears in the heat transfer distribution near the leeward meridian. The depression persists up to a yaw angle of 8°. This behavior is apparently related to the boundary layer "hump" on the leeward side, which was found in the probe tests. The bottom of the depression becomes flat beyond 8° of yaw, and in the range $10^{\circ} < \alpha < 16^{\circ}$, the heat transfer at the leeward meridian develops a localized peak which is identified with separation.

(2) On each side of the local heat transfer peak at the leeward meridian (accompanying separation), there are similar depressions in the heat transfer distributions, which fall below the trend of the distributions farther to windward. These may be evidence of the abrupt thickening of the boundary layer produced by the local maximum of

---

* A separated region in a conical, inviscid flow field also contains a constant radial mass flow per unit area normal to the flow, if the shear layer profiles at the outer edge of the viscous flow are invariant with radial distance.

$(d^2p_c/d\phi^2)$ just to windward of the separation line. The heat rate associated with the separation line is apparently very low.

(3) Just away from the windward meridian, the circumferential distributions display a perceptable "kink". Although not quite symmetrical with respect to the plane of symmetry, the "kink" has appeared in all of the data, even after modifications to the surface of the model. The disturbance is consistently more apparent at higher Reynolds numbers and shifts to windward with increased yaw. This phenomenon is attributed to the action of the vortical layer in the following manner: The density variation across the vortical layer does not play a significant role in heat transfer because, with constant pressure, the density-conductivity product is nearly constant across the layer. However, the radial component of velocity contributes directly to the heat transfer.

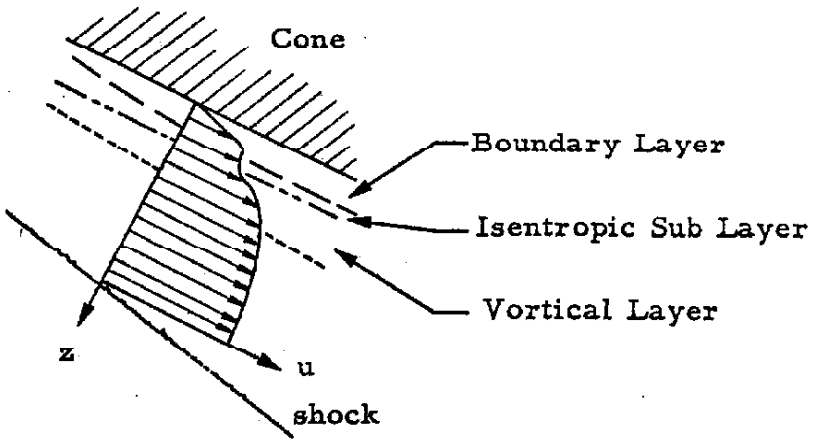

At the base of the vortical layer there must exist an essentially isentropic sub-layer of high entropy but low vorticity. There is a mapping of the entropy variation around the shock onto the entropy variation of the successive lamina of the vortical layer. The circumferential derivative of the entropy just inside the shock vanishes

in the plane of symmetry and so must the entropy gradient at the base of the vortical layer. At some circumferential angle this isentropic sub-layer has been entrained in the boundary layer and subsequently, the radial velocity acting at the edge of the boundary layer rapidly increases.

A more pronounced occurrence of this phenomenon at a more leeward meridian is to be expected at higher Reynolds numbers where the boundary layer is thinner. In data (not presented) at $Re_{\infty,x} = 9.7 \times 10^5$ and $T_{t\infty} = 760^\circ R$ the "kink" was so severe that at $\alpha = 12^\circ$ the heat transfer rate actually increased with ϕ in the range $30^\circ < \phi < 35^\circ$.

III. 2. 3. Analysis of the Probe Data in the Plane of Symmetry

Because the meridian planes of symmetry are stream surfaces and therefore planes of constant entropy in the inviscid flow, the pitot-pressure data, in conjunction with the experimentally determined shock shape, permit quantitative analysis in these planes. The analysis is extended to the viscous region by estimating the static pressure between the inviscid flow and the surface.

III. 2. 3. 1. Static Pressure Profiles

The pitot-pressures in the windward and leeward meridian planes of symmetry were plotted against the normal height, z. The angular elevation of points above the cone surface can be calculated from the normal height according to the relation $(\theta - \theta_c) = \arctan (z/3.45)$. Each profile was extrapolated to the shock wave. The stagnation pressure in the meridian plane was computed from the apparent shock angle, and the static pressures were then calculated from the pitot pressures. The static pressures are plotted in Figures 12a and 12b. The faired curve

passes through the point computed from the pitot pressure extrapolated to the shock. The static pressure given by the apparent shock angle is also plotted. The error in stagnation pressure introduced into the calculations by the use of the apparent shock angle rather than the correct local shock inclination is insignificant in all cases.

In the windward meridian plane the difference between the local shock angle and the apparent shock angle decreases from about 0.3° at zero yaw, to zero at 10° yaw. At larger yaw there is an apparent anomaly: the local shock inclination exceeds the apparent shock angle by up to 0.2° at 24° yaw. This disparity is attributed to a systematic error in estimating the shock position from the probe data. The discrepancy is equivalent to an error in the shock position of 0.012 in. (probe radius = 0.014 in.), and is within the experimental accuracy in the windward meridian where the probe-shock intersections were not well defined.

In the leeward meridian the angle by which the apparent shock inclination exceeds the local shock inclination increases with yaw to a maximum of about 0.6° at 8° of yaw. The discrepancy rapidly subsided with further yaw, and by 24° has fallen to 0.1°, which is within the accuracy of the shock data near the leeward meridian. This behavior is consistent with the following concept of the viscous flow on the leeward meridian: Below about 8° of yaw, there is no evidence of boundary layer separation (Sections III. 2. 1. and III. 2. 2.). The attached boundary layer is very thick and its parabolic displacement growth introduces an appreciable departure from conical flow in the inviscid field. At somewhat larger yaw angles, when boundary layer separation becomes complete, the location of the shear layer is controlled by the inviscid flow, and the adjustments for viscous displacement appear within the

separated region, leaving the outer, inviscid flow essentially conical.

At zero yaw the shock wave is displaced outward by 0.5° from the exact inviscid value. The angle between local shock inclination and the apparent shock angle was found to be 0.3° from the static pressure calculations. Since the displacement effect of the boundary layer on an unyawed cone decays as the inverse square root of the radius (the deviation from conical flow is parabolic), the confirmation of this fact is taken as a measure of the accuracy with which the local shock inclination is inferred from the probe data of the present tests.

III. 2. 3. 2. Mach Number Profiles in the Leeward Meridian

Using the static pressure profiles and the cone surface pressure, the static pressure in the viscous region was estimated (Figure 12b). The pitot-pressure data were used to obtain the Mach number profiles presented in Figure 14 from the pitot pressure profiles of Figure 13.

The pitot pressures are well defined in the inviscid flow, as are the derived static pressures. The Mach number there is considered to be accurate within $\pm$ 2 %. However, the pitot pressures in the viscous region are very low, typically from 2 % to 5 % of full scale. These pressures have been read within an estimated 15 % of the correct value. The estimated static pressures in the viscous region are considered to be within 10 % of the correct values. Consequently, the indeterminacy of the Mach number in the viscous region is approximately: $|\Delta M| < 0.3$. The profile of the shear layer at the outer edge of the viscous region is estimated, since the probe data is sufficient to define only an approximate upper limit to the thickness of this shear layer.

The features of special interest are: (1) the substantially supersonic flow in the separated region; (2) the relatively thin outer shear layer; (3) the apparently inflected Mach number profiles near the wall for yaw angles up to 8°, where no separation is suspected.

These tests cannot be considered as boundary layer surveys because of the absence of total temperature and static pressure data, and because of the large diameter of the probe. A definite probe interaction was observed throughout the pitot-pressure surveys as the probe approached and entered the boundary layer. This effect was magnified when the probe was near the wall, particularly at stations within 0.1 in. of the surface. Thus the inflected Mach number profiles near the surface may be the result of this probe interaction.

The Mach number profiles indicate that a large core of the separated region is essentially free of severe velocity gradients, and may be considered to be an imbedded, nearly inviscid flow. Viscous effects are apparently confined to the relatively thin, outer shear layer and a region near the wall. Although the Mach number in the imbedded flow is only about 1/3 that of the external flow, the radial component of velocity represents a much larger fraction. If the Crocco relation for planar flows (with Prandtl number unity) is invoked in lieu of a knowledge of the total temperature distribution, the radial component of velocity in the separated region is 70 % of the external velocity.

The high radial velocity component and total enthalpy in the "inviscid" core of the separated flow, and the apparently thin boundary layer at its base, easily account for the significant heat transfer which was observed beneath the separated region. A detailed model of the separated flow must be constructed in order to make a quantitative comparison and to account for the observed Reynolds number independence of the heat transfer.

IV. CONCLUSIONS

IV. 1. The Implications of the Tests

IV. 1. 1. Small Yaw

The probe surveys established that the boundary layer on the leeward half of the cone thickens rapidly with yaw and that a pronounced viscous hump appeared in the vicinity of the leeward meridian. The boundary layer, including the "hump", grew exponentially with yaw to 8°, the maximum yaw angle for which the surface pressure decreased monatonically to leeward. In this yaw range the displacement thickness and heat transfer exhibited the conventional inverse square root of Reynolds number dependency. Thus, even though the displacement effect of the viscous "hump" may substantially alter the inviscid flow at practical Reynolds numbers, the effect can be calculated iteratively or, in principle, by expanding the solution in inverse powers of Reynolds number. That is, the solution of the problem in the limit of very large Reynolds number converges to the inviscid solution.

If allowance is made for the local displacement angle of the boundary layer on the unyawed cone, the second order inviscid theory of Stone-Kopal represents the surface pressure on the entire cone at very small yaw, and on all but the leeward portion of the cone up to 8° of yaw. The boundary layer theory for the windward meridian, as well as the local inviscid variables of the flow, were well confirmed experimentally. No boundary layer theory is available for the remainder of the cone so that a test of the effect of the error in the Kopal values of the velocity components at the cone surface could not be made. (This error is associated with the vortical layer, which vanishes at the windward meridian where

agreement was found.)

The second order theory of Cheng was less able to represent surface pressure; however, the test conditions did not approach the criteria demanded by this shock layer theory. Its application to higher Mach numbers and/or blunter cones is expected to produce good agreement in the range of small yaw (pressure decreasing monatonically to leeward). The theory is particularly valuable in providing a representation of the inviscid streamlines throughout the flow field (except at the leeward generator) which is correct to the first order in yaw.

It is reasoned that the entire boundary layer, including the "hump", is well represented by the conically-transformed, three-dimensional equations for a thin, compressible boundary layer, and especially so if the external flow which is used is corrected for the displacement effect of the layer, i. e., if coupling is included. This calculation poses a formidable analytic problem, but it is apparently necessary since the restriction of the equations to the leeward meridian cannot yield a quantitative value for the boundary layer thickness, nor is there any a priori criterion by which the indeterminacy of multiple solutions can be resolved (when such solutions arise).

IV. 1. 2. Larger Yaw

Beyond 8° of yaw in the present tests (and almost certainly in general, whenever a pressure recovery appears at the leeward side of the cone) a change in the rate of growth of the "hump" with yaw signalled the onset of a qualitative change in the viscous flow near the leeward meridian. This transition is accompanied by the appearance of a surface pressure distribution which is nearly identical to that found on the

aft side of a circular cylinder in a two-dimensional, supersonic flow. Concurrently, the heat transfer to the leeward meridian rose markedly and its Reynolds number dependence vanished, as did that of the displacement effect of the viscous "hump". These findings are clearly indicative of boundary layer separation. There are two factors which influence the change in the viscous flow and which always appear together: (1) the pressure recovery at the leeward meridian acts to reverse the circumferential velocity component at the base of the boundary layer and the flow is formally separated; (2) the inviscid flow diverges from the surface of the cone in the leeward meridian plane by an amount that increases with the magnitude of the pressure recovery, and the viscous layer grows as required to entrain fluid from this divergent flow.

The latter effect governs the extent of the viscous growth in a manner that is independent of the structure of the separated flow. As the yaw angle is increased, the pressure recovery becomes greater, and the rate of flow divergence is caused to increase; but the accompanying increase in the thickness of the viscous layer alters the body shape so as to diminish the pressure recovery. Within a few degrees of yaw beyond 8°, the separated flow is virtually "free" of the cone surface and is solely responsive to the demands of the inviscid flow, so that no further change in the pressure recovery is observed as the yaw angle is increased. The region occupied by the separated flow is essentially conical. Although there is at present no theoretical model with which to describe this flow, it is clear that the location and extent of the pressure recovery (and the structure of the local inviscid flow) are essentially dependent upon the strong viscous interaction. The interaction, once

established, is found to be nearly independent of Reynolds number; that is, the flow field which exists in the limit of large Reynolds number does not approach the "inviscid" flow over the circular cone for the range of moderate to large yaw being considered.

It is not clear what role is played in the separation process by the reversal of the circumferential velocity component. It is possible that the circulation of the flow within the separated region controls the rate at which the shear layer at the edge of the viscous region transfers mass to the interior of the viscous flow and thus provides the mechanism which couples the viscous growth to the pressure recovery.

A lack of dependence upon yaw of the thickness of the boundary layer over the remainder of the cone was evident in these tests beyond an angle of 8°. It is plausible to relate this independence to the appearance of substantial regions of the flow field in which the circumferential velocity component is supersonic. The upstream influence of boundary layer development is communicated only through the base of the boundary layer (or by means of a gross thickening or separation of the boundary layer farther upstream, which was absent in these tests). Thus, not only the imbedded shock waves near the viscous hump, but the freedom of the windward portion of the flow field from any influence of the strong leeward viscous interaction, may be dependent upon the attainment of this supersonic transverse velocity component of velocity at or below the yaw angle for which separation occurs.

Tests in which the product, $M_{\infty}\theta_c$ is approximately unity or less, should display a qualitatively different mode of separation and an absence of imbedded shock waves, except at very large yaw. Indeed,

vapor screen photographs of slender cones at low Mach numbers confirm both of these suppositions; however, there are insufficient data to ascertain the windward extent of the viscous interaction.

The surface pressure distributions given by the perturbation theories were generally unsatisfactory beyond about 8° of yaw. The agreement on the windward meridian was fair at all of the yaw angles of the test; however, the confidence to be placed in such predictions is low. That is, even in the absence of any effect of viscosity, the second order perturbation is qualitatively inadequate beyond about 8° of yaw and the agreement at larger angles is not significant.

The flow over the windward two-thirds of the cone is apparently neither influenced significantly by local boundary layer displacement effects nor by the gross interaction at the leeward side of the cone. The failure of the inviscid theories at large yaw is attributable in part to an insufficient number of terms (i. e., not carried to high enough order in yaw). A more basic problem is the inability of the theories to (properly) represent phenomena which are essentially associated with large yaw and for which the appropriate derivative is not to be found at zero yaw. Thus, it is not clear that even an extension to fourth order in yaw (the minimum required to alter the theoretical prediction at $\phi = 90^{\circ}$) would promote any substantial improvement except possibly in the windward meridian.

The Newtonian flow theory gave an excellent approximation to the surface pressure over most of the cone at all of the yaw angles of the test.

IV. 2. Further Investigations

Many of the difficulties of these tests are absent when data is gathered solely in the plane of symmetry. It is clearly essential for the construction of a theory of the separated flow to obtain detailed surveys of pitot pressure, static pressure and total temperature in the leeward meridian plane. This data would also provide a basis for evaluation of boundary layer solutions in the leeward plane of symmetry.

A substantial repetition of the present tests at a lower Mach number (or with a much more slender cone) would resolve the question of the structure of the separated region in the presence of a subsonic cross flow velocity component.

Tests at a higher Mach number (or with a much less slender cone) would be of interest in providing a valid basis for comparison with Cheng's theory.

Finally, the theoretical problem of determining the correct inviscid flow field, including an approximation to the displacement thickness, appears to demand additional numerical integration. The formulation of Stocker and Mauger appears to be ideally suited to this problem, and the computations should be facilitated by the use of the experimentally determined shock shape. The integration of the full boundary layer equations would be needed to complete the solution; however, an examination of the solutions to the boundary layer equations, restricted to the leeward plane of symmetry, should be of some value.

REFERENCES

1. Kopal, Z.: Tables of Supersonic Flow Around Cones. Massachusetts Institute of Technology, Department of Electrical Engineering, Report TR-1, 1947.

2. Kopal, Z.: Tables of Supersonic Flow Around Yawing Cones. Massachusetts Institute of Technology, Department of Electrical Engineering, Report TR-3, 1947.

3. Kopal, Z.: Tables of Supersonic Flow Around Cones of Large Yaw. Massachusetts Institute of Technology, Department of Electrical Engineering, Report TR-5, 1949.

4. Ferri, A.: The Linearized Characteristics Method and Its Application to Practical Non-Linear Supersonic Problems. NACA TN 2515, 1951.

5. Ferri, A.: Supersonic Flow Around Circular Cones at Angles of Attack. NACA TN 2236, 1950.

6. Cheng, H. K.: Hypersonic Flows Past a Yawed Circular Cone and Other Pointed Bodies. Journal of Fluid Mechanics, Vol. 12, Part 2, pp. 169-191, February, 1962.

7. Stocker, P. M. and F. E. Mauger: Supersonic Flow Past Cones of General Cross-Section. Journal of Fluid Mechanics, Vol. 13, Part 13, pp. 383-399, July, 1962.

8. Allen, H. J.: Pressure Distribution and Some Effects of Viscosity on Slender Inclined Bodies of Revolution. NACA TN 2044, 1950.

9. Young, G. B. W. and C. P. Siska: Supersonic Flow Around Cones at Large Yaw. Journal of the Aeronautical Sciences, Vol. 19, No. 2, pp. 111-119, February, 1952.

10. Moore, F. K.: Three-Dimensional Compressible Laminar Boundary Layer Flow. NACA TN 2279, 1951.

11. Moore, F. K.: Laminar Boundary Layer on a Circular Cone in Supersonic Flow at Small Angle of Attack. NACA TN 2521, 1951.

12. Moore, F. K.: Laminar Boundary Layer on a Cone in Supersonic Flow at Large Angle of Attack. NACA TN 2844, 1952.

13. Reshotko, E.: Laminar Boundary Layer with Heat Transfer on a Cone at Angle of Attack in a Supersonic Stream. NACA TN 4152, 1957.

14. Reshotko, E. and I. E. Beckwith: Compressible Laminar Boundary Layer over a Yawed Infinite Cylinder with Heat Transfer and Arbitrary Prandtl Number. NACA TN 3986, 1957.

15. Cooper, M. and R. A. Webster: The Use of an Uncalibrated Cone for Determination of Flow Angles and Mach Numbers at Supersonic Speeds. NASA TN 2190, 1951.

16. Jack, J. R.: Aerodynamic Characteristics of a Slender Cone-Cylinder Body of Revolution at a Mach Number of 3.85. NACA RM E51H17, 1951.

17. Hold, M. and J. Blackie: Experiments on Circular Cones at Yaw in Supersonic Flow. Journal of the Aerospace Sciences, Vol. 23, No. 10, pp. 931-936, October, 1956.

18. Reller, J. O. and F. M. Hamaker: Temperature Recovery Factors on a Slender 12° Cone-Cylinder at Mach Numbers from 3.0 to 6.3 and Angles of Attack up to 45°. NACA RM A55G20, 1955.

19. Smetana, F. O.: A Preliminary Investigation of the Effects of Variations in Reynolds Number and Surface Temperature on Four Surface Pressures on a Slightly Blunted $7\frac{1}{2}^{\circ}$ Half-Angle Cone at Mach Numbers 5 and 8 for Angles of Attack up to 24°. ASD-TDR-62-360, 1962.

20. Sands, N. and J. R. Jack: Preliminary Heat-Transfer Studies on Two Bodies of Revolution at Angle of Attack and a Mach Number of 3.12. NACA TN 4378, 1958.

21. Burbank, P. B. and L. Hodge: Distribution of Heat Transfer on a 10° Cone at Angles of Attack from 0° to 15° for Mach Numbers of 2.49 to 4.65 and a Solution to the Heat Transfer Equation that Permits Complete Machine Calculations. NACA RM-6-4-59L, 1959.

22. Julius, J.: Measurement of Pressure and Local Heat Transfer on a 20° Cone at Angles of Attack up to 20° at a Mach Number of 4.95. NASA TN D-179, 1959.

23. Conti, R. J.: Laminar Heat Transfer and Pressure Measurements at a Mach Number of 6 on Sharp and Blunt 15° Half-Angle Cones at Angles of Attack up to 90°. NASA TN D-962, 1961.

24. Pasiuk, L.: Supersonic Aerodynamic Heat Transfer and Pressure Distribution on a Sphere-Cone Model at High Angles of Yaw. NOL-TR-62-35, 1962.

25. Dewey, C. F., Jr.: Measurements in Highly Dissipative Regions of Hypersonic Flow. California Institute of Technology, Pasadena, California, Ph. D. Thesis, June, 1963.

26. Baloga, P. E. and H. T. Nagamatsu: Instrumentation of GALCIT Hypersonic Wind Tunnels. GALCIT Hypersonic Research Project, Memorandum No. 29, July 31, 1955.

APPENDIX A

THE ERRORS IN THE MEASURED RATIO OF HEAT TRANSFER COEFFICIENTS

1. Lateral Conduction Effects

If a local Cartesian coordinate system is erected with its origin at the base of a thin insulating layer of constant thickness covering a

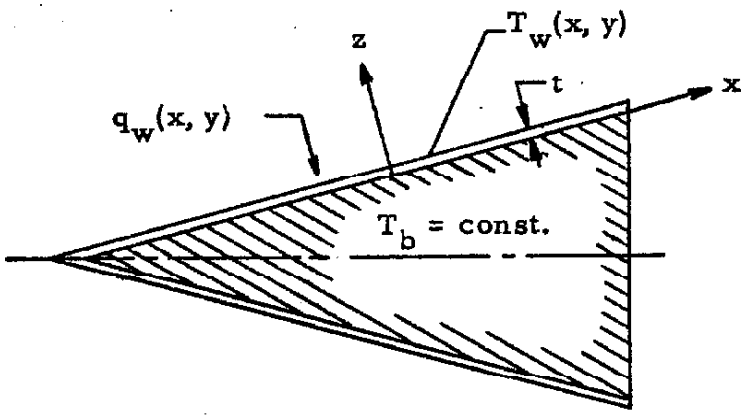

highly conducting body, such that the z- axis is the outward normal; and if it is assumed that the lateral distribution of temperature is similar throughout the layer ($0 \leq z \leq t$), then the temperature can be represented as

$$T = T_w(x, y)\, f(z) + T_b \quad , \qquad \text{(A-1)}$$

where the temperature of the body at the base of the insulating layer, T_b, is considered constant. The steady heat conduction equation in a medium of constant conductivity,

$$\nabla^2 T = 0 \quad , \tag{A-2}$$

becomes simply

$$f'' + (1/L^2) f = 0 \quad , \tag{A-3}$$

where $(1/L^2)$ stands for $(\nabla^2 T_w)/T_w$ which is independent of z. The condition at z = 0 that f(0) = 0 restricts the solution to

$$f = A \sin (z/L) \quad . \tag{A-4}$$

The constant A is determined from the heat flux at the wall,

$$q_w = k(\partial T/\partial z)_w = k T_w f'(t) = \left[(k T_w A)/L\right] \cos (t/L) \quad .$$

Therefore,

$$A = (q_w L)/(kT_w \cos \frac{t}{L}) \quad ,$$

and the temperature distribution is

$$T(x, y; z) = \frac{q_w (x, y)}{k} \quad \frac{L}{\cos (t/L)} \quad \sin (z/L) + T_b \quad . \tag{A-5}$$

The measured temperature difference between the body and the surface, $T_w - T_b$, is used to determine the heat transfer rate by assuming a linear temperature profile, thus

$$\bar{q}_w = (k/t) (T_w - T_b) = q_w (L/t) \tan (t/L) \quad , \tag{A-6}$$

and the fractional error in the heat rate so obtained is

$$\epsilon = (\bar{q}_w - q_w)/q_w = (L/t) \tan (t/L) - 1 \quad . \tag{A-6}$$

It is apparent that for vanishing thickness, the error also vanishes. Furthermore, since for a suitably smooth distribution of $q_w(x, y)$, the wall temperature distribution $T_w(x, y)$ is also smooth and the quantity $L = \sqrt{(T_w/\nabla^2 T_w)}$ is therefore of the order of the body transverse dimension, while t is by assumption much smaller, the error can be approximated as

$$\epsilon \approx (1/3)(t/L)^2 \quad , \tag{A-7}$$

or

$$\epsilon \approx (t^2/3) \left[(\nabla^2 T_w)/T_w \right] \quad . \tag{A-7a}$$

The meridional conduction error can be easily determined for any conical body since the local heat transfer rate (and also local wall temperature variation as $\epsilon \longrightarrow 0$) varies inversely as the square root of the distance along rays from the apex, thus

$$q_w \sim T_w \sim r^{-\frac{1}{2}} \quad ,$$

so that

$$(1/T_w)(\partial^2 T_w/\partial r^2) = (3/4)\, r^{-2}$$

and

$$\epsilon_r = (1/4)(t/r)^2 \tag{A-8}$$

Likewise, if the circumferential wall temperature distribution due to yaw is locally approximated by

$$T_w \sim \cos(n\phi)$$

then,

$$\left[\frac{1}{T_w (r \sin \theta_c)^2} \frac{\partial^2 T_w}{\partial \phi^2} \right]_{max.} = - \left(\frac{n}{r \sin \theta_c} \right)^2 , \qquad (A\text{-}9)$$

and the maximum error is

$$\epsilon_\phi = - (1/3) \left(\frac{n t}{r \sin \theta_c} \right)^2$$

It is apparent that for $n^2 > (3/4) \sin^2 \theta_c$, which is generally the case for circular cones even at relatively small yaw, the circumferential conduction error exceeds the meridianal error.

In the present case, for example, the local maximum in heat transfer which appears on the leeward side of the cone at moderate yaw angles can be characterized by $n \leq 6$. Then, even at the forward station, taking $r = 1$ inch and $t = 3 \times 10^{-3}$ inch, for the 10° cone:

$$\epsilon_\phi \leq - (1/3) \left[(18 \times 10^{-3})/.1736 \right]^2 \approx - 0.4 \% .$$

Whereas,

$$\epsilon_r = (1/4) \left[(3 \times 10^{-3})/1 \right]^2 \approx 0.0002 \% .$$

It should be noted that the circumferential gradients are elsewhere not as severe as those in the case just cited, being characterized by $n \leq 2$, and thus producing errors an order of magnitude less.

2. Effects Caused by Variable Thermometric Properties

The ratio of the heat transfer coefficient at yaw to that for the unyawed cone is

$$\frac{h}{h_o} = \frac{q_w(H_{aw}-H_w)^{-1}}{q_{wo}(H_{awo}-H_{wo})^{-1}} = \frac{k_w(\partial T/\partial z)_w\,[c_p(T_{aw}-T_w)]^{-1}}{k_{wo}(\partial T/\partial z)_{wo}[c_{p_o}(T_{awo}-T_{wo})]^{-1}} . \quad \text{(A-10)}$$

If the temperature gradient at the wall is replaced by the temperature difference across the layer divided by the thickness of the layer, neglecting here the error discussed in Section 1 of this appendix, equation (A-10) becomes

$$\frac{h}{h_o} = \frac{k_w(T_w-T_b)\,[c_p(T_{aw}-T_w)]^{-1}}{k_{wo}(T_{wo}-T_b)\,[c_{p_o}(T_{awo}-T_{wo})]^{-1}} , \quad \text{(A-10a)}$$

where T_b, the temperature at the base of the insulating layer is taken as constant. The ratio of the electrical signal produced by the thermocouple temperature difference $\Delta T = T_w - T_b$, at yaw to that at zero yaw is, then

$$\frac{\Delta E}{\Delta E_o} = \frac{E_w-E_b}{E_{wo}-E_b}$$

$$= \left[\frac{\Delta E/\Delta E_o}{\Delta T/\Delta T_o}\right]\left[\frac{k_{wo}}{k_w}\right]\left[\frac{c_p}{c_{p_o}}\right]\left[\frac{T_{aw}-T_w}{T_{awo}-T_{wo}}\right]\frac{h}{h_o} . \quad \text{(A-11)}$$

Each factor on the right hand side of equation (A-11) can be identified with an error, thus:

$$\frac{\Delta E}{\Delta E_o} = (1 + \epsilon_E)(1 + \epsilon_k)(1 + \epsilon_{c_p})(1 + \epsilon_T)\frac{h}{h_o} \qquad \text{(A-11a)}$$

Variable Conductivity

The conductivity of the insulating material generally depends upon the temperature, $k = k(T)$, and, for a small temperature excursion, can be expanded about its value at T_{wo} in a power series,

$$\frac{k_{wo}}{k_w} = \frac{k(T_{wo})}{k(T_{wo}) + (T_w - T_{wo})(\partial k/\partial T)_{wo} + \cdots}$$

$$= 1 - (T_w - T_{wo})\frac{(\partial k/\partial T)_{wo}}{k(T_{wo})} + \cdots \qquad \text{(A-12)}$$

Now, since T_b is constant

$$(T_w - T_{wo}) = \Delta T - \Delta T_o \quad ,$$

and the error arising from variable conductivity is

$$\epsilon_k = \frac{k_{wo}}{k_w} - 1 \approx \Delta T_o\left(\frac{\Delta T}{\Delta T_o} - 1\right)\frac{(\partial k/\partial T)_{wo}}{k(T_{wo})} \qquad \text{(A-13)}$$

where the ratio $(\Delta T/\Delta T_o) \approx (q_w/q_{wo})$ depends upon the yaw angle and circumferential location.

The maximum error occurs at the highest local heat transfer ratio and is proportional to the fractional change in conductivity with temperature. No specific information is available concerning this property for the F. E. P. -type teflon dispersion coating employed as an insulating layer. A conservative estimate given by the manufacturer, Du Pont Corp., claims $\left[(dk/dT)/k\right] \leq 10^{-3}$ per ^{o}R near room temperature. The largest value of $(\Delta T/\Delta T_o)$ encountered in the tests was 4.4 at the aft station on the windward meridian at $p_{t\infty} = 245$ p. s. i. g., and the associated value of ΔT_o was 8.5 ^{o}R; thus

$$\epsilon_k \leq -(8.5)(4.4 - 1)(10^{-3}) = -2.9\ \% \quad ,$$

whereas the largest value of ΔT_o was 19.8 ^{o}R at the forward station at $p_{t\infty} = 245$ p. s. i. g., for which $(\Delta T/\Delta T_o) = 3.3$, so that

$$\epsilon_k \leq -(19.8)(3.3 - 1)(10^{-3}) = -4.6\ \% \quad .$$

Thermocouple Non-Linearity

The variable recorded during the tests was the ratio of the thermocouple output difference across the insulating layer at yaw to that at zero yaw. An error is incurred by assuming that this electrical signal ratio is equal to the temperature difference ratio. The output of a copper-constantan thermojunction in milli-volts is very well represented over a large temperature range ($150 < {}^{o}R < 800$) by the expression

$$(E + B) = AT^{m} \quad ; \begin{cases} A = 1.76 \times 10^{-4} \\ B = 6.20 \text{ (for } 0^{o}C \text{ reference junction)} \\ m = 1.69 \end{cases} \qquad \text{(A-14)}$$

Thus, the measured voltage difference can be expressed in a series

developed around T_b ,

$$\Delta E = E_w - E_b = (E + B)_w - (E + B)_b$$

$$= (T_w - T_b)\left[\frac{d(E + B)}{dT}\right]_b + \tfrac{1}{2}(T_w - T_b)^2\left[\frac{d^2(E + B)}{dT^2}\right]_b + \ldots$$

$$= (\Delta T)\, mA\, T_b^{m-1} + \tfrac{1}{2}(\Delta T)\, m\,(m-1)\, A T_b^{m-2} + \ldots \quad .$$

The ratio of the voltage differences at yaw and zero yaw is

$$\frac{\Delta E}{\Delta E_o} = \frac{\Delta T\, m\, A\, T_b^{n-1} + \frac{1}{2}(\Delta T)^2 m\,(m-1)\, A\, T_b^{n-2} + \ldots}{\Delta T_o\, m\, A\, T_b^{n-1} + \frac{1}{2}(\Delta T_o)^2\, m\,(m-1)\, A\, T_b^{n-2} + \ldots}$$

$$\approx (\Delta T/\Delta T_o)\left[1 + \frac{m-1}{2T_b}(\Delta T - \Delta T_o)\right] \quad .$$

Thus the error arising from the assumption of proportionality between the thermocouple signal and the temperature is

$$\epsilon_E = \frac{(\Delta E/\Delta E_o)}{(\Delta T/\Delta T_o)} - 1 = \Delta T_o\left(\frac{\Delta T}{\Delta T_o} - 1\right)\left(\frac{m-1}{2T_b}\right) \quad . \qquad \text{(A-15)}$$

The dependence of ϵ_E and ϵ_k (equation A-13) upon the temperature difference across the layer, and thus upon the local heat transfer rate, is seen to be the same; however, these errors are of opposite sign. Consider the condition that was critical for ϵ_k : at the forward station when $p_{t\infty} = 245$ p. s. i. g. and $T_b = 567^\circ R$,

$$\epsilon_E = \frac{0.69}{(2)(567)}(19.8)(3.3 - 1) = 2.8\,\% \quad .$$

It is of interest that where the conductivity variation and/or thermocouple non-linearity can be chosen freely, the errors from these two sources can be made to cancel according to the criterion:

$$\frac{(dk/dT)_{wo}}{k(T_{wo})} = \frac{m - 1}{2\,T_b}$$

or for $\Delta T_o << T_{wo}$:

$$m \approx 1 + 2\,\frac{(dk/dT)_{wo}}{(k/T)_{wo}}$$

3. The Effect of Variation of Thermodynamic Potential

The difference between the adiabatic wall enthalpy and the enthalpy at the cooled wall is the thermodynamic potential normalizing the heat transfer coefficient. The variation of specific heat with temperature, and the change in the enthalpy excess caused by variations in the recovery temperature with yaw are, strictly speaking, not errors in measurement, but rather a part of the external heat transfer phenomena being studied. That is, these effects would not appear at all if the ratio of heat transfer rate at yaw to that at zero yaw were being determined rather than the ratio of coefficients. However, the available theory is developed in terms of the ratio of the heat transfer coefficients. Since there is, in any case, an actual error introduced into the enthalpy excess by the variations of the temperature difference across the insulating layer, the variation of the thermodynamic potential stemming from all sources is considered as an error herein.

The specific heat is sensibly constant at the surface temperatures

realized in these tests. For example, caloric imperfections alter c_p by less than 0.2 % at 550 °R (nominal wall temperature). The effect of these imperfections is henceforth neglected.

The adiabatic wall temperature depends upon a recovery factor, r, which is very nearly constant for laminar flow; T_{aw} is given by

$$T_{aw} = T_c + r\,(T_{t\infty} - T_c) = T_{t\infty}\,\frac{\left[1 + r\left(\frac{\gamma-1}{2}\right) M_c^{\,2}\right]}{\left[1 + \left(\frac{\gamma-1}{2}\right) M_c^{\,2}\right]}\,, \qquad \text{(A-16)}$$

where the subscript c denotes conditions at the cone surface but external to the boundary layer. Using this relation, the fourth member on the right-hand side of equation (A-11) can be written,

$$\frac{T_{aw}-T_w}{T_{awo}-T_{wo}} = \frac{\left[\dfrac{1 + r\left(\frac{\gamma-1}{2}\right)M_c^2}{1 + \left(\frac{\gamma-1}{2}\right)M_c^2}\right] - \dfrac{T_{wo} + \Delta T - \Delta T_o}{T_{t\infty}}}{\left[\dfrac{1 + r\left(\frac{\gamma-1}{2}\right)M_c^2}{1 + \left(\frac{\gamma-1}{2}\right)M_c^2}\right] - \dfrac{T_{wo}}{T_{t\infty}}}$$

$$= \frac{1 - \dfrac{(1-r)\left(\frac{\gamma-1}{2}\right)M_c^2}{1 + \left(\frac{\gamma-1}{2}\right)M_c^2} - \dfrac{T_{wo}}{T_{t\infty}}\left[1 + \left(\frac{\Delta T_o}{T_{wo}}\right)\left(\frac{\Delta T}{\Delta T_o} - 1\right)\right]}{\dfrac{(1-r)\left(\frac{\gamma-1}{2}\right)M_{co}^2}{1 + \left(\frac{\gamma-1}{2}\right)M_{co}^2} - \dfrac{T_{wo}}{T_{t\infty}}} \qquad \text{(A-17)}$$

$$= 1 - \left\{\frac{(1-r)\left[\dfrac{\left(\frac{\gamma-1}{2}\right)M_c^2}{1 + \left(\frac{\gamma-1}{2}\right)M_c^2} - \dfrac{\left(\frac{\gamma-1}{2}\right)M_{co}^2}{1 + \left(\frac{\gamma-1}{2}\right)M_{co}^2}\right] + \dfrac{\Delta T_o}{T_{t\infty}}\left(\dfrac{\Delta T}{\Delta T_o} - 1\right)}{1 - (1-r)\dfrac{\left(\frac{\gamma-1}{2}\right)M_{co}^2}{1 + \left(\frac{\gamma-1}{2}\right)M_{co}^2} - \dfrac{T_{wo}}{T_{t\infty}}}\right\},$$

where the constancy of the base temperature, T_b, has been used as well as the invariance of the total temperature external to the boundary layer. Thus the error produced by the variation of the thermodynamic potential is

$$\epsilon_T = \frac{T_{aw} - T_w}{T_{aw_o} - T_{w_o}} - 1$$

$$= \frac{(1-r)\left[\frac{(\frac{\gamma-1}{2})M_{c_o}^2}{1+(\frac{\gamma-1}{2})M_{c_o}^2} - \frac{(\frac{\gamma-1}{2})M_c^2}{1+(\frac{\gamma-1}{2})M_c^2}\right] - \frac{\Delta T_o}{T_{t\infty}}\left(\frac{\Delta T}{\Delta T_o} - 1\right)}{1 - (1-r)\left[\frac{(\frac{\gamma-1}{2})M_{c_o}^2}{1+(\frac{\gamma-1}{2})M_{c_o}^2}\right] - \frac{T_{w_o}}{T_{t\infty}}} \quad . \tag{A-18}$$

The second term is seen to be of the same form as that appearing in the conductivity error and the thermocouple effect, whereas the first term is the anticipated Mach number effect on the recovery temperature. Now consider as critical the forward station at $p_{t\infty} = 245$ p. s. i. g., and take $\gamma = 1.4$, $r = 0.85$, $M_c \simeq 2.6$ at 24° yaw (from tangent 34° cone approximation), $M_{c_o} = 6.2$, $\Delta T_o = 19.8^\circ R$, $T_{t\infty} = 1360^\circ R$, $(\Delta T/\Delta T_o) = 3.3$, and $T_{w_o} = 587^\circ R$; then

$$\epsilon_T = (10.7 - 7.7) \times 10^{-2} = 3.0\ \% \quad .$$

The regions of high heat transfer are generally associated

with high local surface inclination and low external Mach number. Thus the increase of thermodynamic potential caused by the local reduction of Mach number is always opposed by the reduction of the thermodynamic potential which results from the greater temperature difference across the insulating layer. The magnitude of both effects subsides rapidly as the yaw is reduced. For example a reduction of yaw from 24° to 20° causes the error, ϵ_T, to fall to 2 %.

APPENDIX B

WIND TUNNEL CALIBRATION

At the conclusion of the tests, an abbreviated calibration of the empty tunnel was conducted. The survey consisted of vertical traverses in the midplane of the tunnel at each of the supply pressures of the tests (129. 3 and 259. 3 p. s. i. a.) and at axial locations corresponding to the forward and aft measuring stations on the models (x = 1 in. and 4 in.). In addition the supply temperature was varied through the entire range for which the flow could be maintained.

The results of the four vertical traverses at the normal supply temperatures (1360^{o}R) are presented in Figure 15. The Mach number distribution is nearly the same at each station and for each tunnel pressure, except for a 1 % increase in Mach number at the high pressure. The probe model provided circumferential distributions of the pitot-pressure in the free stream, and these data indicated a nearly axisymmetric distribution of Mach number. This symmetry is indicated by points taken from the probe data in the horizontal plane (the top of the figure in this case corresponds to the south side of the tunnel). The greatest departure from axial symmetry occurs in the vertical plane in which the traverses were made. The boundary layer restricts the test core to a diameter of about 3 in.; however, the flow is satisfactorily uniform within a 4 in. diameter.

The reduction of supply temperature at the maximum supply pressure produced the variation of pitot-pressure shown in Figure 16. There is virtually no effect on the pitot-pressure at 1160^{o}R (700^{o}F) at

either station; however, below about 1010°R (550°F) the pitot pressure displays very erratic behavior. The condensation of air in the stream can be expected to produce erroneous data under these flow conditions.

TABLE I

SURFACE PRESSURE MEASUREMENTS

Figure	x (in.)	$p_{t\infty}$ (p. s. i. a.)	$T_{t\infty}$ (^{o}R)	M_{∞}	$Re_{\infty, x} \times 10^{-5}$	$T_w/T_{t\infty}$
S 1 a, b	4.0	259.3	1360	7.95	4.2	0.40
S 2 a, b	4.0	129.3	1360	7.87	2.1	0.40
S 3	1.0	259.3	1360	7.95	1.04	0.42
S 4	1.0	129.3	1360	7.87	0.52	0.42

TABLE II

HEAT TRANSFER MEASUREMENTS

Figure	x (in.)	$p_{t\infty}$ (p. s. i. a.)	$T_{t\infty}$ (^{o}R)	M_{∞}	$Re_{\infty, x} \times 10^{-5}$	$T_w/T_{t\infty}$	ΔT_o (^{o}R)
S 5	4.0	259.3	1360	7.95	4.2	0.40	8.5
S 6	4.0	129.3	1360	7.87	2.1	0.40	6.0
S 7	4.0	259.3	1160	8.	5.3	0.46	5.8
S 8	4.0	259.3	960	8.	7.3	0.56	3.3

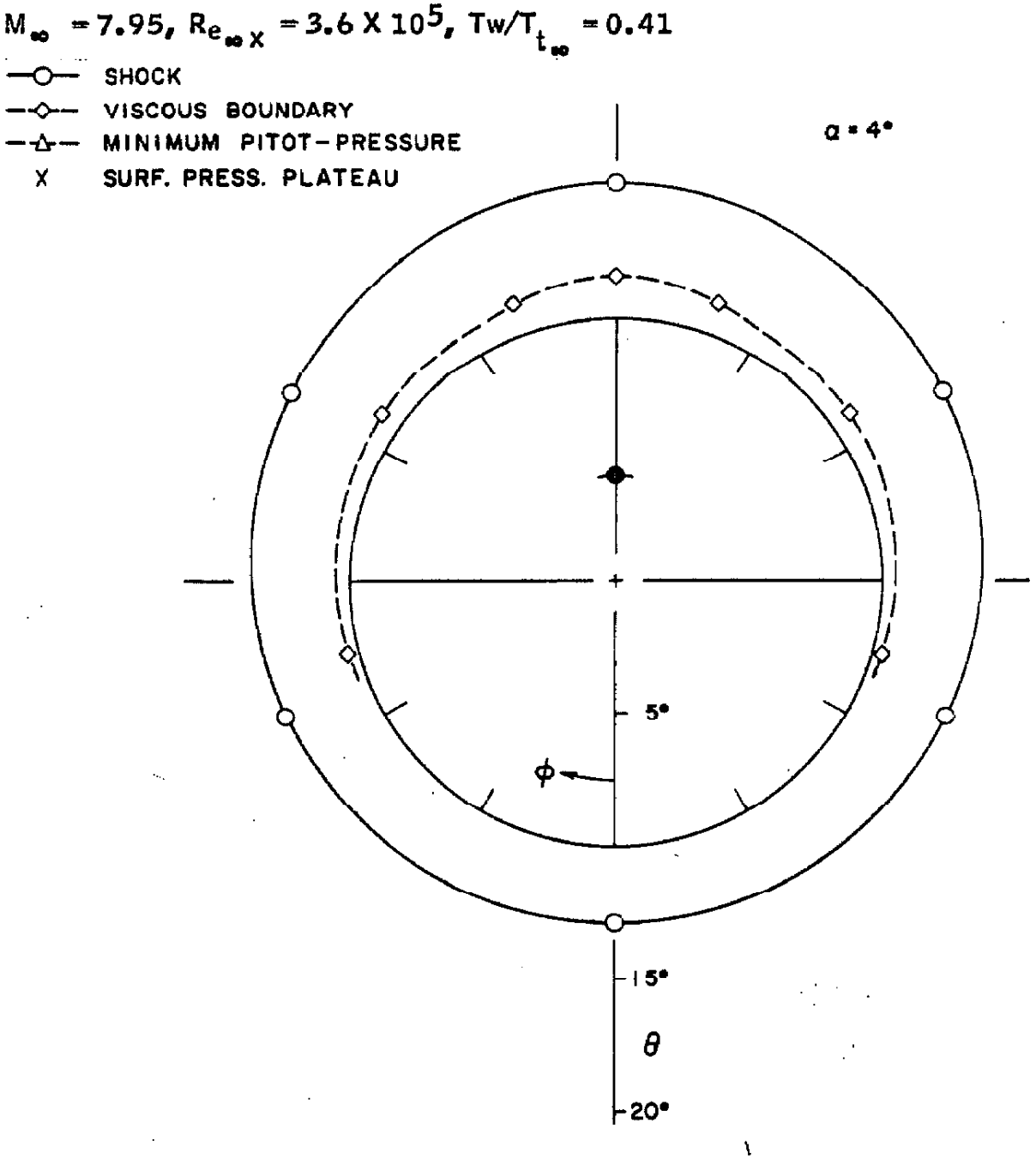

Figure 4a. Geometry of the Flow Field — 4° Yaw

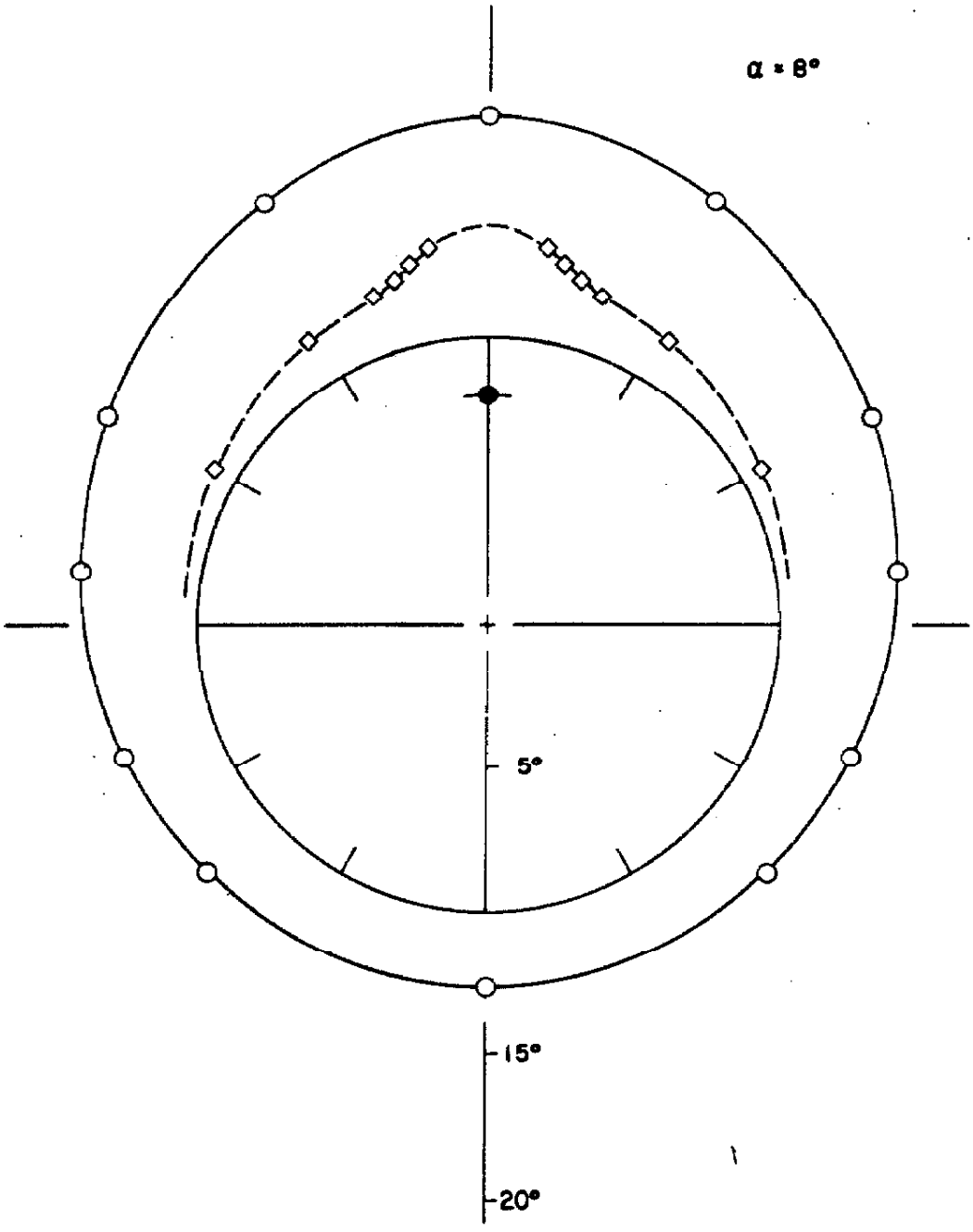

Figure 4b. Geometry of the Flow Field -- 8^0 Yaw

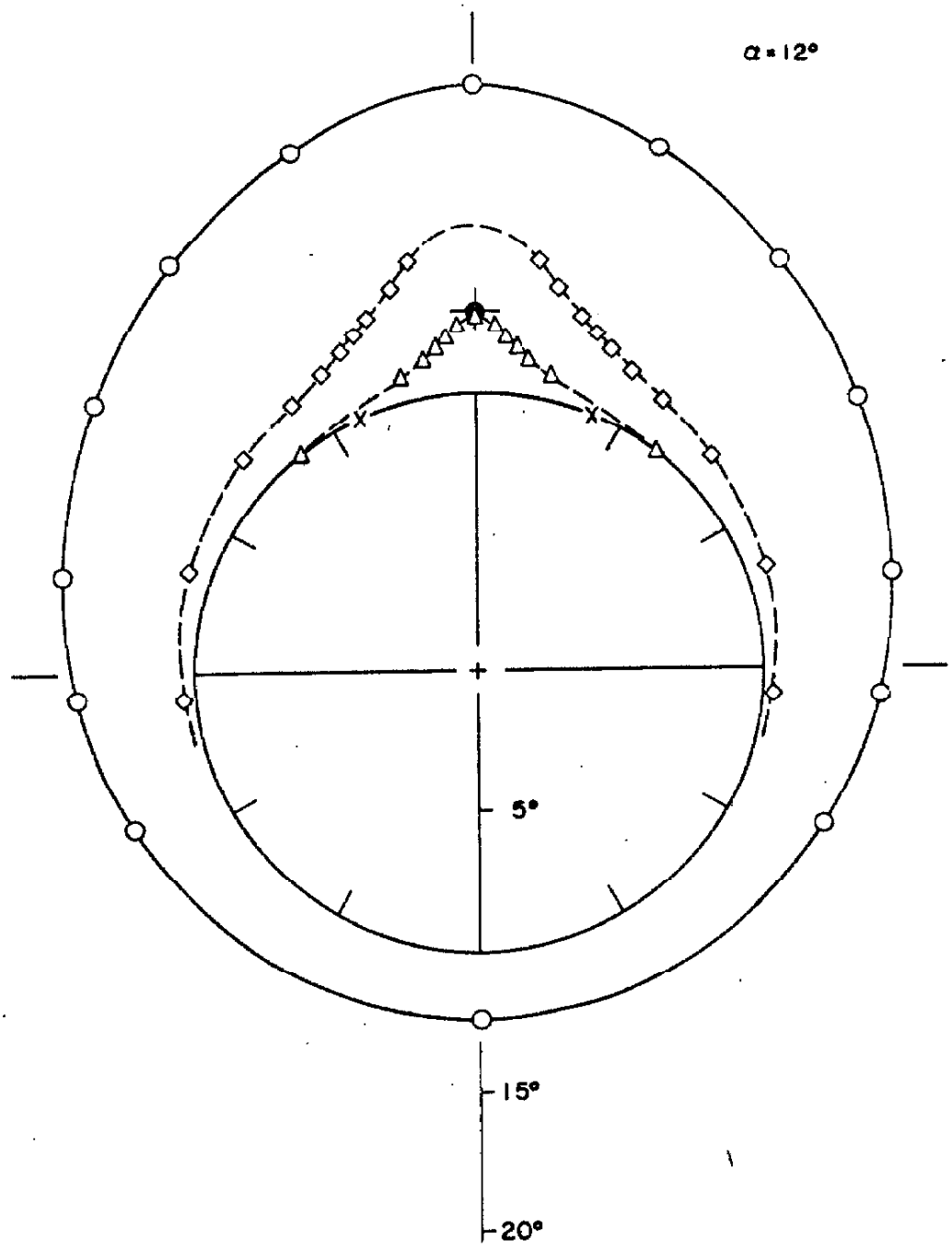

Figure 4c. Geometry of the Flow Field — 12° Yaw

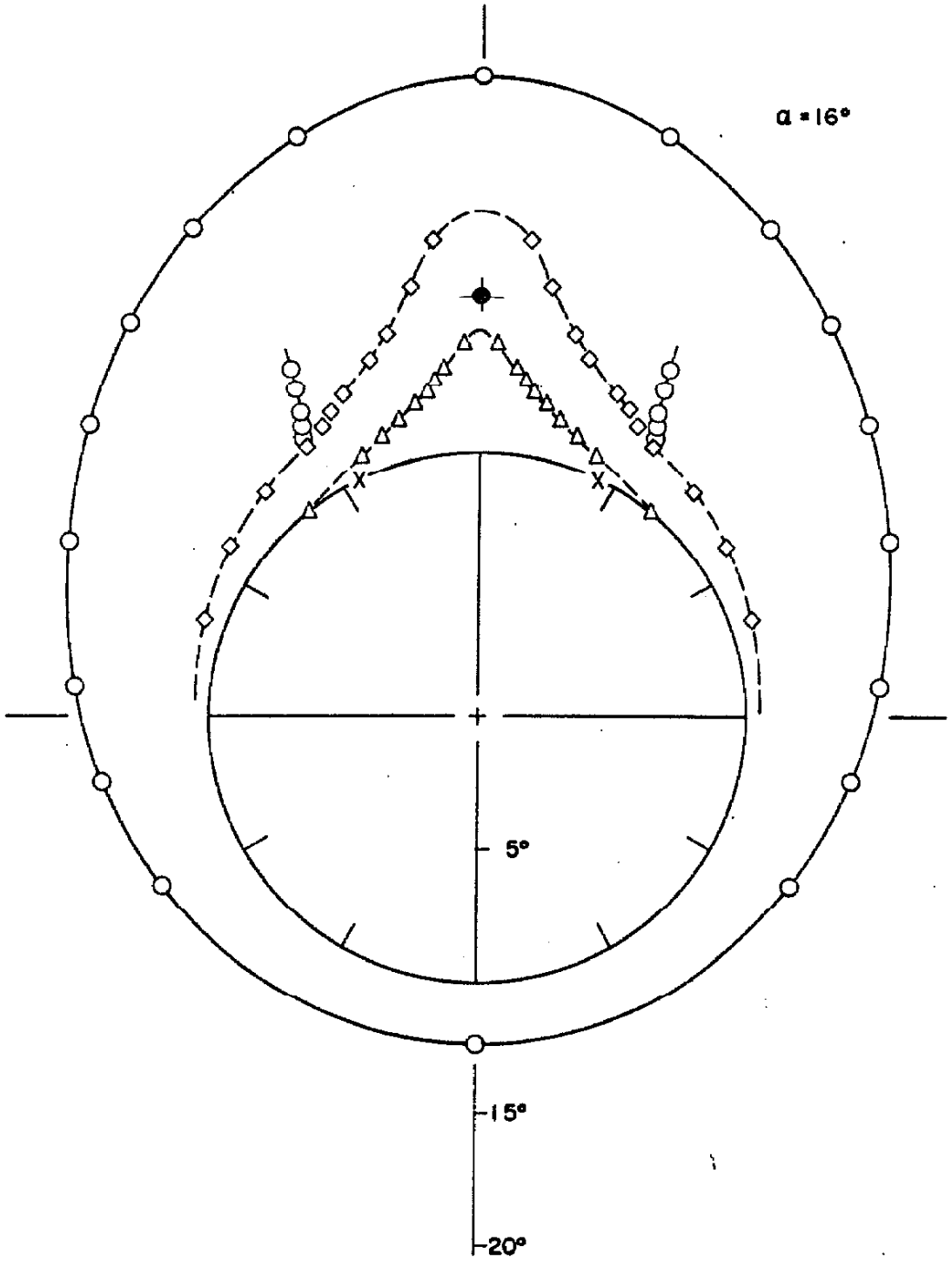

Figure 4d. Geometry of the Flow Field -- 16° Yaw

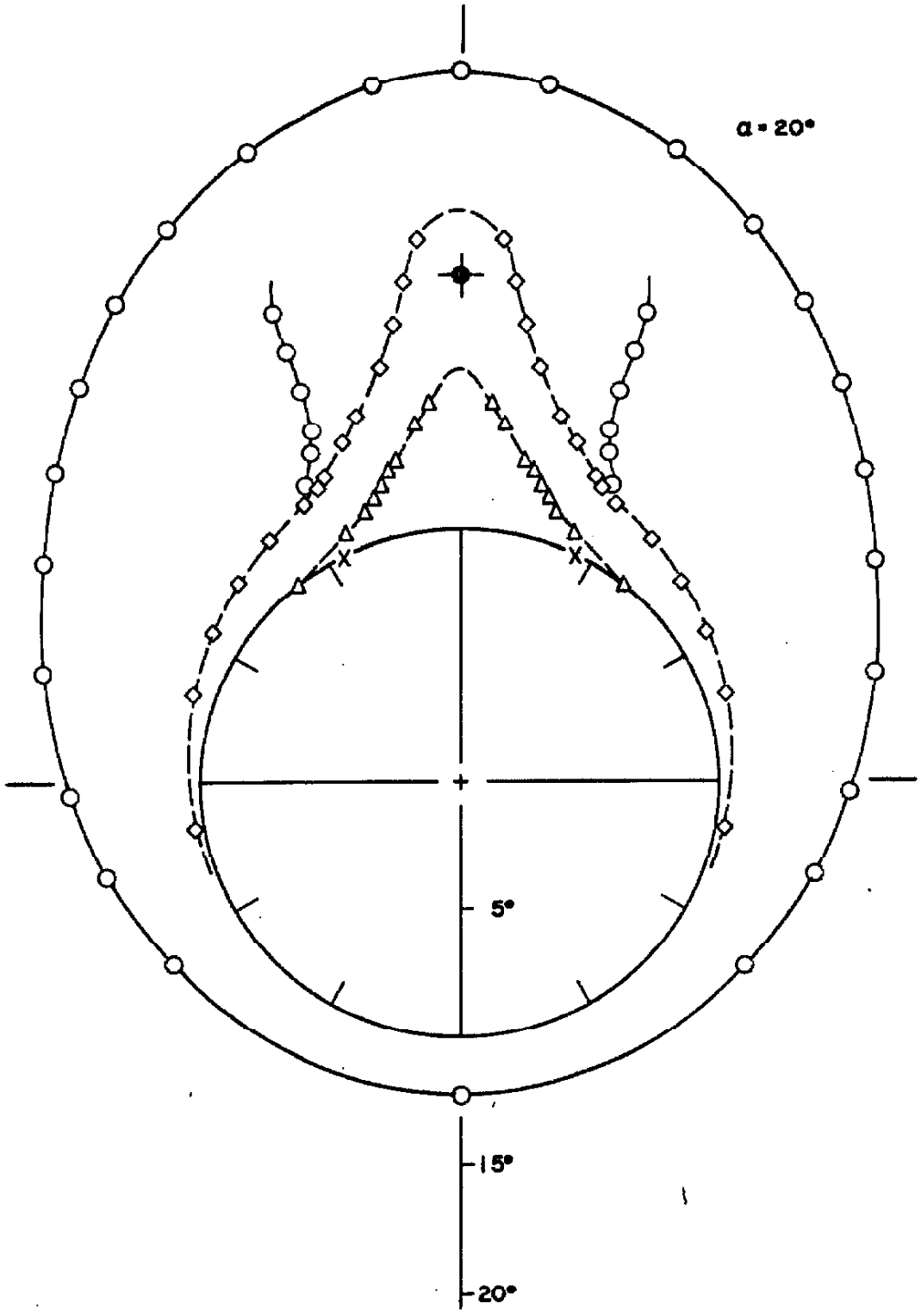

Figure 4e. Geometry of the Flow Field -- 20° Yaw

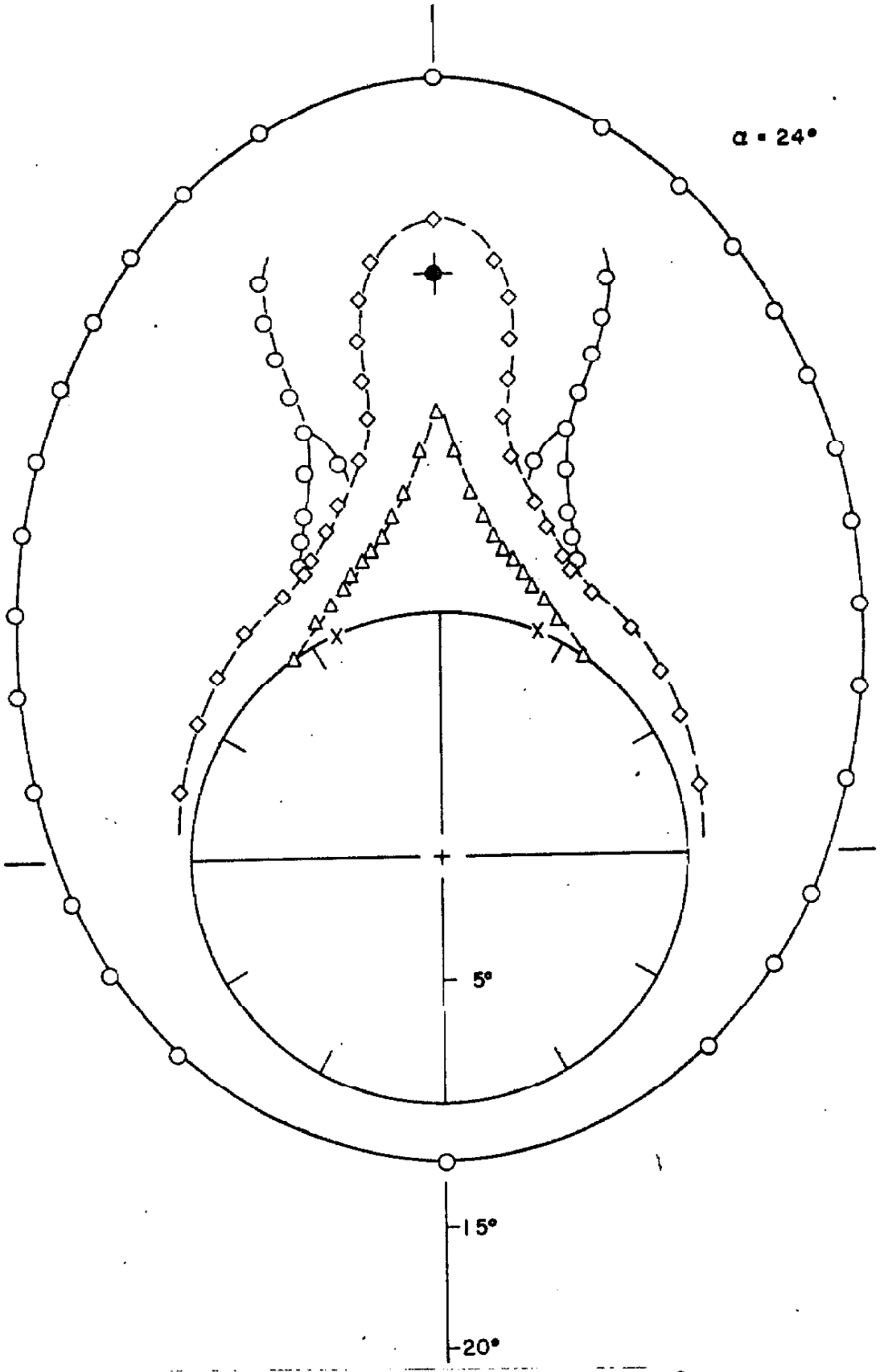

Figure 4f. Geometry of the Flow Field — 24° Yaw

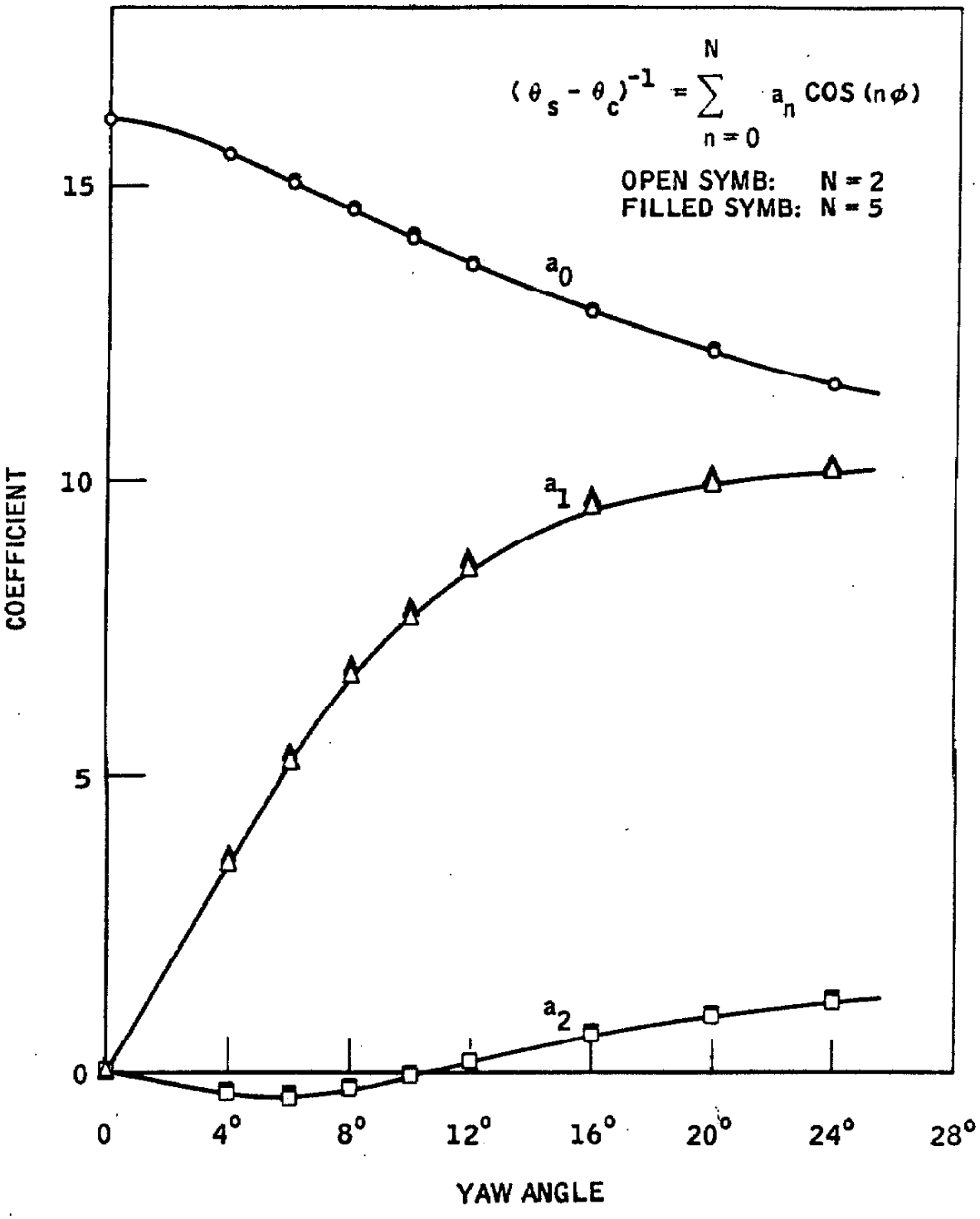

Figure 5. Fourier Representation of Shock Shape

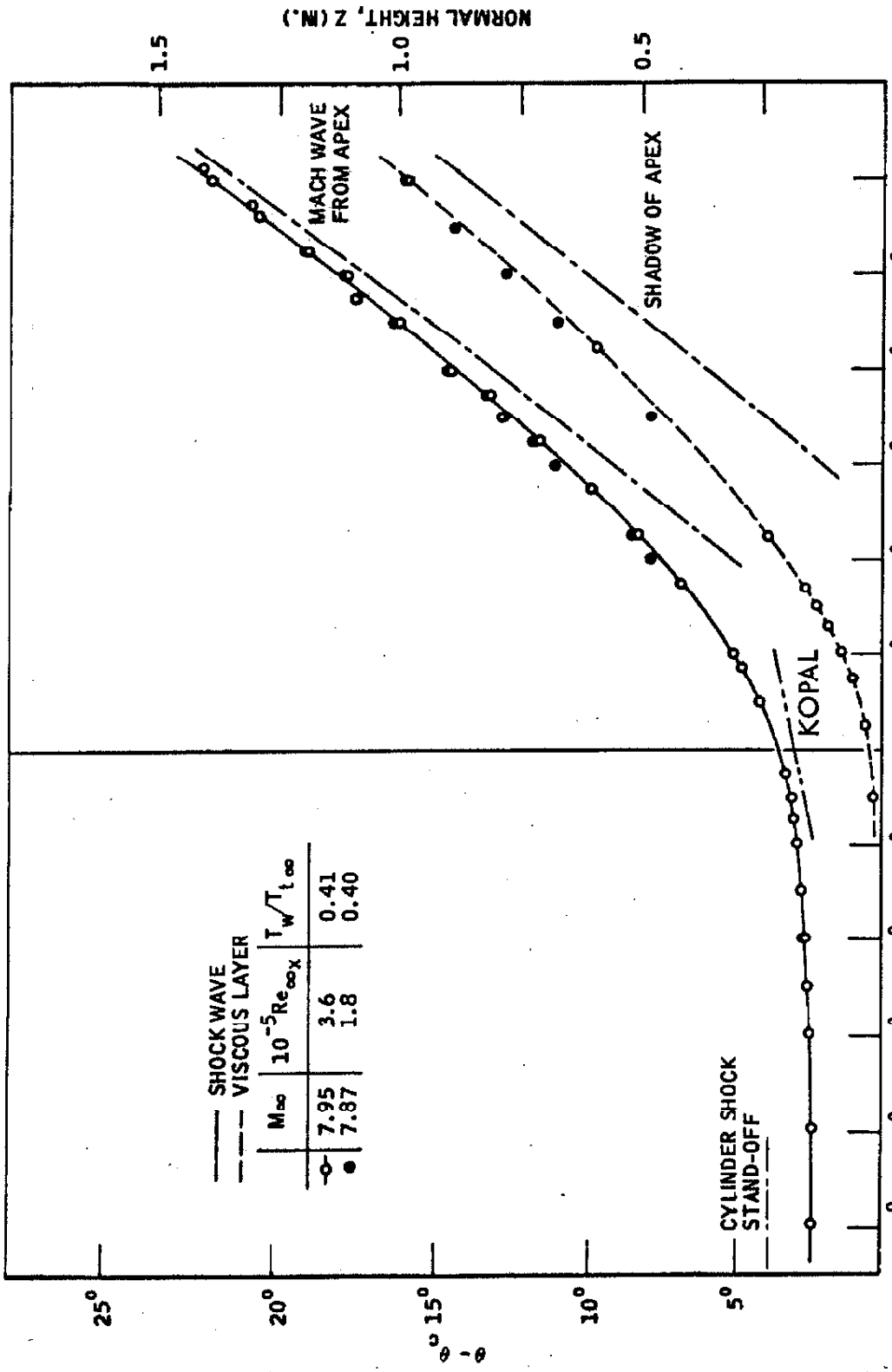

Figure 6. Shock Layer in the Plane of Symmetry

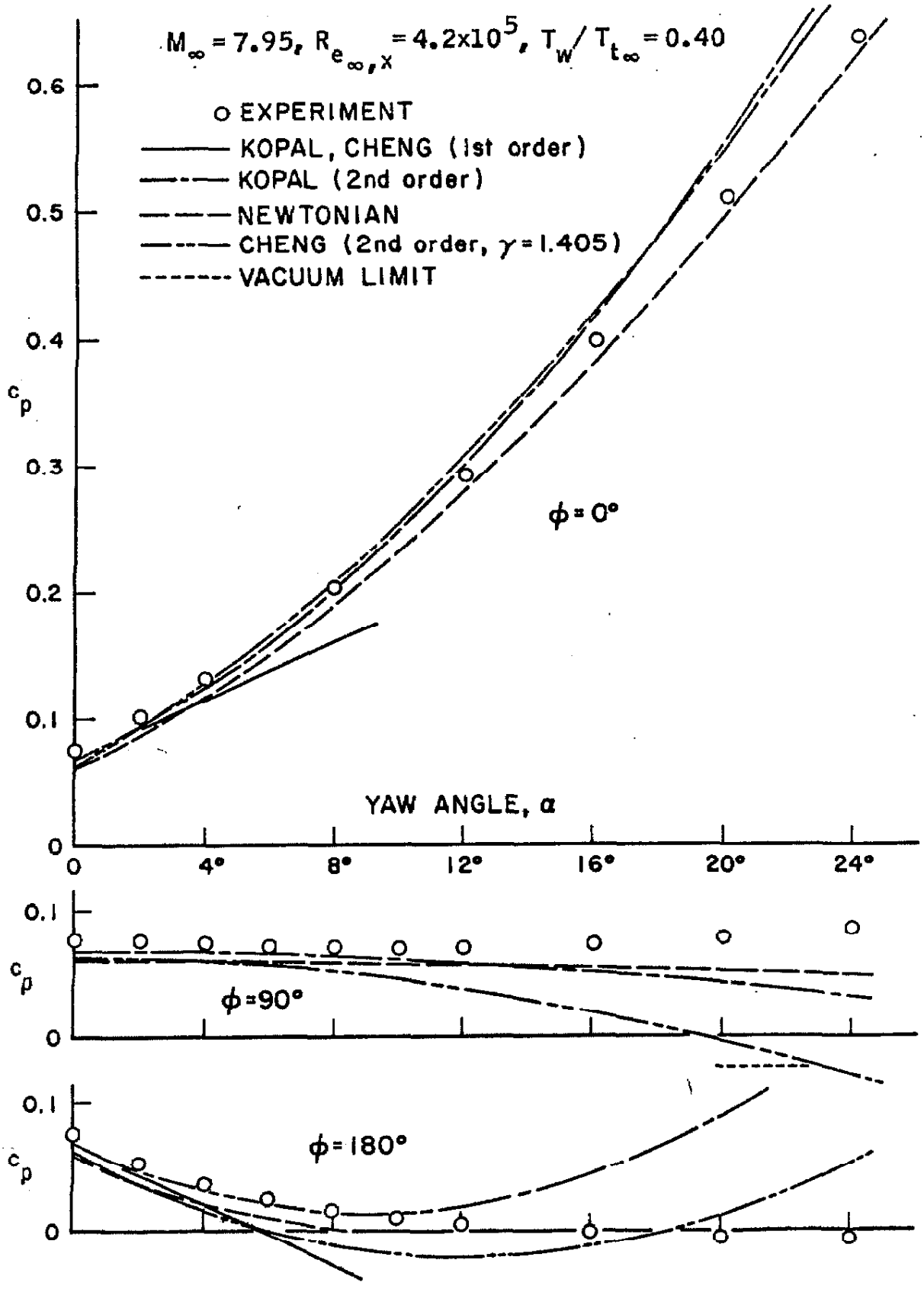

Figure 7. Pressure Variation with Yaw in Meridian Planes

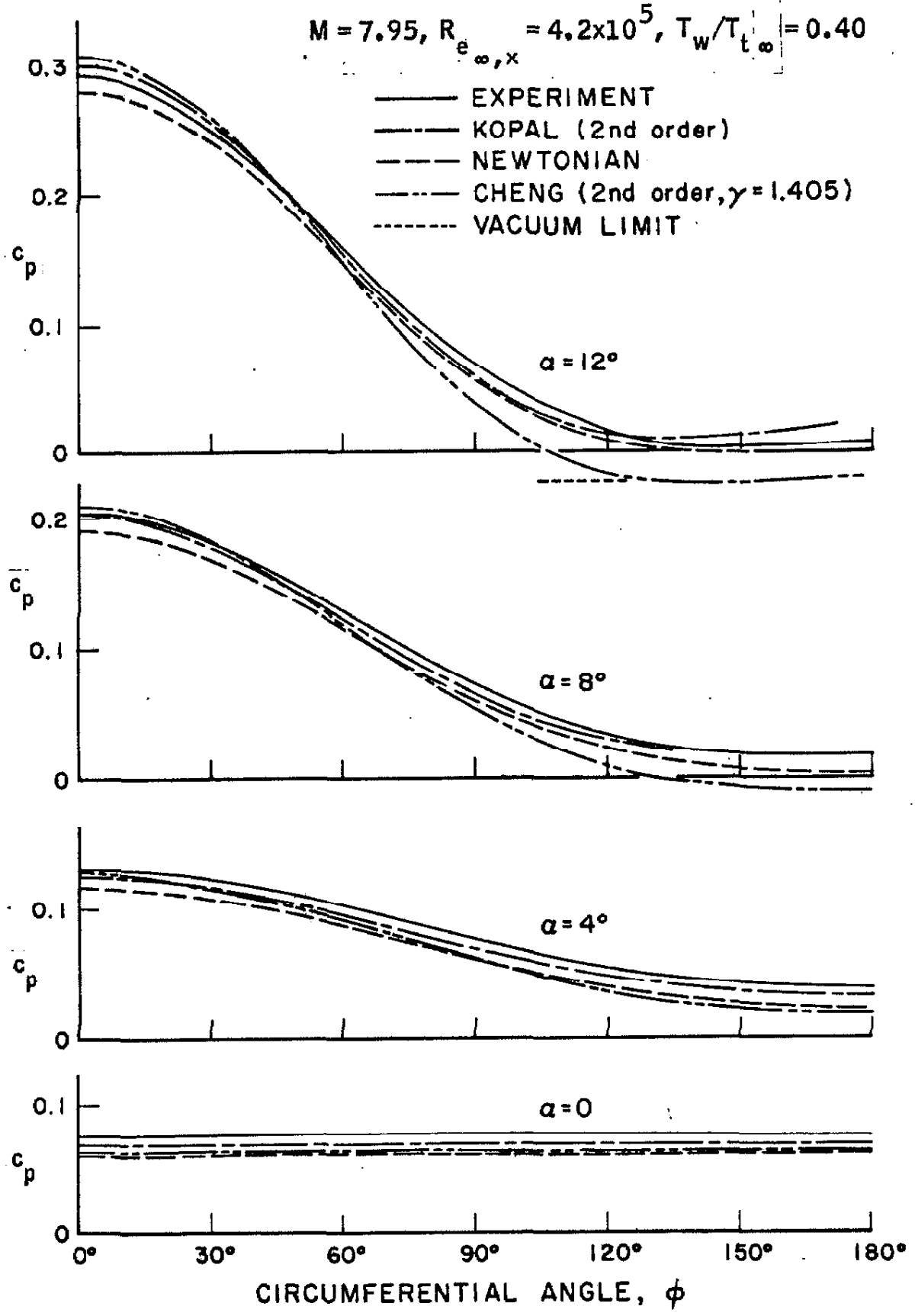

Figure 8. Circumferential Pressure Distribution; a. Moderate Yaw

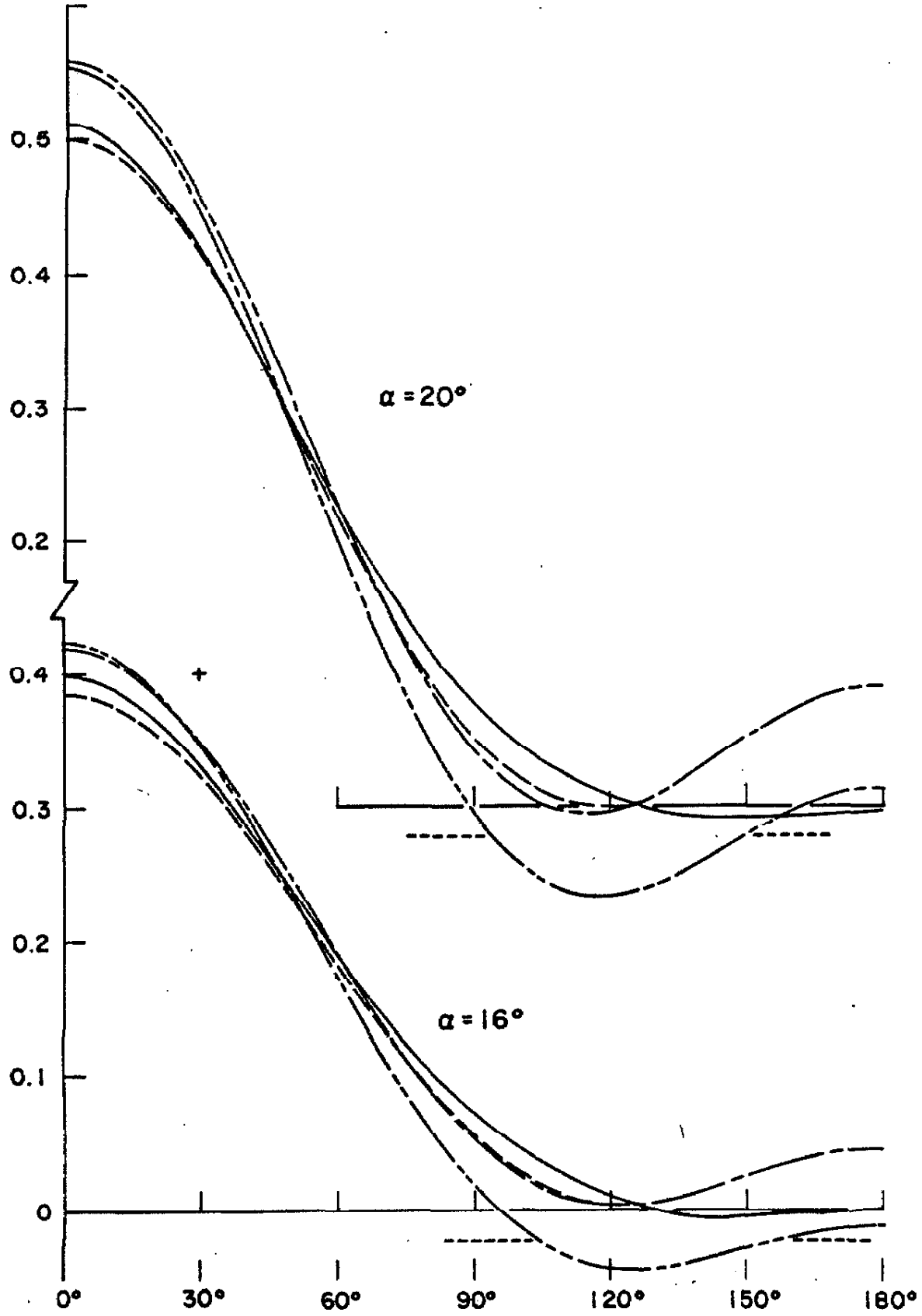

Figure 8 (continued), b. Large Yaw

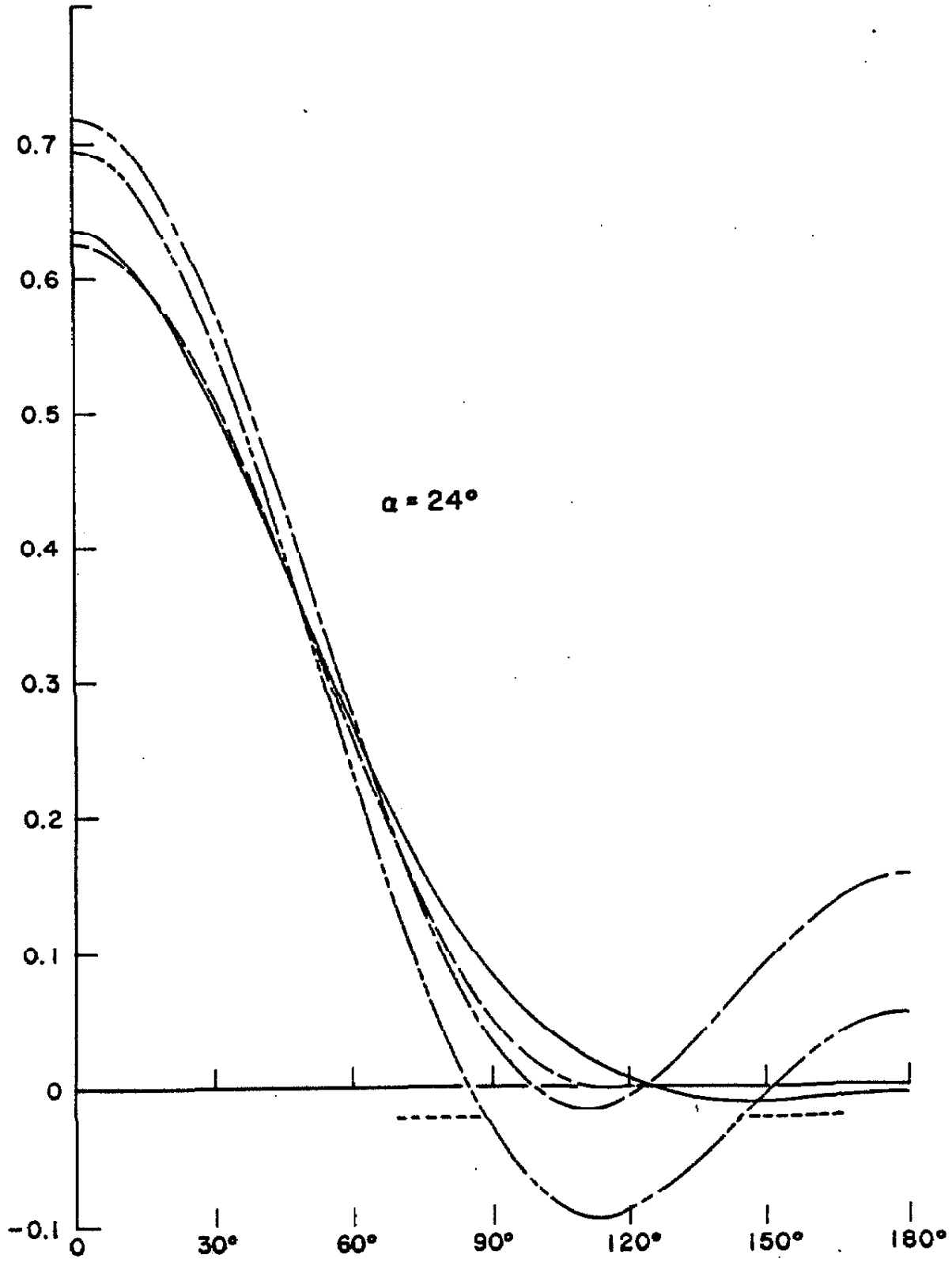

Figure 8 (concluded), c. Very Large Yaw

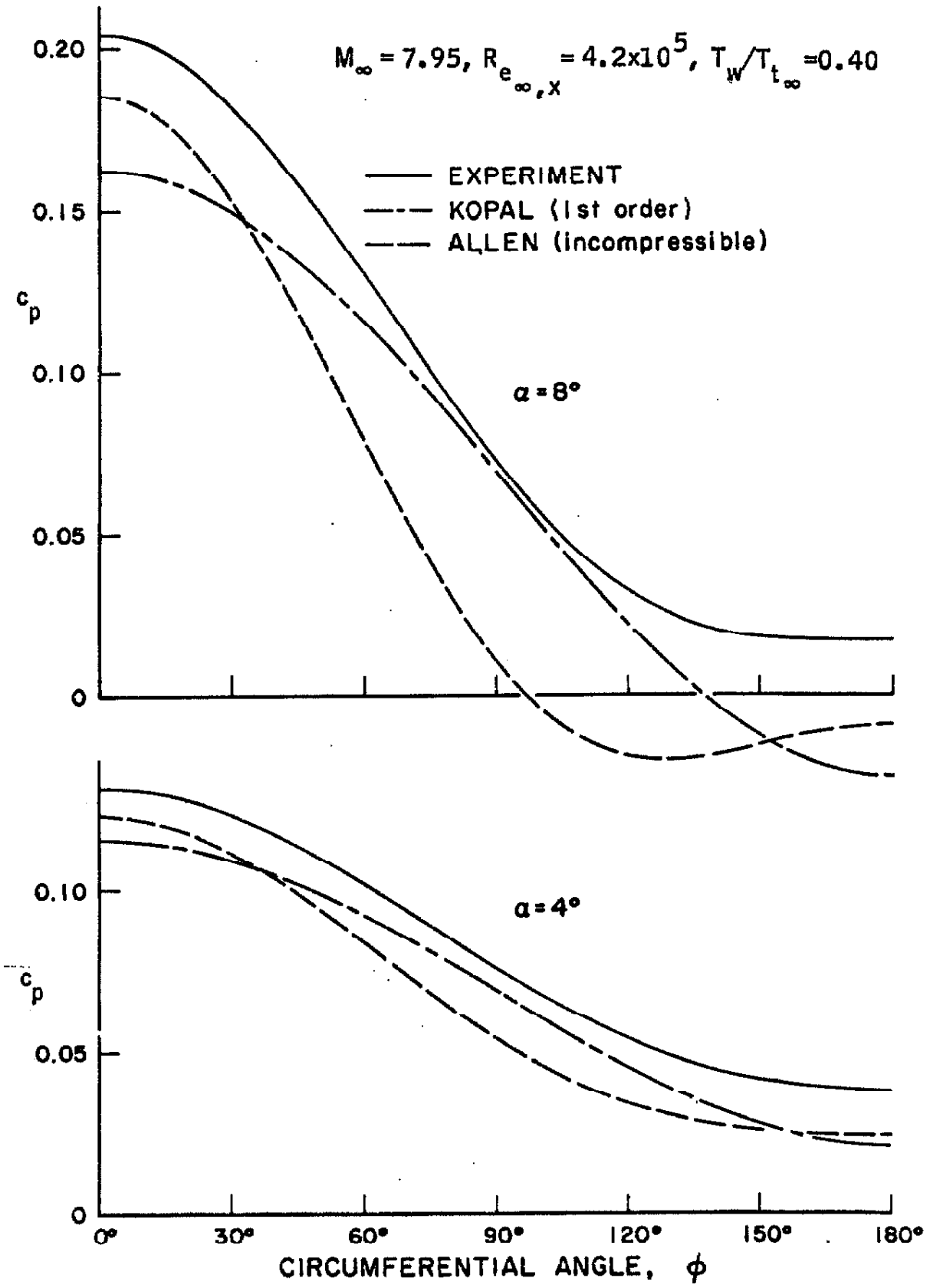

Figure 9. Pressure Distribution at Small Yaw

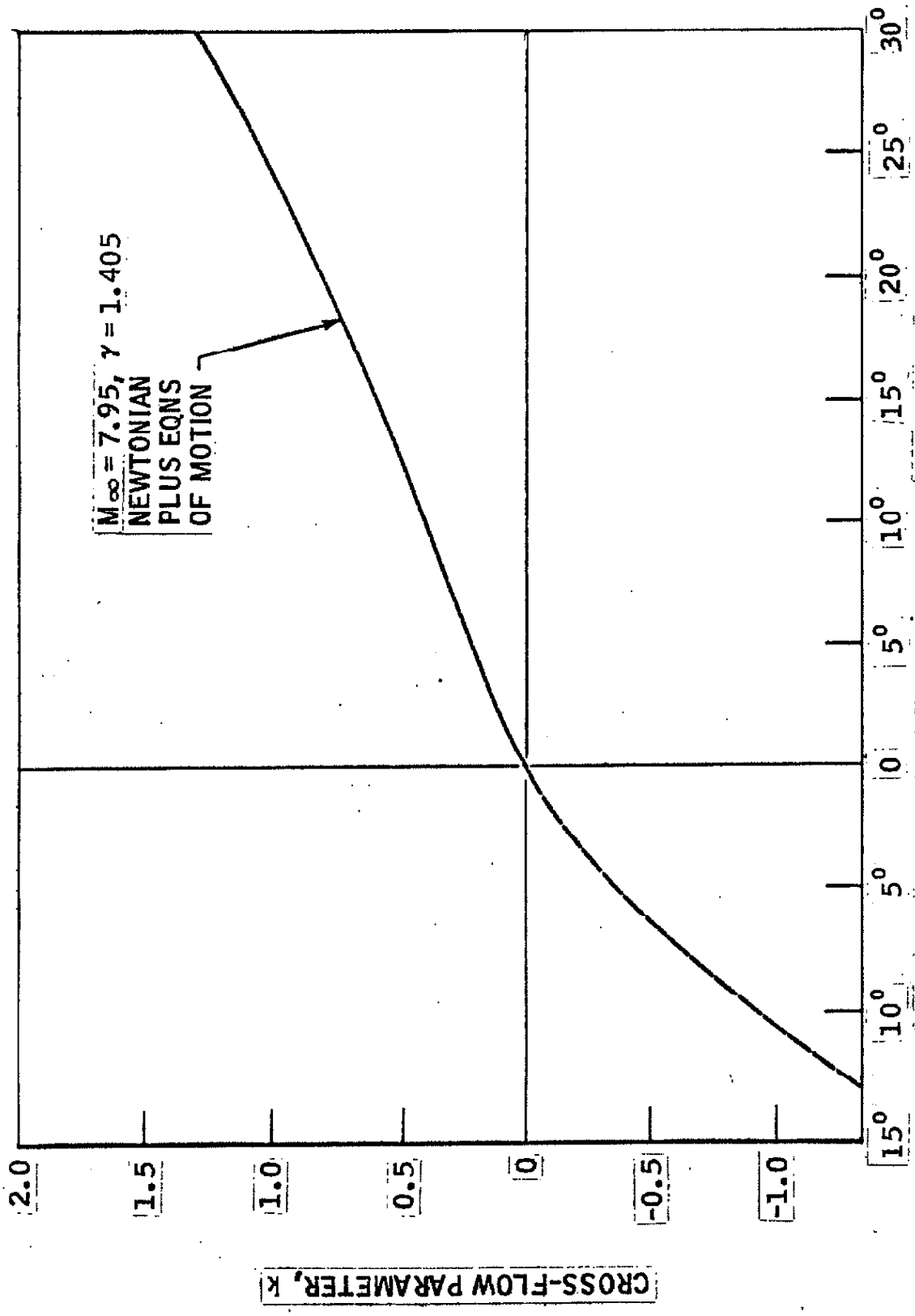

Figure 10. Theoretical Flow, Plane of Symmetry; a. Cross-Flow Parameter

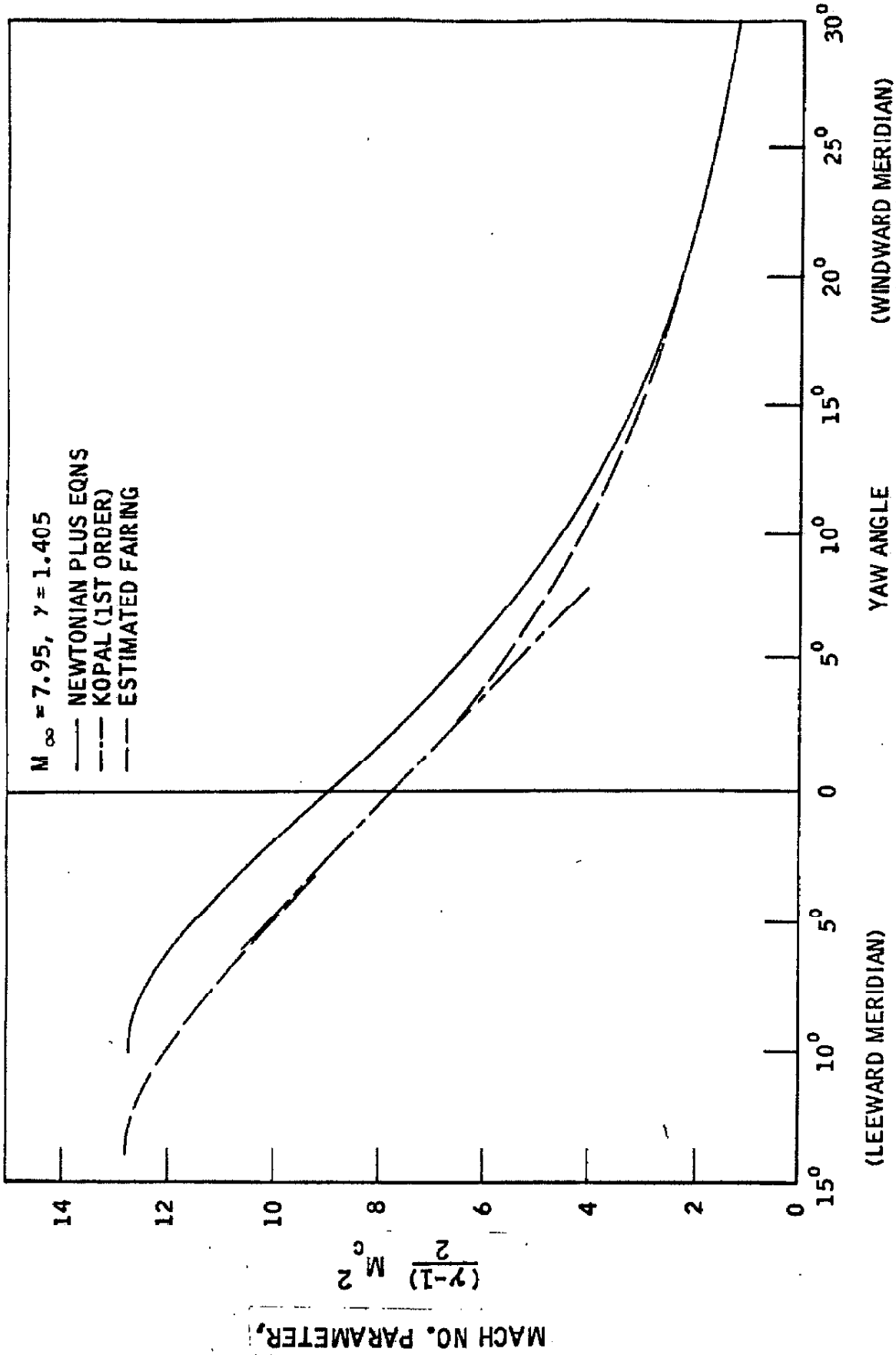

Figure 10 (continued); b. Mach Number Parameter

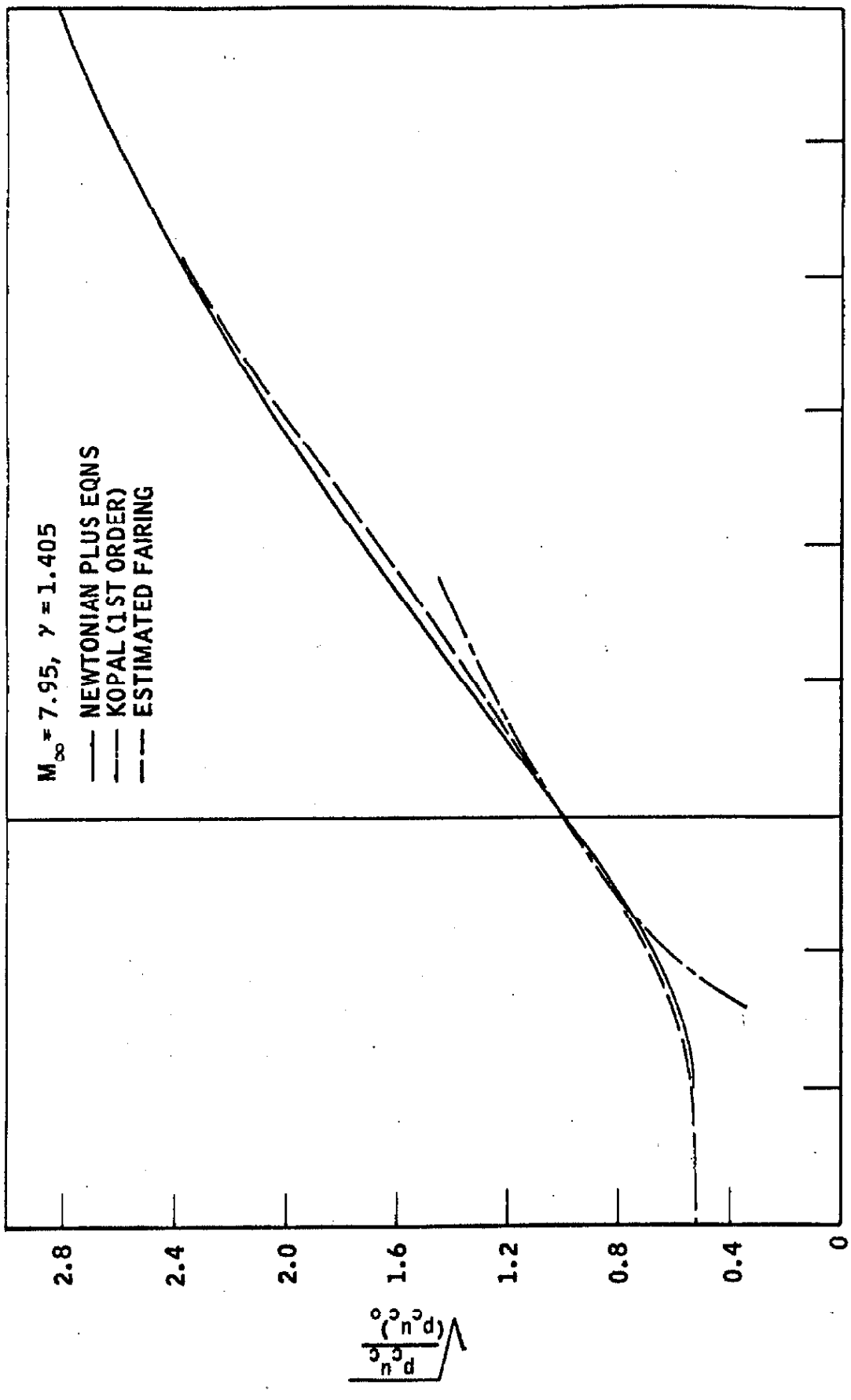

Figure 10 (concluded); c. Pressure - Velocity Product

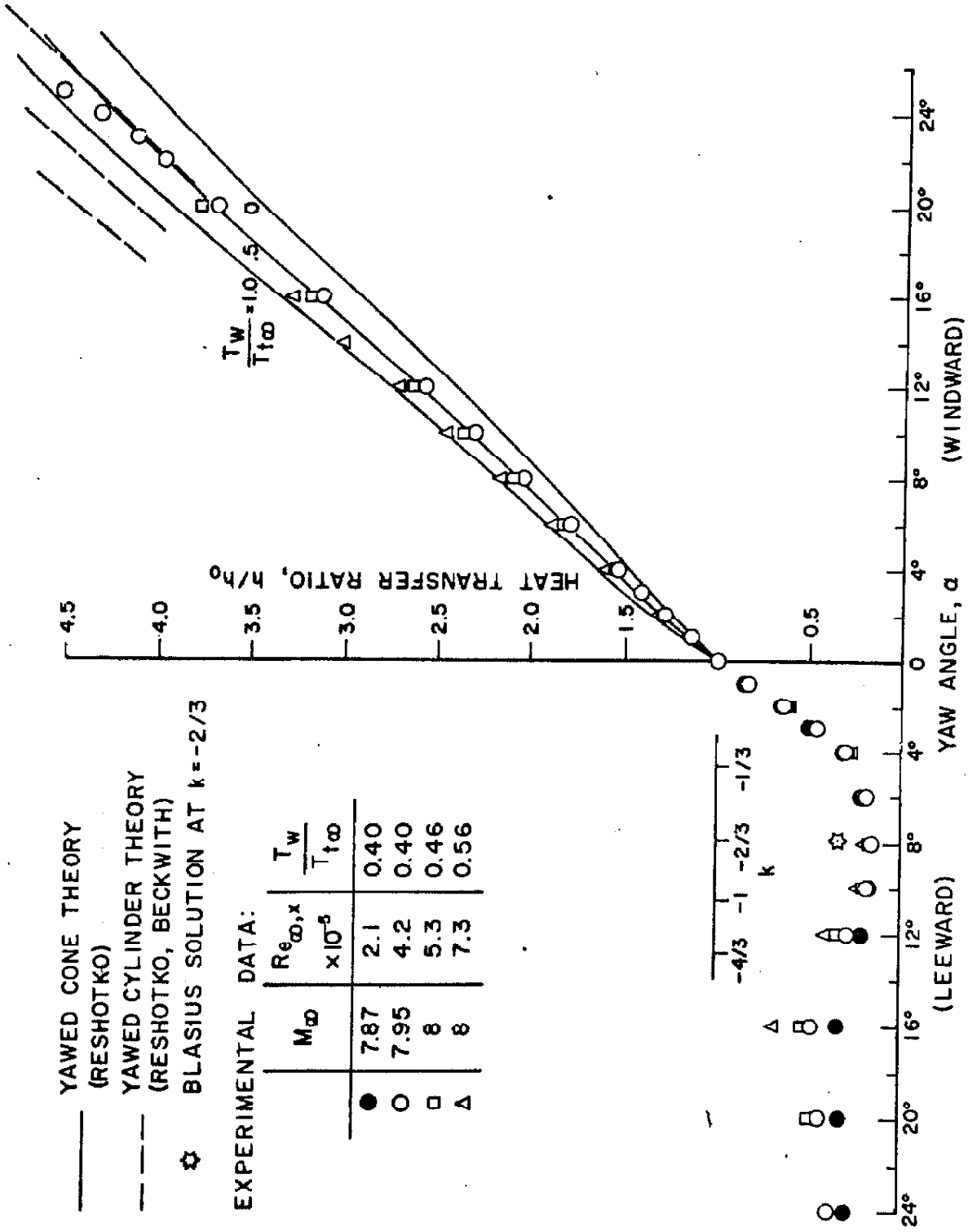

Figure 11. Heat Transfer in the Plane of Symmetry

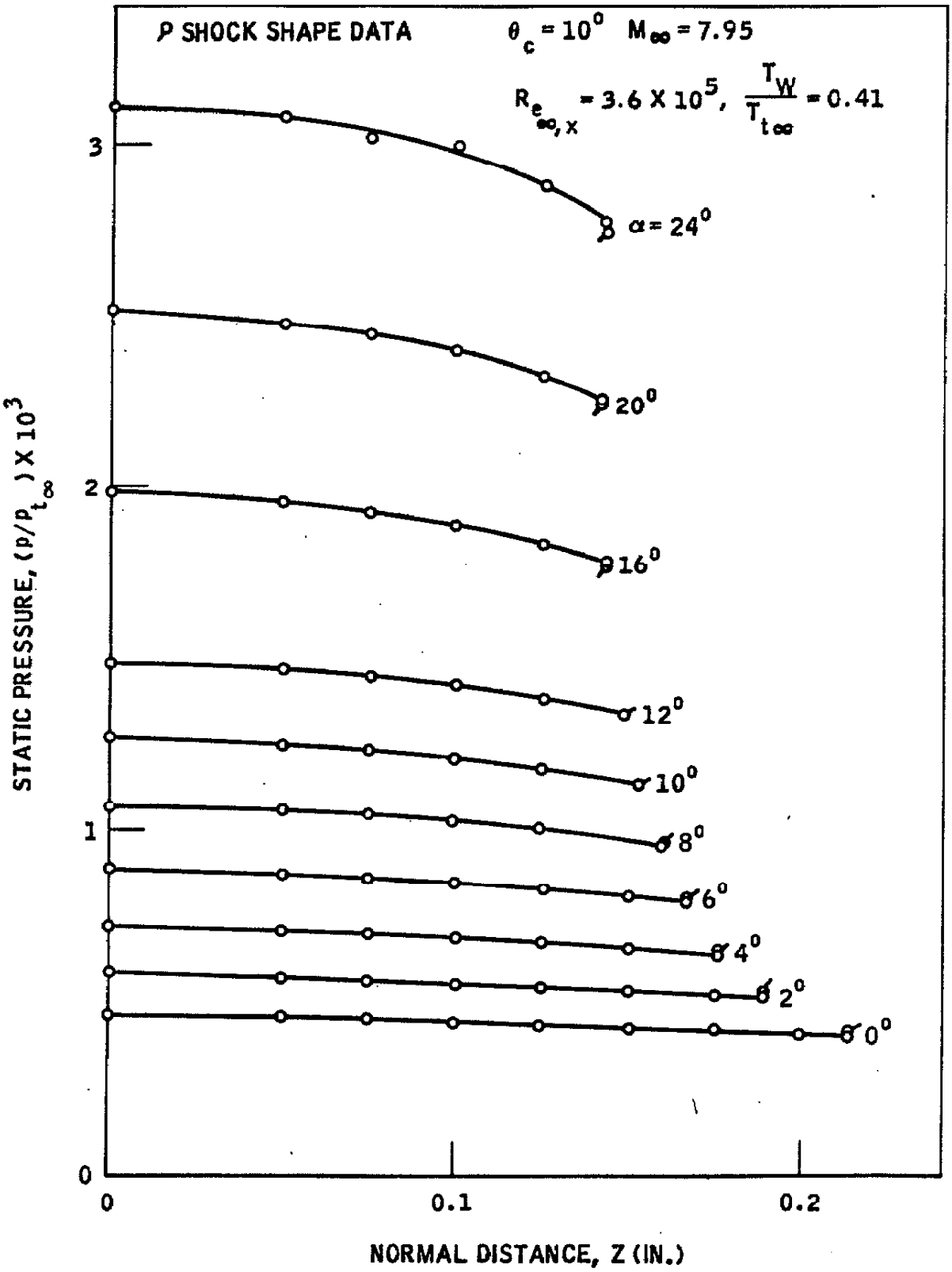

Figure 12. Static Pressure Profiles - Plane of Symmetry;
a. Windward Meridian

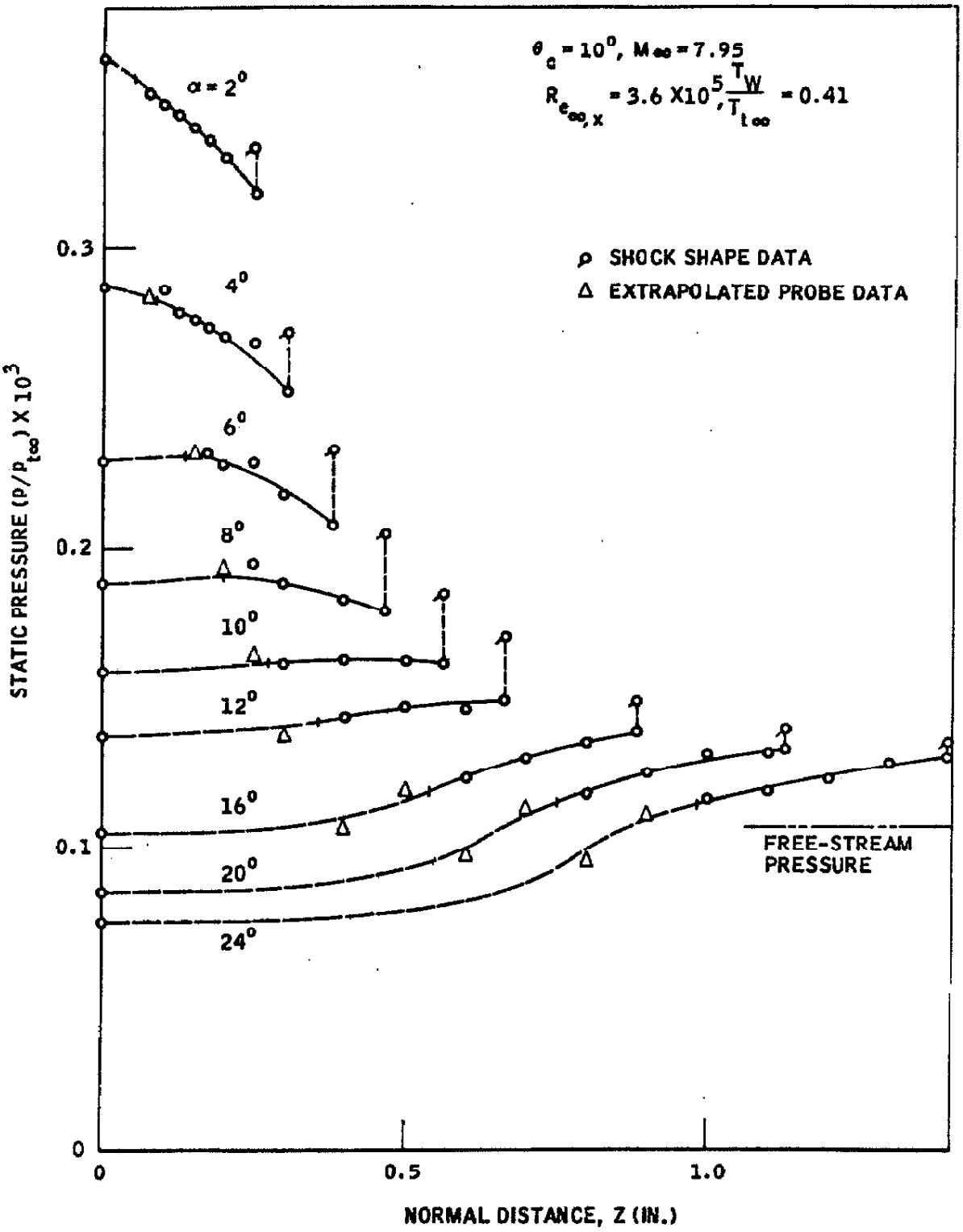

Figure 12. (concluded); b. Leeward Meridian

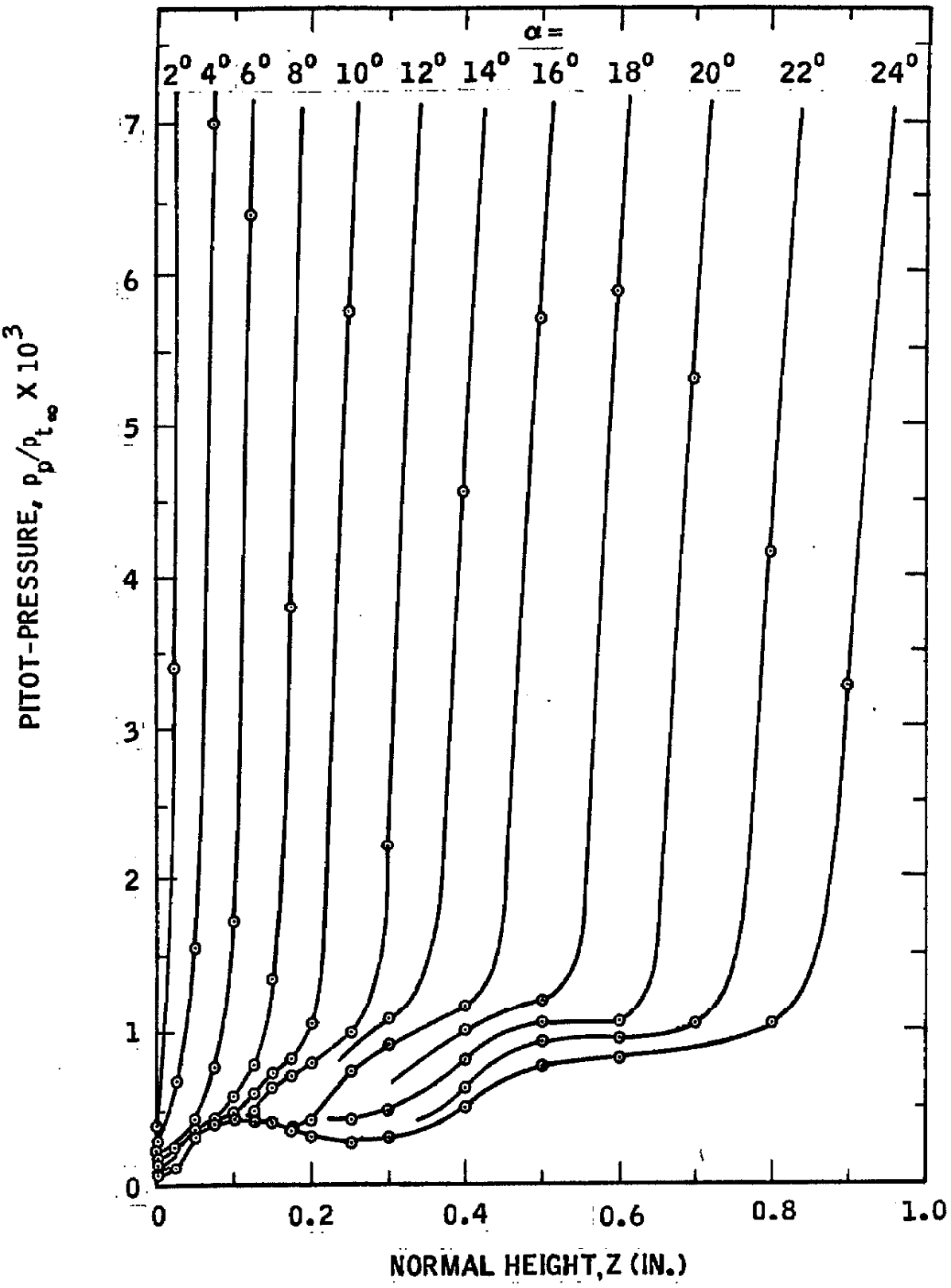

Figure 13. Pitot Pressure Profiles in the Viscous Layer at the Leeward Meridian ($M_\infty = 7.95$, $R_{e_{\infty x}} = 3.6 \times 10^5$, $Tw/T_{t_\infty} = 0.41$)

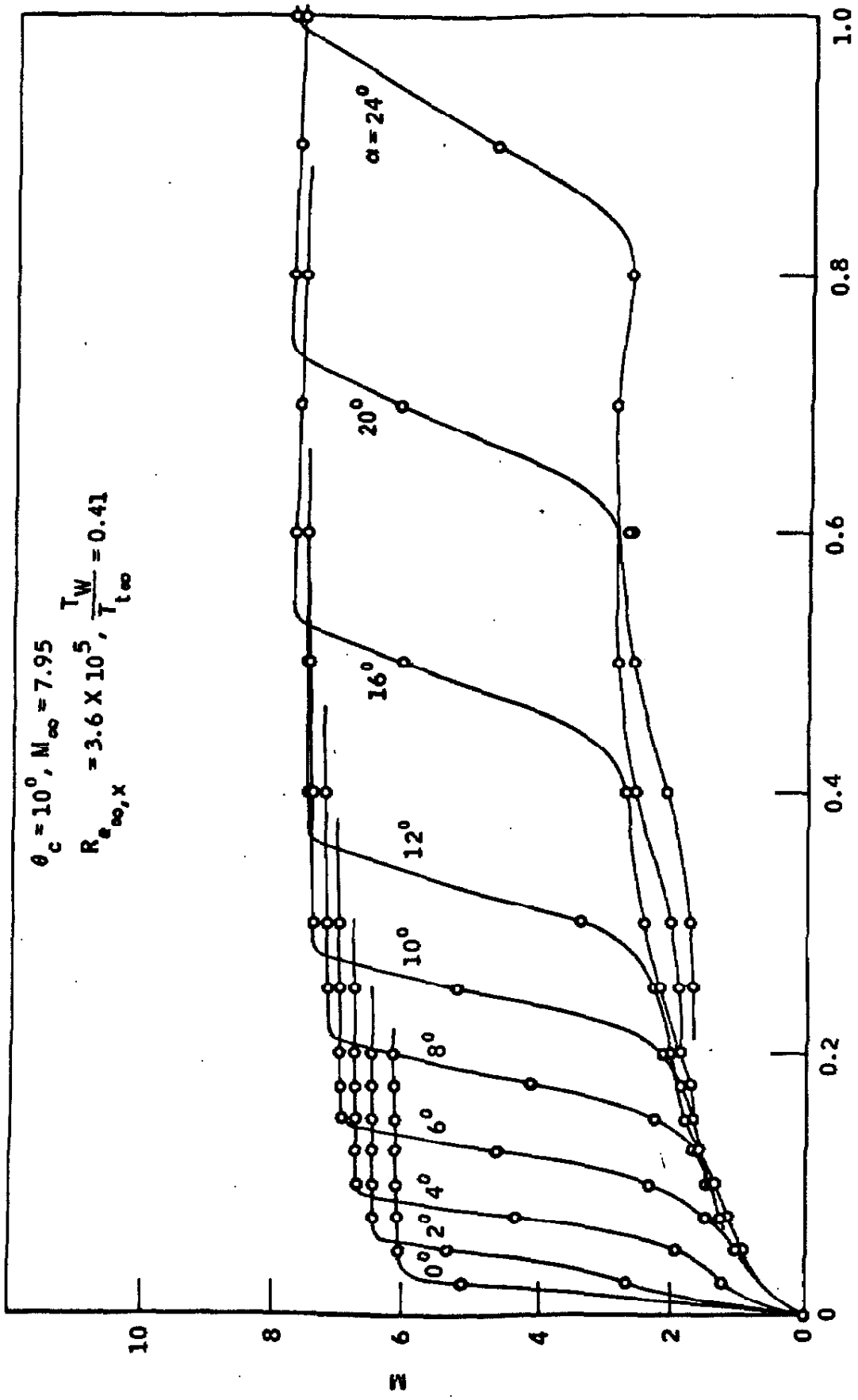

Figure 14. Mach Number Profiles - Leeward Meridian

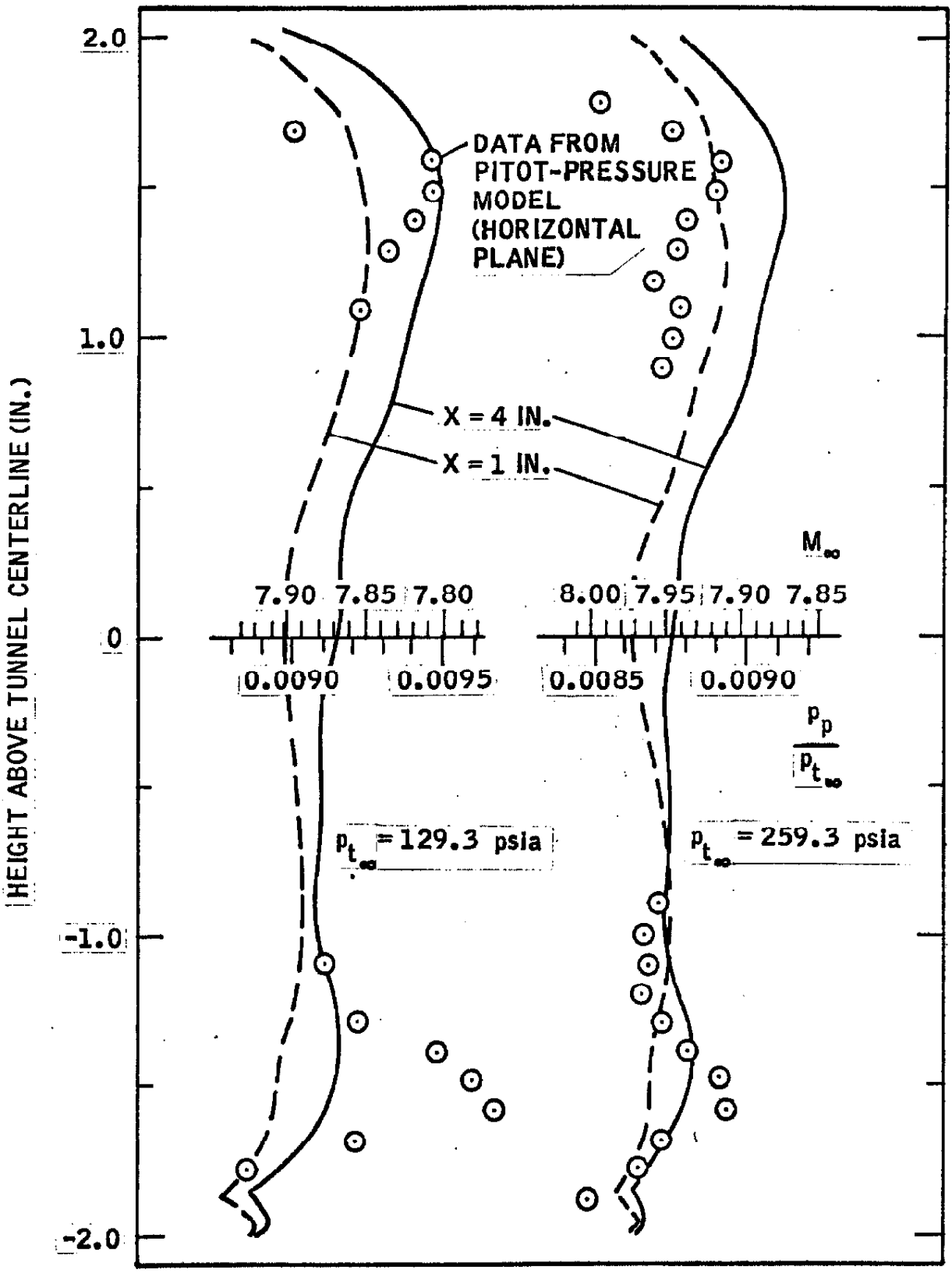

Figure 15. Wind Tunnel Calibration

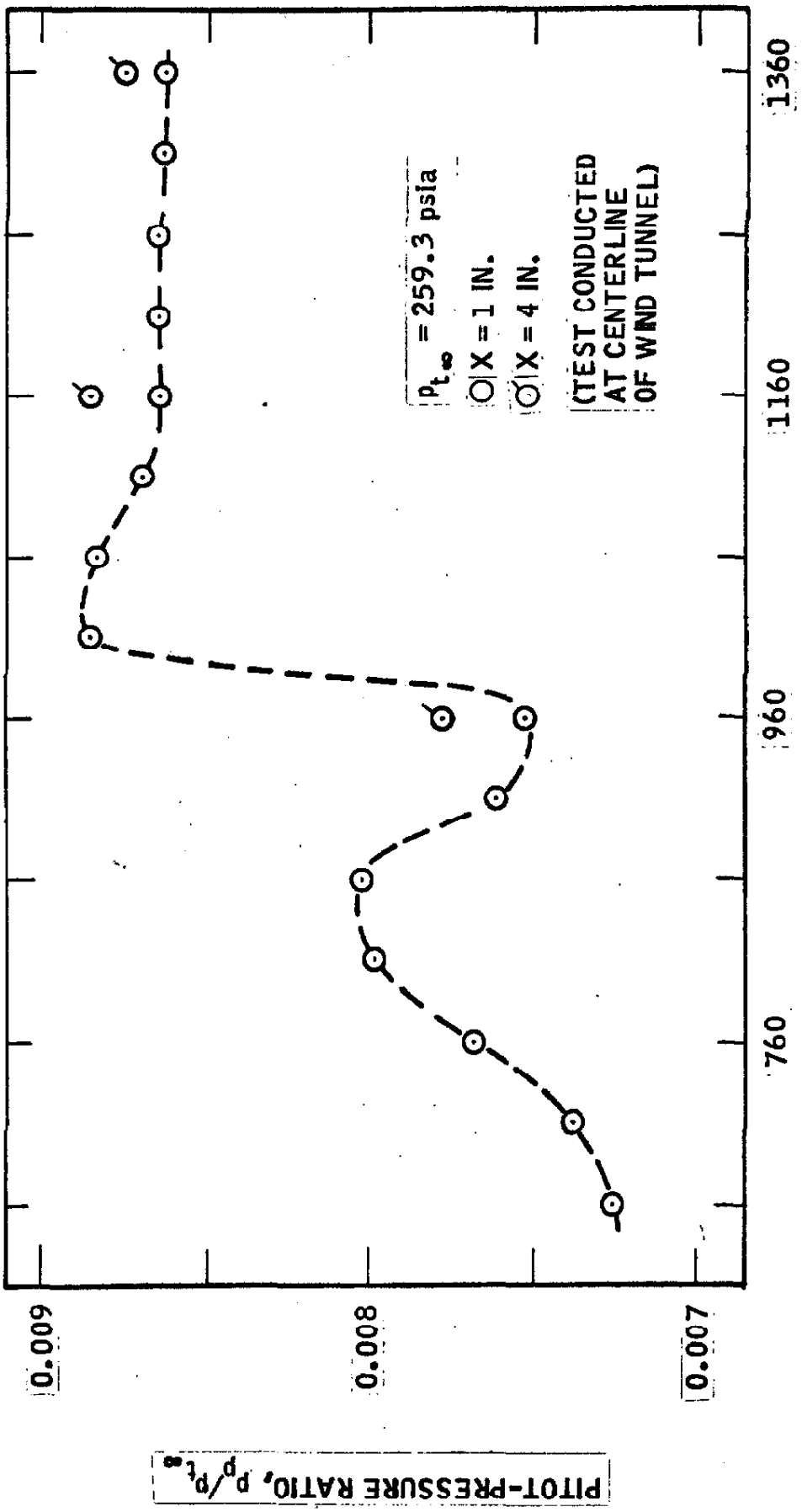

Figure 16. Supply Temperature Effect on Pitot-Pressure

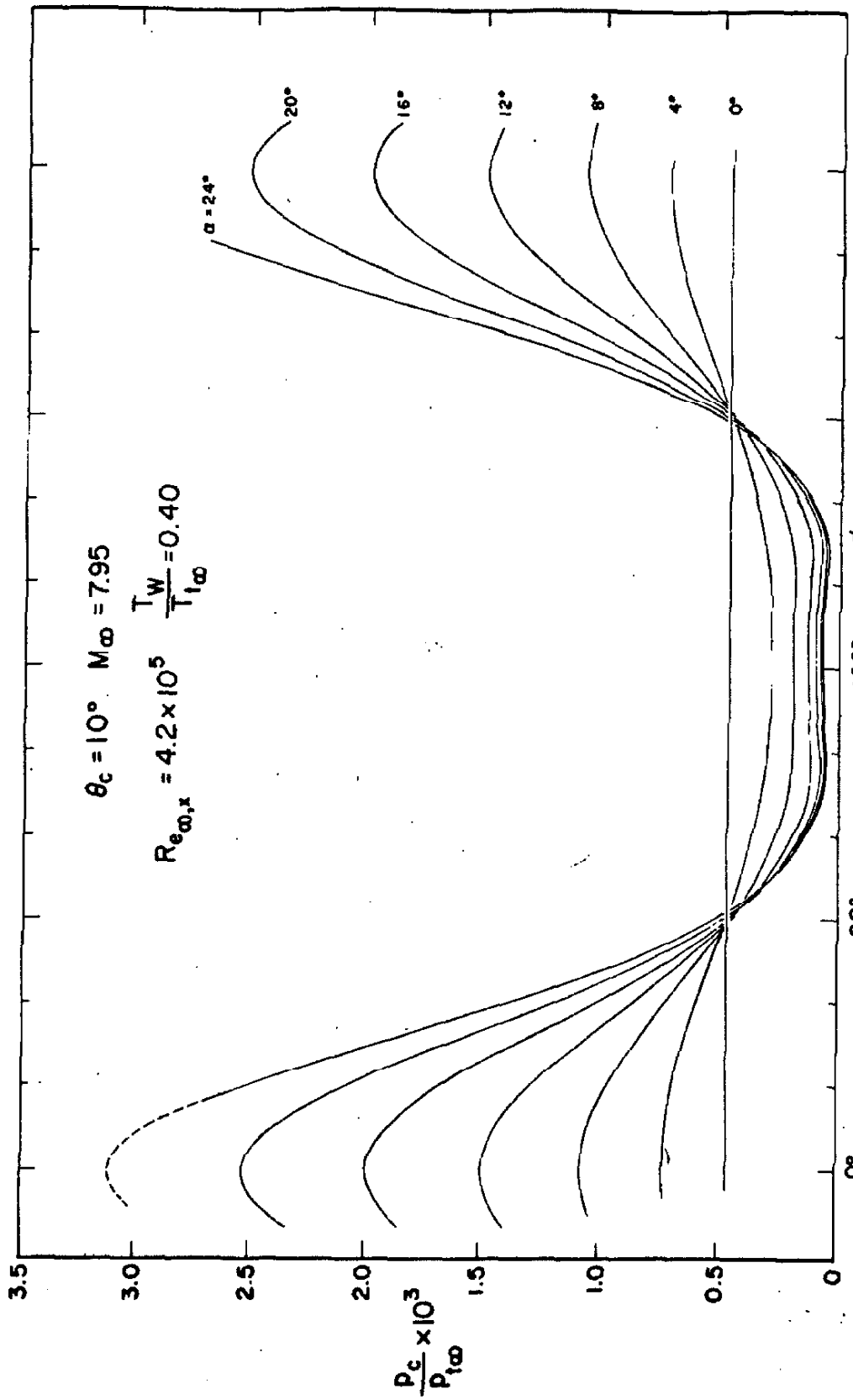

Figure S1a. Surface Pressure - Model No. 1

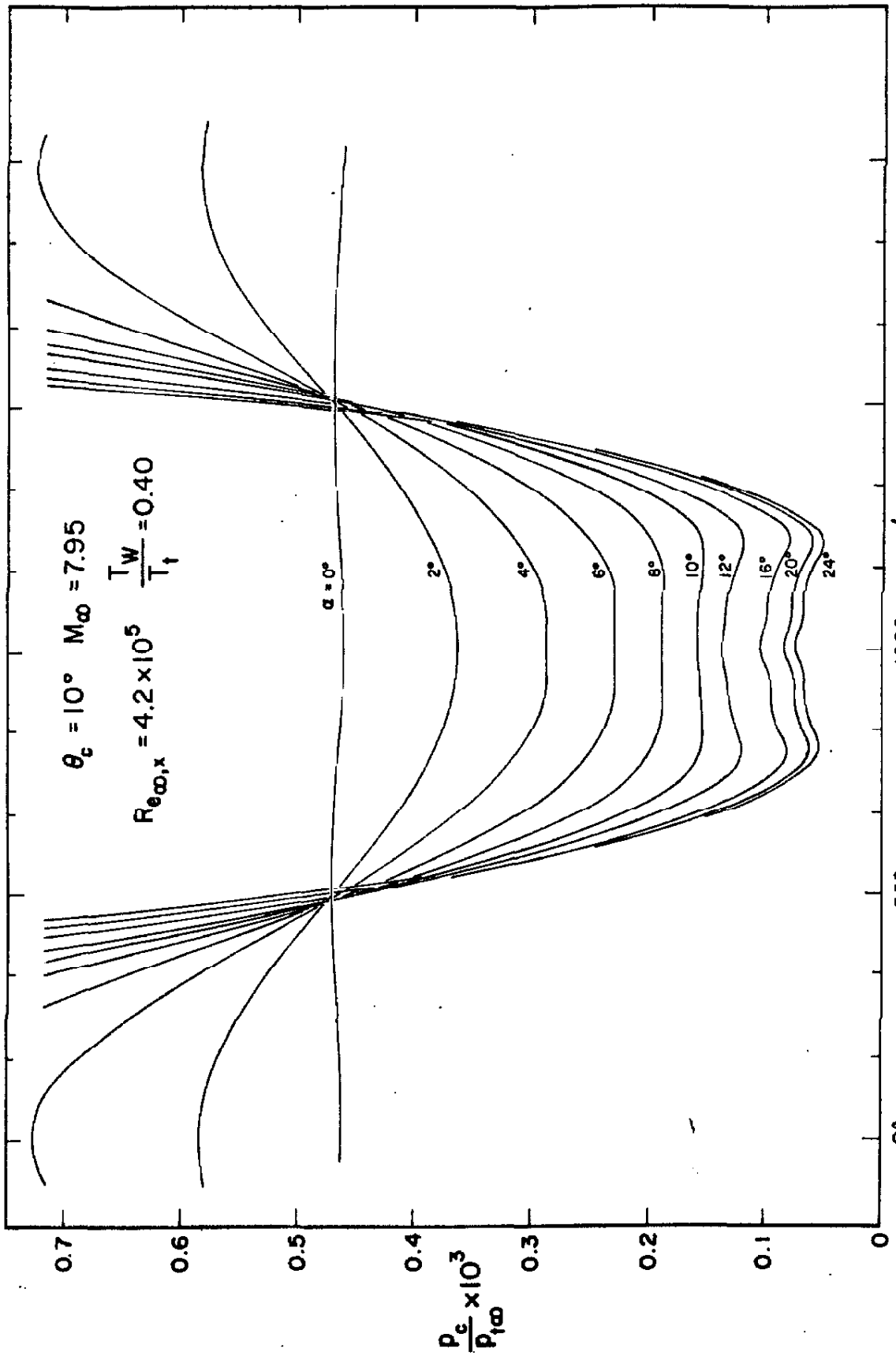

Figure S1b. Surface Pressure Details - Model No. 1

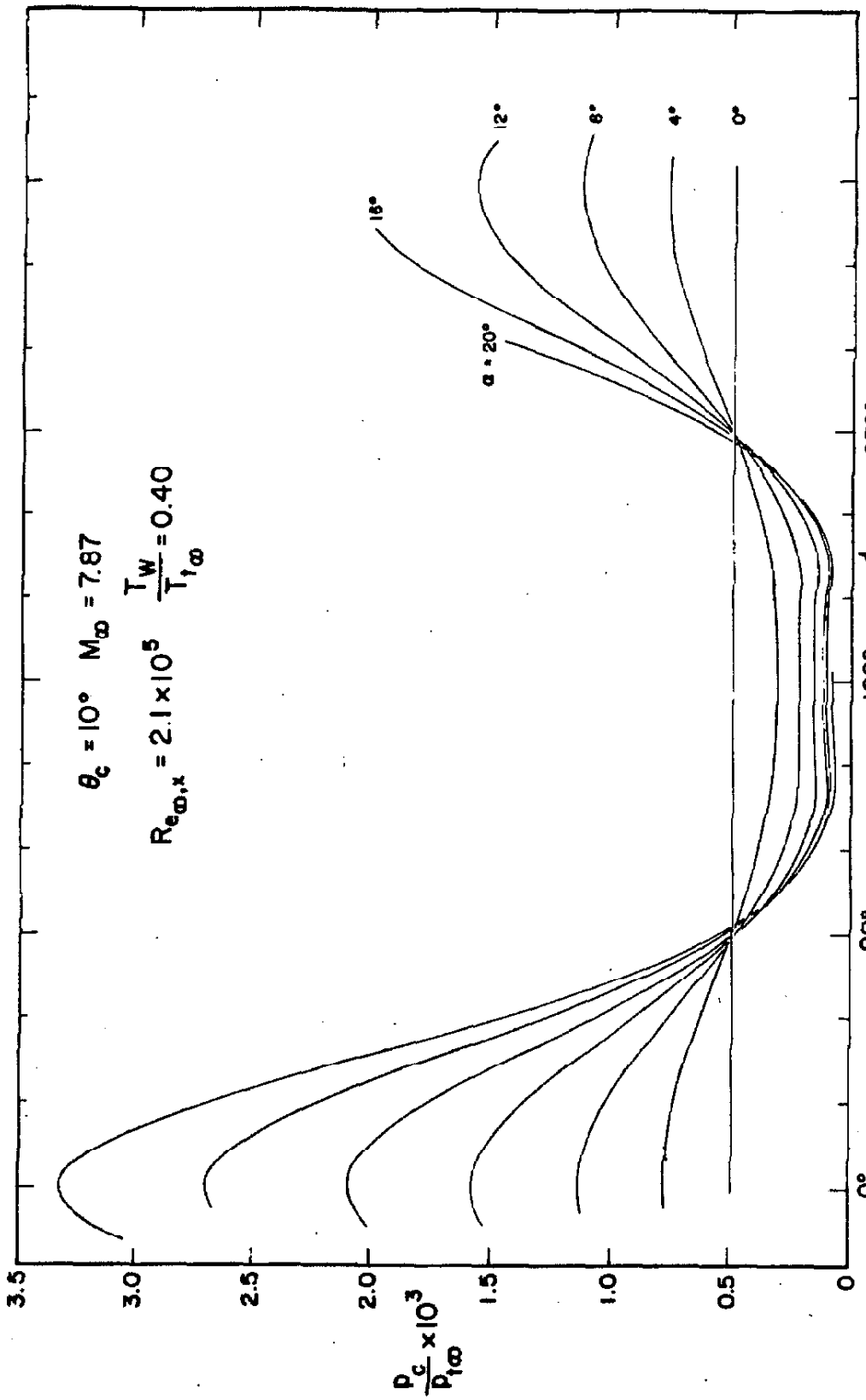

Figure S2a. Surface Pressure - Model No. 1

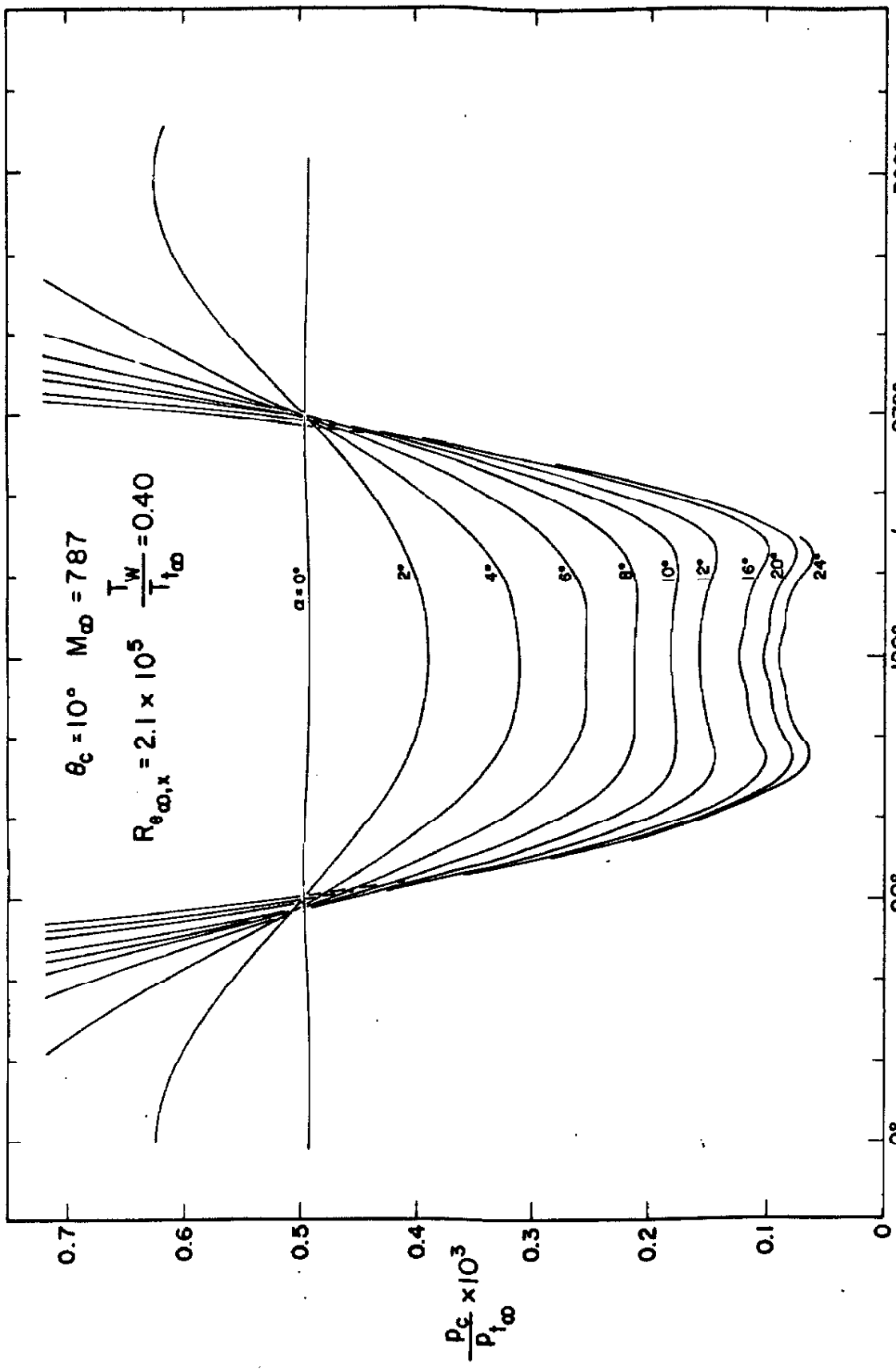

Figure S2b. Surface Pressure Details - Model No. 1

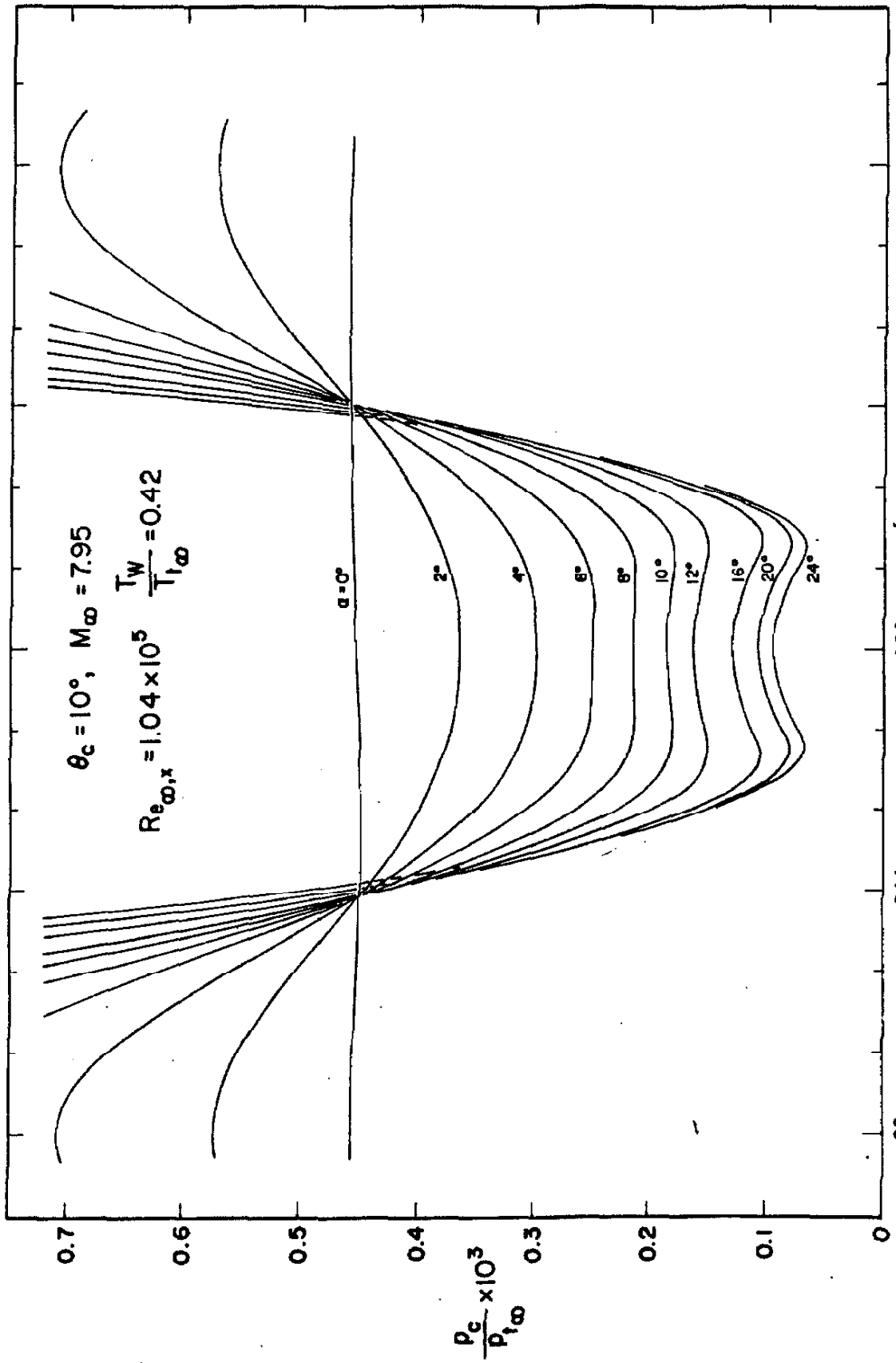

Figure S3. Surface Pressure Details – Model No. 2

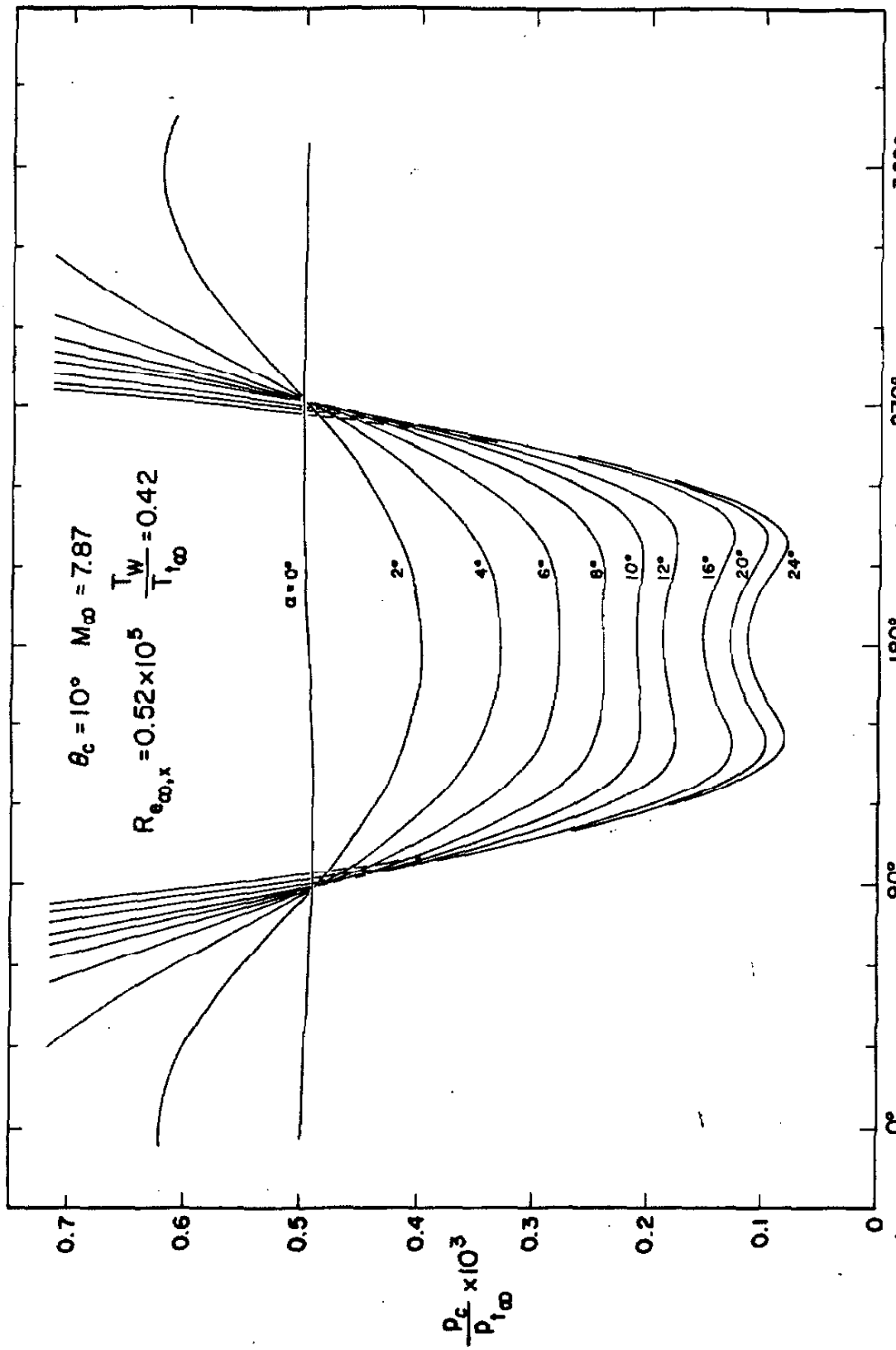

Figure S4. Surface Pressure Details - Model No. 2

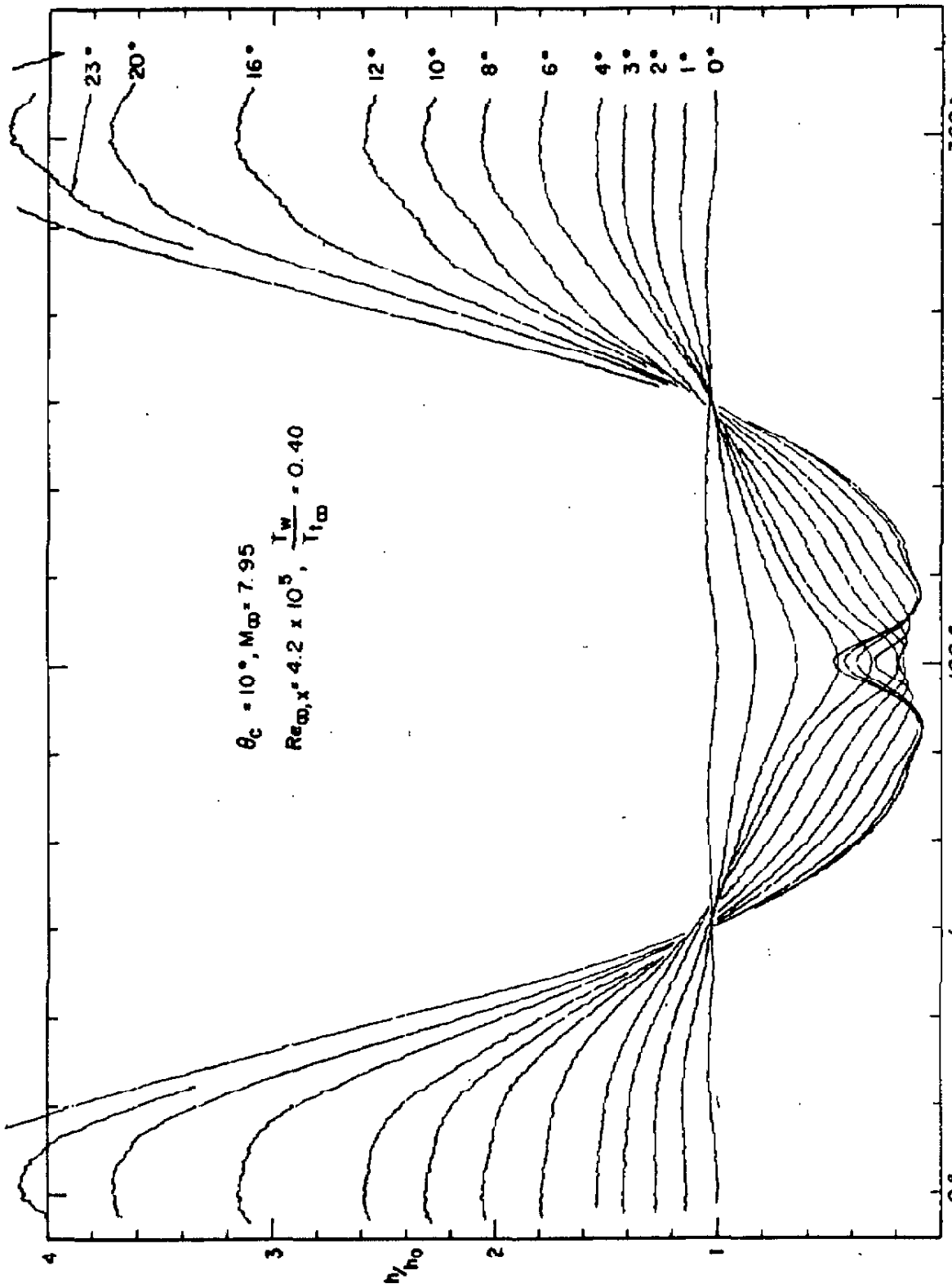

Figure S5. Normalized Local Heat Transfer

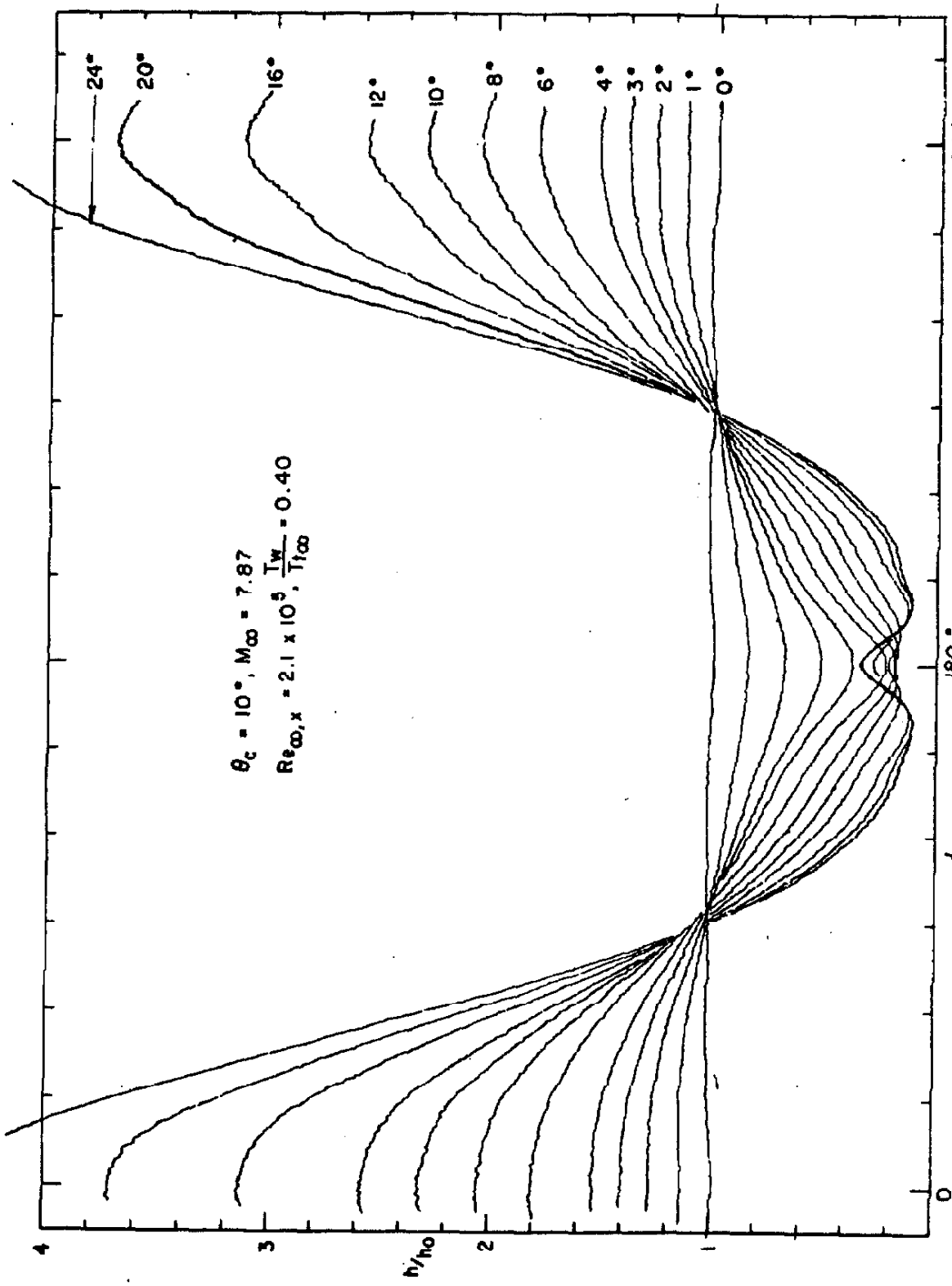

Figure S6. Normalized Local Heat Transfer

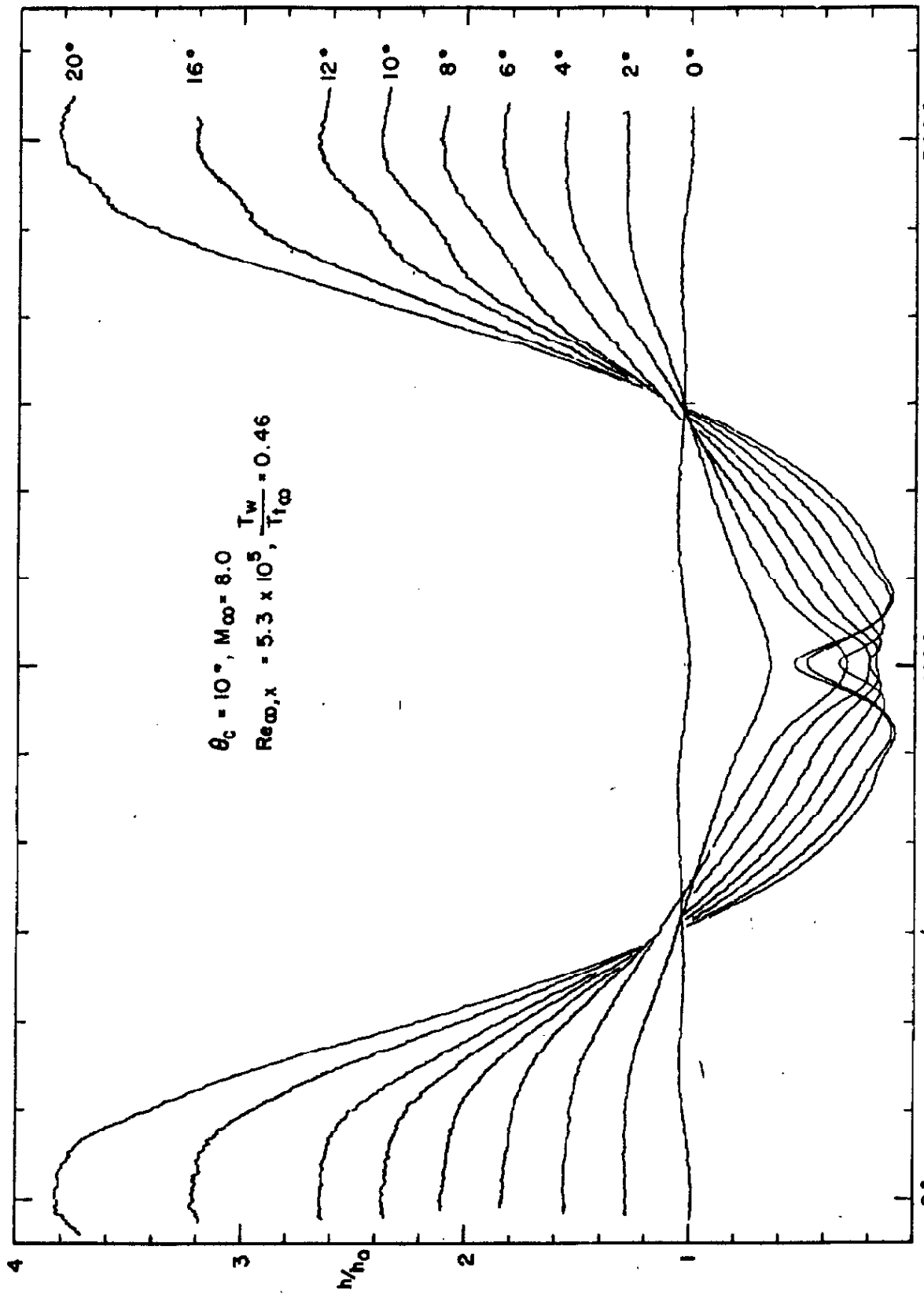

Figure S7. Normalized Local Heat Transfer

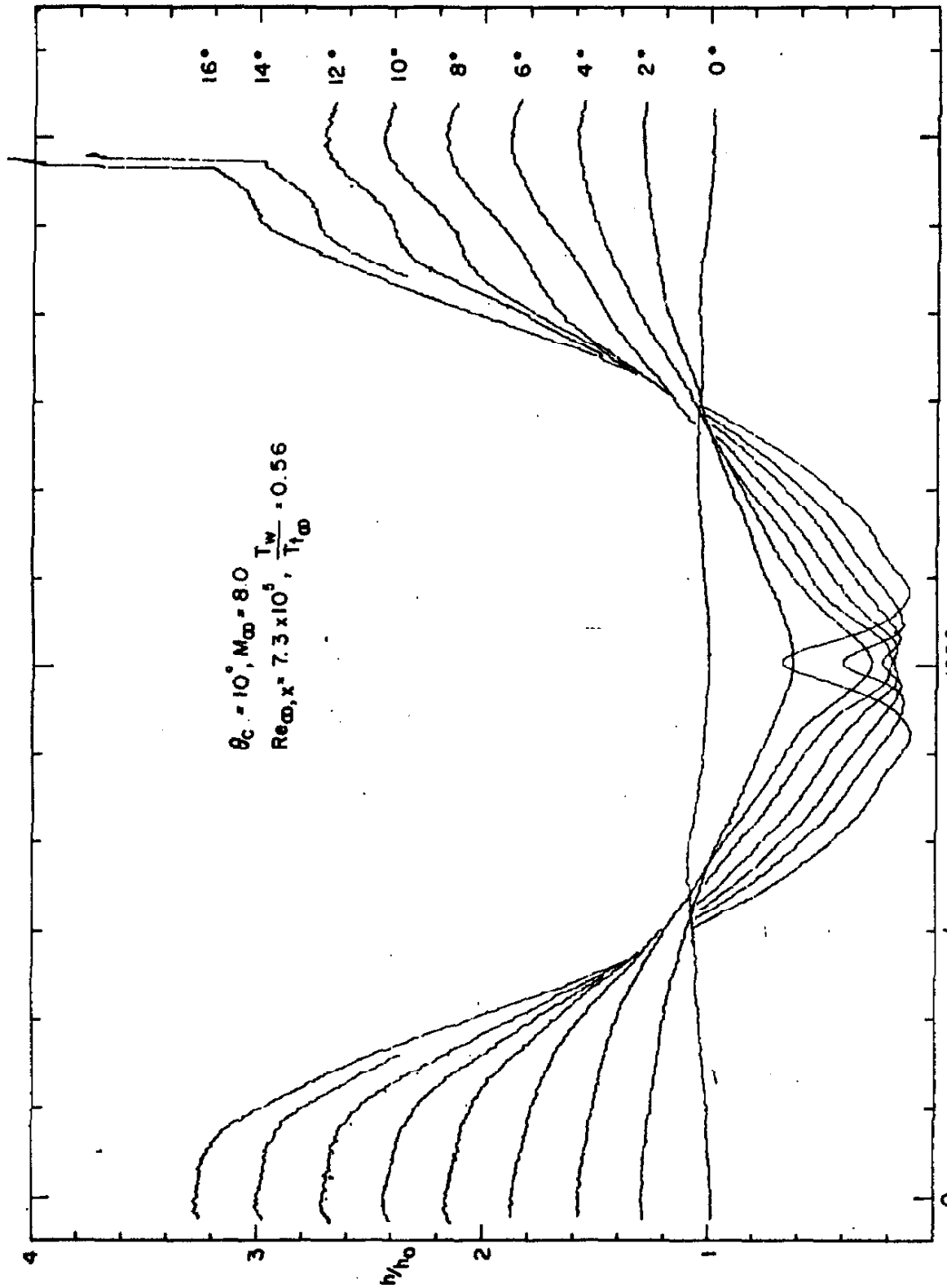

Figure 58. Normalized Local Heat Transfer

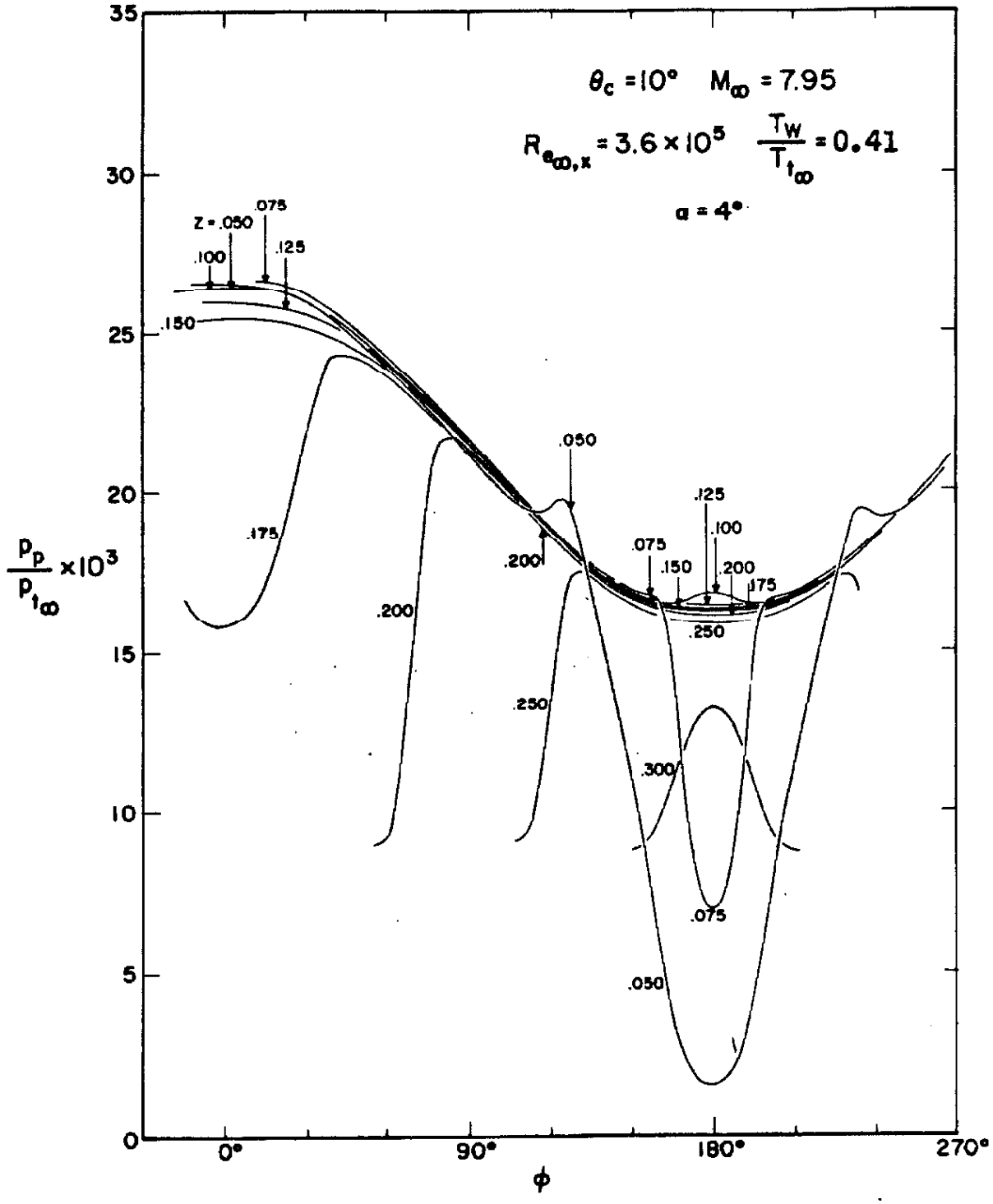

Figure S9. Pitot Pressure Survey - 4^0 Yaw

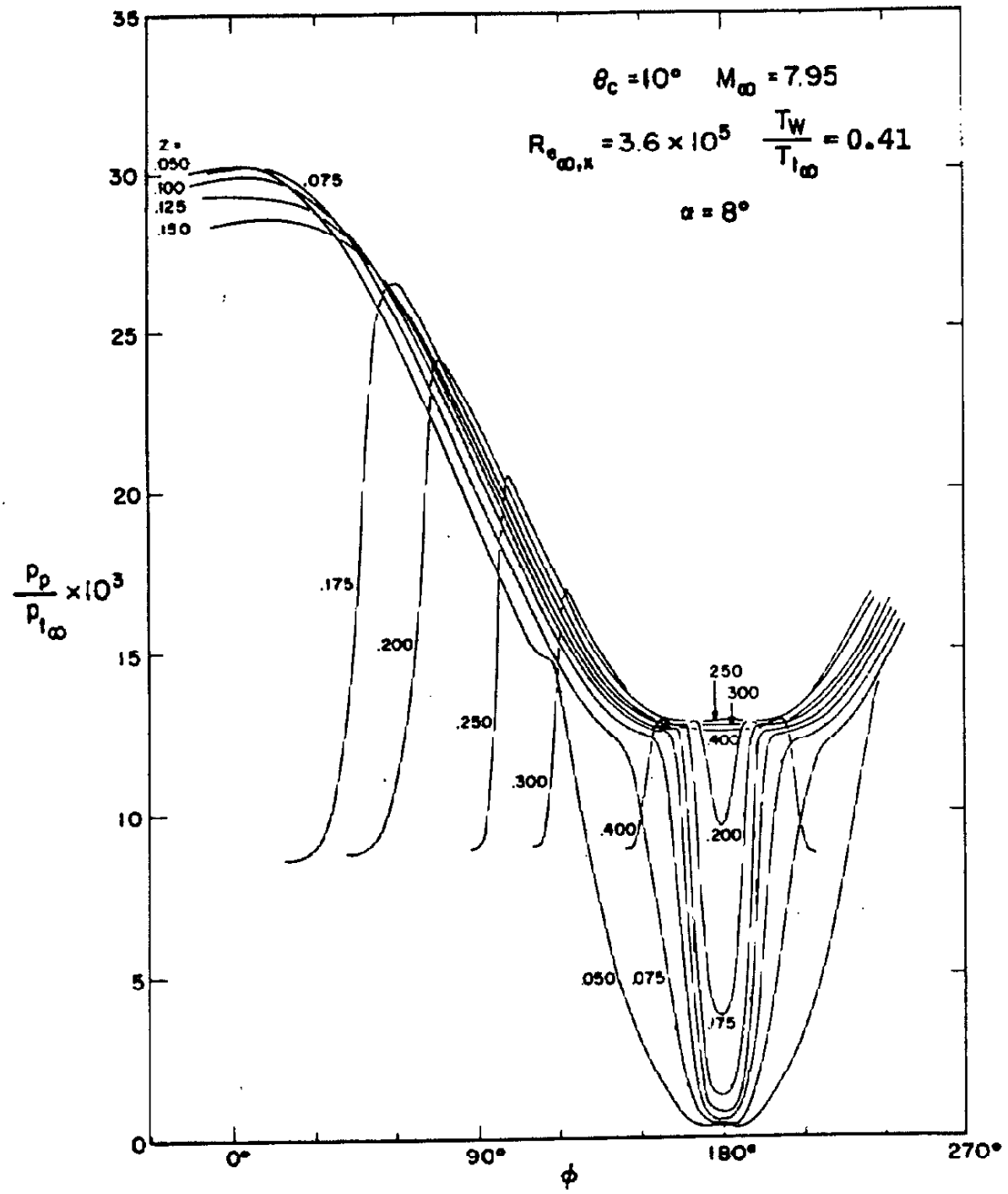

Figure S10. Pitot Pressure Survey - 8^0 Yaw

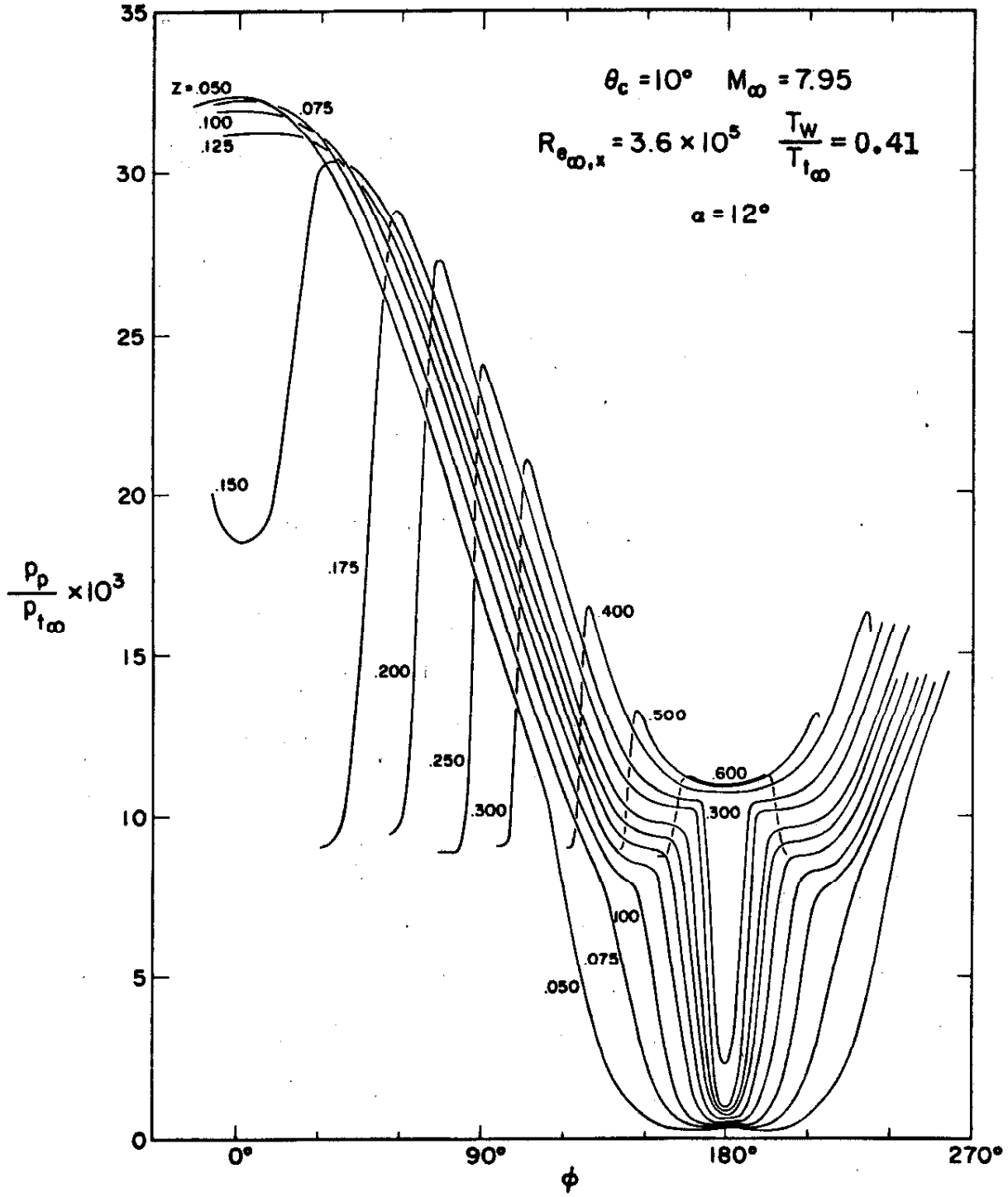

Figure S11. Pitot Pressure Survey - 12° Yaw

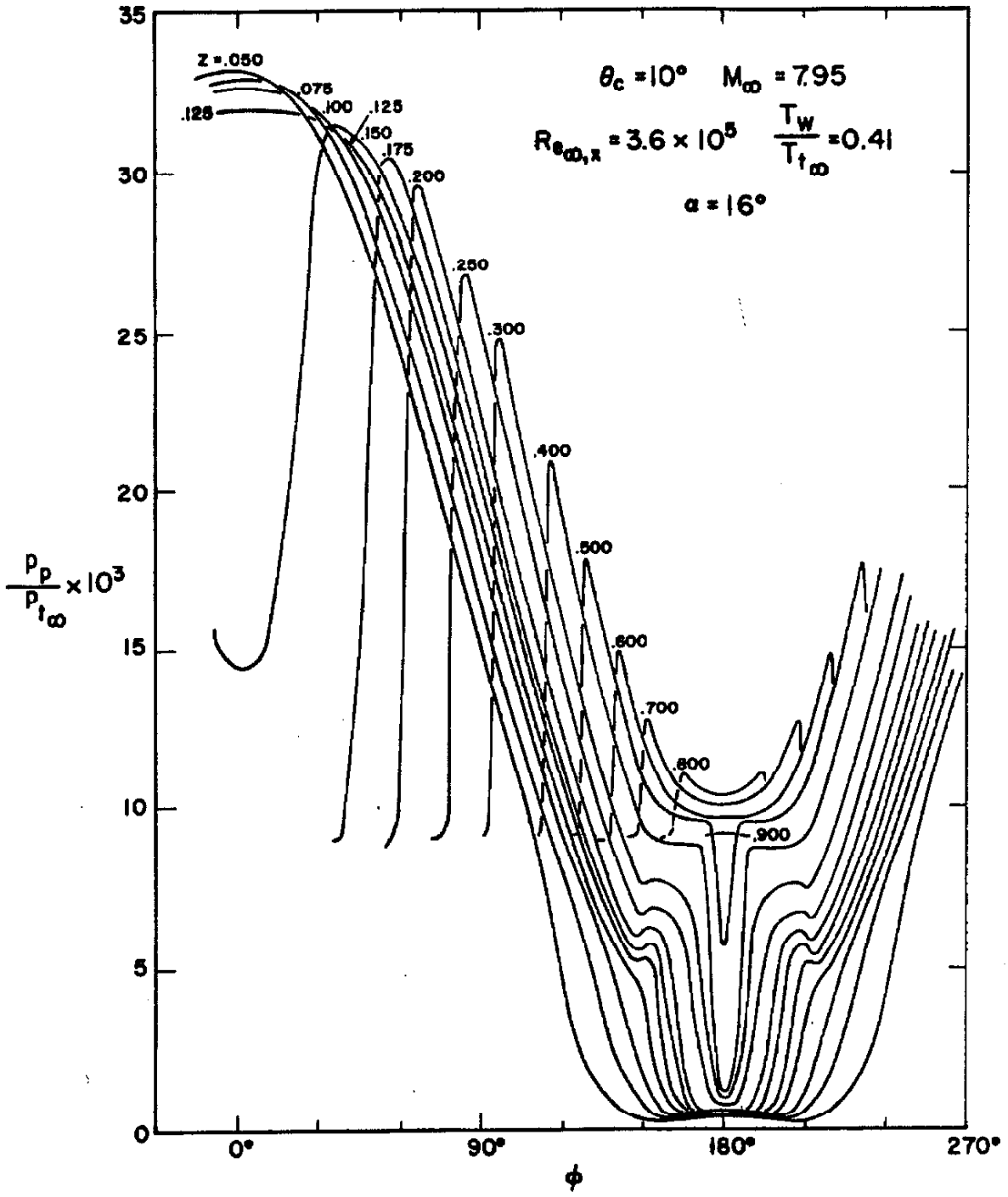

Figure S12. Pitot Pressure Survey - 16° Yaw

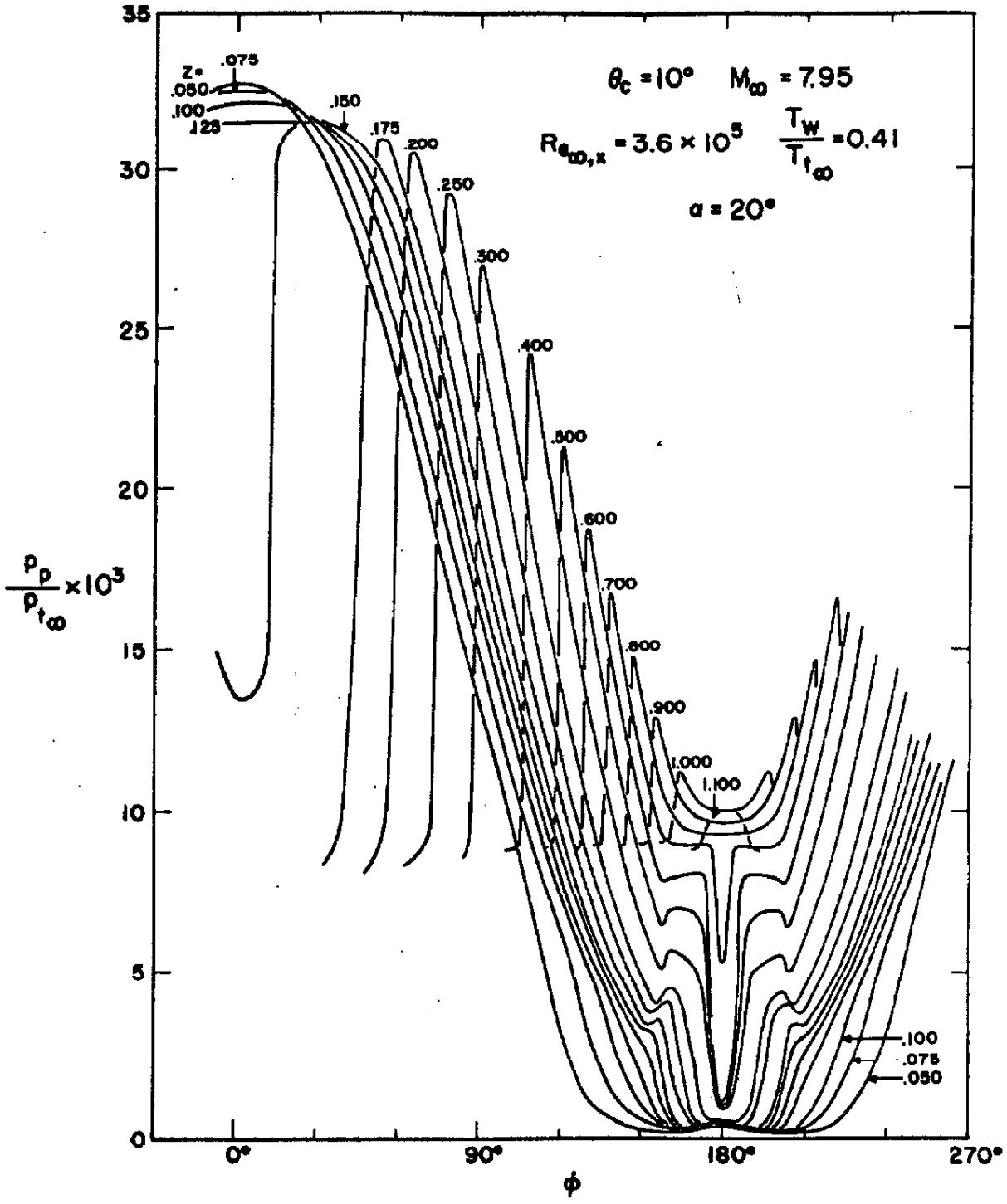

Figure S13. Pitot Pressure Survey - 20^0 Yaw

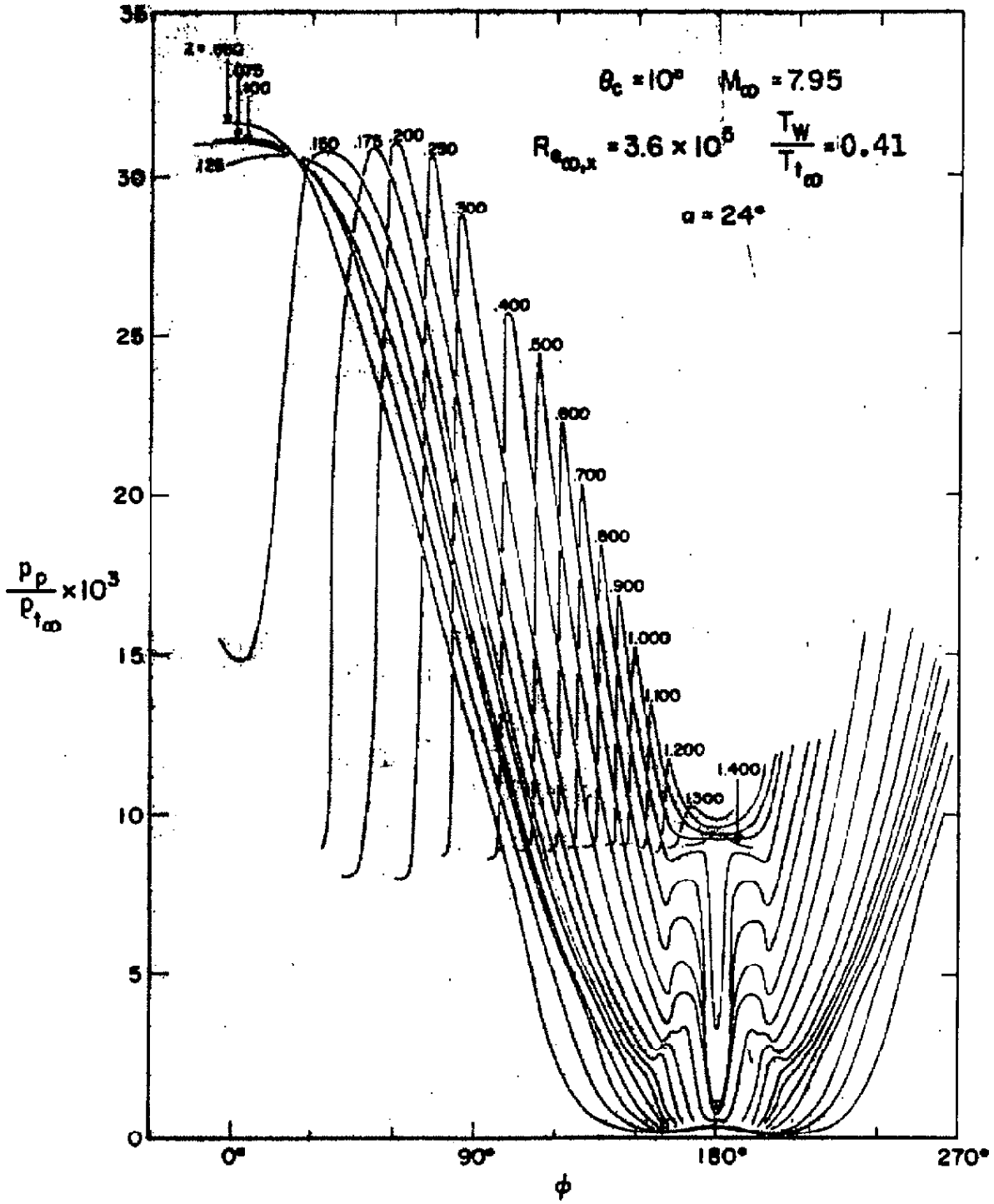

Figure S14. Pitot Pressure Survey - 24^0 Yaw

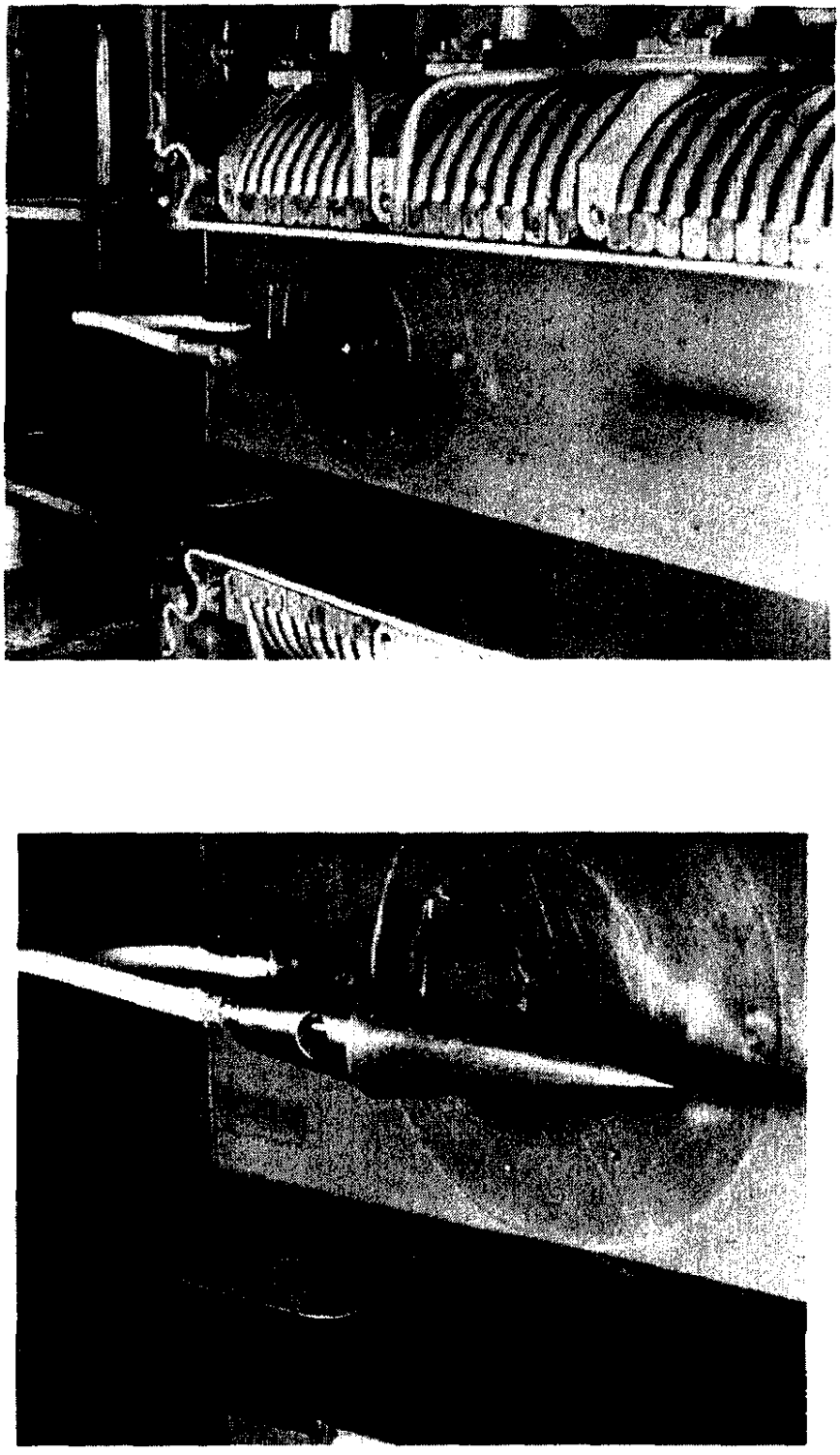

Figure 1. Model Installation in Leg 2 - GALCIT Hypersonic Wind Tunnel

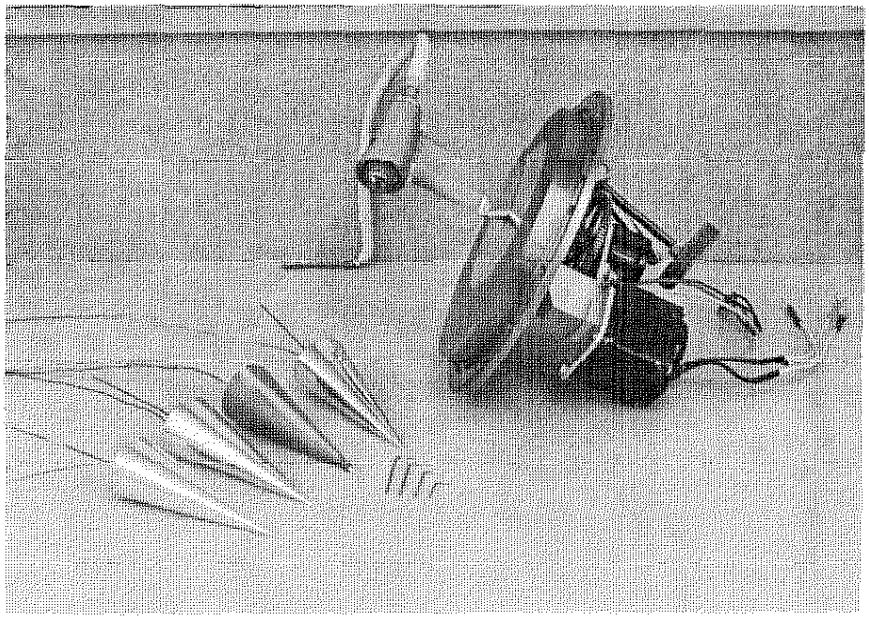

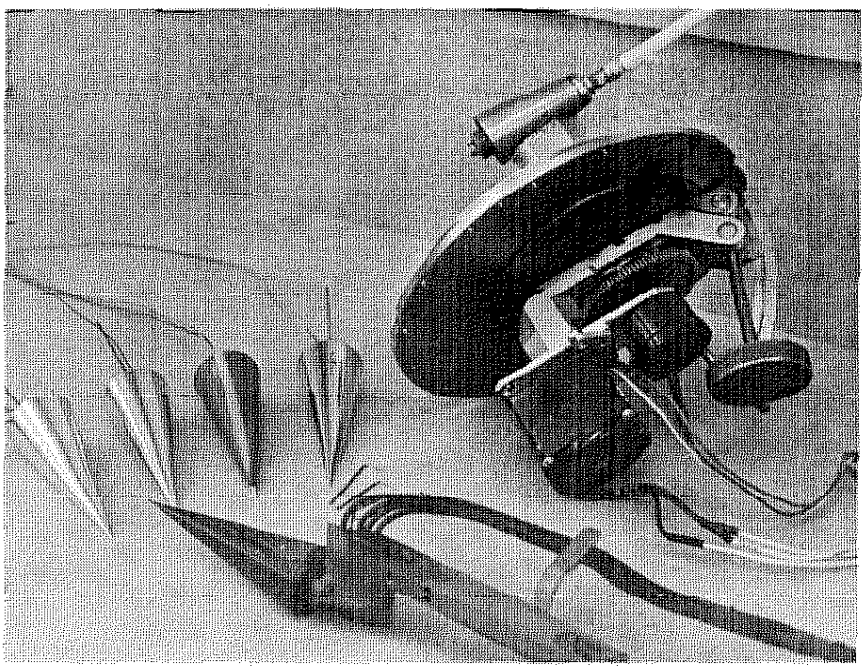

Figure 2. Test Models and Support System

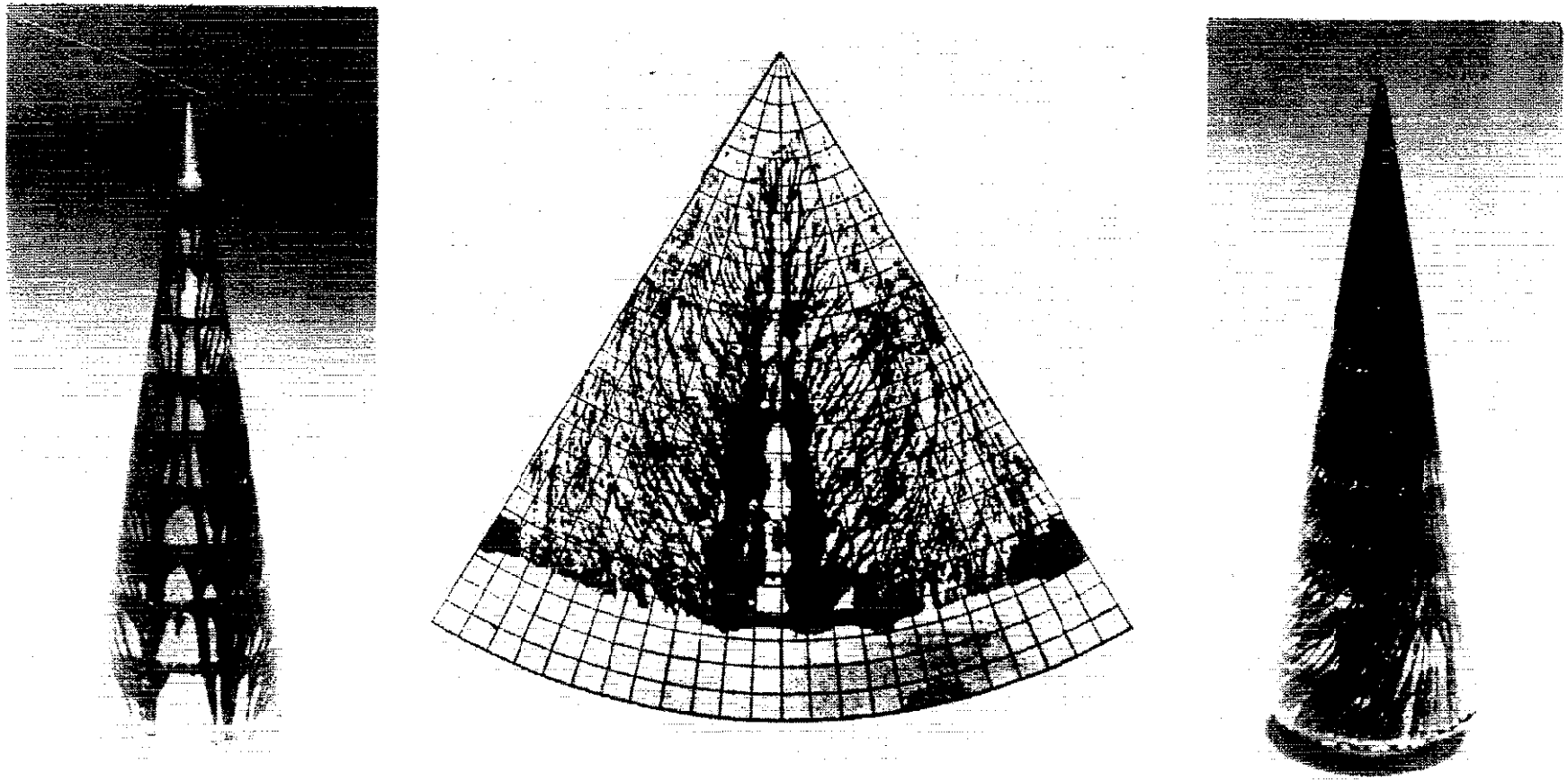

$M_\infty = 7.9$, $R_{e_\infty} \approx 1.0 \times 10^6$/FT, $T_w/T_{t_\infty} \approx 0.8$; $\alpha = 11^\circ$

(EACH RADIAL DIVISION = 0.2 IN.)

Figure 3. Surface Flow Patterns